

FRACTAL STRUCTURES

Paul Meakin

Central Research and Development Department,
E. I. du Pont de Nemours and Company,
Wilmington, DE 19880-0356, U.S.A.

INTRODUCTION

Much of our understanding of the properties and behavior of physical systems depends on quantitative models for their structure. Until quite recently, most of these models have been based on Euclidean geometry (straight lines, planar surfaces, spherical volumes, etc.). For such structures the familiar symmetries of invariance to translation, rotation, reflection and inversion play an important role in the development of an understanding of a broad range of properties and processes. However, many systems of considerable practical and scientific importance (colloidal aggregates, practical catalysts, polymer molecules, many porous materials and biological structures for example) cannot be adequately described in such terms. In many cases, the lack of an adequate way of describing such structures has inhibited a systematic study of their physical and chemical behavior. Many of these apparently complex structures possess an important symmetry that has frequently been overlooked in the past. This symmetry is an invariance to a change in length scale or magnification. Objects that possess this symmetry are now called fractals.¹⁻⁴ The most simple type of fractals are those that are invariant to an isotropic change of length scales. Familiar examples include clouds, coastlines and the vascular system. In many other cases, the fractal structure is invariant to a "self-affine" transformation in which the length scale is changed by different factors in different directions. Examples of such self-affine fractals include mountains and a wide range of rough surfaces. Invariance to self-affine or self-similar transformations can be used to obtain an understanding of some of the properties of fractal systems without the need to be encumbered by physical and chemical details in much the same way that group theory can be used in areas such as molecular and atomic spectroscopy, solid state physics, reaction mechanisms and high energy physics. In the first part of this review the basic concepts of fractal geometry are described. This section emphasizes the distinction between self-affine and self-similar fractals and introduces some more general approaches to the description of fractal structures.

Many of the most important processes in solid state chemistry occur at surfaces and interfaces. In many cases these interfaces have a complex fractal geometry. To a large extent this review is concerned with structure and dynamics of these surfaces and their importance in solid state chemistry. In recent years a variety of simple models for the formation of rough surfaces have been developed. Computer simulation results almost invariably indicate that these surfaces have a self-affine fractal geometry and in some cases the geometric scaling (fractal) properties of these surfaces can be understood in terms of analytic theories. Computers and computer graphics have played a critical role in the application of fractal geometry to the physical sciences. Without the ability to see the complex and often beautiful structures generated by even very simple models, it is doubtful if fractal geometry would have reached its present level of development and it is certain that the dissemination of the concepts of fractal geometry would have been a much more slow and painful process without the digital computer.

Fractal geometry is still a young and vigorous area of mathematics. The range of its applications to physics and chemistry has not yet been fully delineated. At this stage it is apparent that the concepts of fractal geometry can be usefully applied to a quite broad range of problems relevant to solid state chemistry.

Consequently, it seems worthwhile to describe areas in which progress has been made and to indicate some newer directions that seem to be quite promising. This is the main objective of this review.

FRACTAL GEOMETRY

The concepts of fractal geometry were developed primarily by B. B. Mandelbrot¹⁻³ (who invented the word fractal) during the past 20-30 years. These concepts are based on work by late 19th century and early 20th century mathematicians but it is only within the last 5-10 years that these ideas have become widely disseminated and applied to many problems in physics, chemistry, biology and other areas. A fascinating account of the genealogy of fractals can be found in ref. 3. There is no concise definition of a fractal but in general terms a fractal is a structure that is invariant to a change of length scale (or scales). In real systems this symmetry is an idealization that is not precisely realized. However, models based on fractal geometry are valuable in understanding physical systems in much the same way that idealizations based on Euclidean geometry and its associated symmetries have been used successfully for many decades to describe and understand physical and chemical processes. Such idealizations include planar surfaces, polyhedral crystal forms, spherical particles, etc. In practice, it is extremely difficult to prepare surfaces that closely approach the ideal planar form and such a description breaks down completely at atomic length scales. If the planar approximation is relatively accurate, we may describe deviations from this idealization in terms of "defects". As the concentration of defects increases defect-defect interactions become important and as the surface structure becomes more and more irregular, a fractal description may be found to be more useful.

Many of the most simple and most familiar examples of fractals are generated by systematic hierarchical processes that result in regular structures that do not closely resemble those found in nature. These structures provide exact realizations of the scale symmetries associated with fractal geometry. A variety of simple models (percolation, random walks, diffusion-limited aggregation, etc.) lead to random fractal structures. The structures do not possess an exact scaling symmetry but are self-similar (or self-affine) in a statistical sense only. Both types of fractals are described below.

Self-Similar Fractals

What is probably the most simple example of a self-similar fractal (the Cantor set³) is shown in Figure 1. Starting with a line of length L the middle third is removed to form two lines of length $L/3$ separated by a gap of length $L/3$. In the second stage the middle third of each of the remaining lines is removed leaving 4 lines each of length $L/9$. After n generations the system contains 2^n lines each of length $3^{-n}L$. As $n \rightarrow \infty$ the total number of line segments (2^n) diverges but their total length $(2/3)^n L$ approaches zero. The Cantor set can be extrapolated to infinitely large length scales by placing a pattern of length L a distance L from a similar pattern, etc. In this way we can generate a fractal set covering all length scales from 0 to ∞ . If the Cantor set is dilated by a factor of 3, it can be covered by two replicas of itself and its fractal dimension (D_C) is given by $D_C = \log(2)/\log(3) = 0.6309\dots$. This "definition" of the fractal dimensionality is in accord with our understanding of dimensionality in ordinary Euclidean systems. For example, if a d dimensional Euclidean object (a hypercube, for example) is diluted isotropically by a factor of λ , it can be covered by λ^d replicas of the original (undiluted) hypercube and the fractal dimensionality is given by

$$D_C = \frac{\log(\lambda^d)}{\log(\lambda)} = d \quad (1)$$

In general, there are many different fractal dimensionalities associated with a fractal structure. For example, the Hausdorff-Besicovitch^{3,5} dimension (D_H) can be obtained by determining the number of line segments $N(\delta)$ of length δ (or more generally d dimensional hyperspheres of diameter δ) needed to cover the Cantor set. The determination of the Hausdorff-Besicovitch dimension is based on the quantity $N(\delta)\delta^{D_H}$ in the limit $\delta \rightarrow 0$.

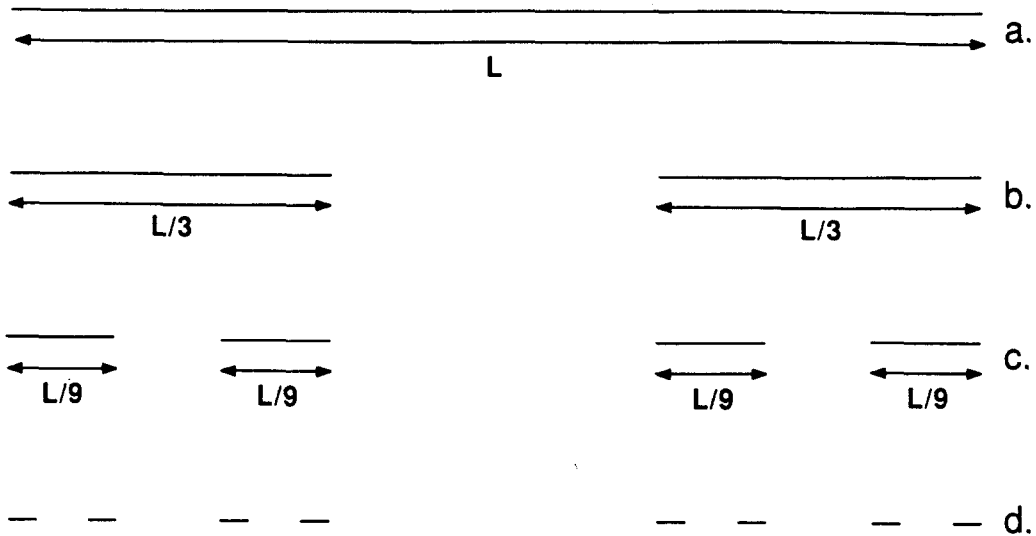


Fig. 1. Three stages in the construction of a Cantor set with a fractal dimensionality of $\log(2)/\log(3)$.

$$M_{D_t} = \lim_{\delta \rightarrow 0} N(\delta) \delta^{D_t} \quad (2)$$

D_H is the critical dimension for which the quantity M_{D_t} diverges if $D_t < D_H$ and approaches zero if $D_t > D_H$. For the triadic Cantor set shown in Figure 1 $D_H = \log(2)/\log(3)$ so that $D_H = D_c$. For simple self-similar fractals all of the approaches used to measure the fractal dimensionality give the same value and we may characterize the fractal by a single, all purpose⁶ fractal dimension D ($D_H = D_c = \dots = D$). The Hausdorff-Besicovitch dimensionality is an important mathematical concept but measurement of the Hausdorff-Besicovitch dimensionality is not a practical general way of determining the all-purpose fractal dimensionality for a self-similar fractal. For the purpose of applications to physics and chemistry, this dimensionality is mainly of historic interest.

A second example^{7,8} of a hierarchical self-similar fractal is shown in Figure 2. In the first stage (Figure 2a) five discs are combined to form a small cross. In the second stage (Figure 2b) five of the patterns shown in Figure 2a are combined to form a larger structure containing 25 discs. Figures 2c and 2d show the next two stages in the construction process in which successively larger and larger structures are assembled. At each stage in the construction process the overall size of the structure is increased by a factor of 3 and the number of discs is increased by a factor of 5. The hierarchical structure can also be extended to infinitesimally small length scales by replacing each of the discs of diameter d_0 in Figure 2a by a small cross consisting of 5 discs with a diameter $d_0/3$, etc. The fractal constructed in this fashion can be covered by five replicas of itself after dilation by a factor of 3 and its fractal dimensionality (D) is $\log(5)/\log(3)$ ($\approx 1.4649\dots$). A finite structure such as that shown in Figure 2d is not rigorously self similar. Instead, it exhibits an approximate self-similarity over a limited range of length scales (approximately d_0 to $81 d_0$ in this case). Structures such as those shown in Figure 2 that are generated during the construction of an asymptotic fractal are often called pre-fractals.³ It is often useful to think of the fractal dimensionality of fractal objects as the exponent that describes the scaling relationship between mass (or measure, μ) (M) and length (L)

$$M \sim L^D \quad (3)$$

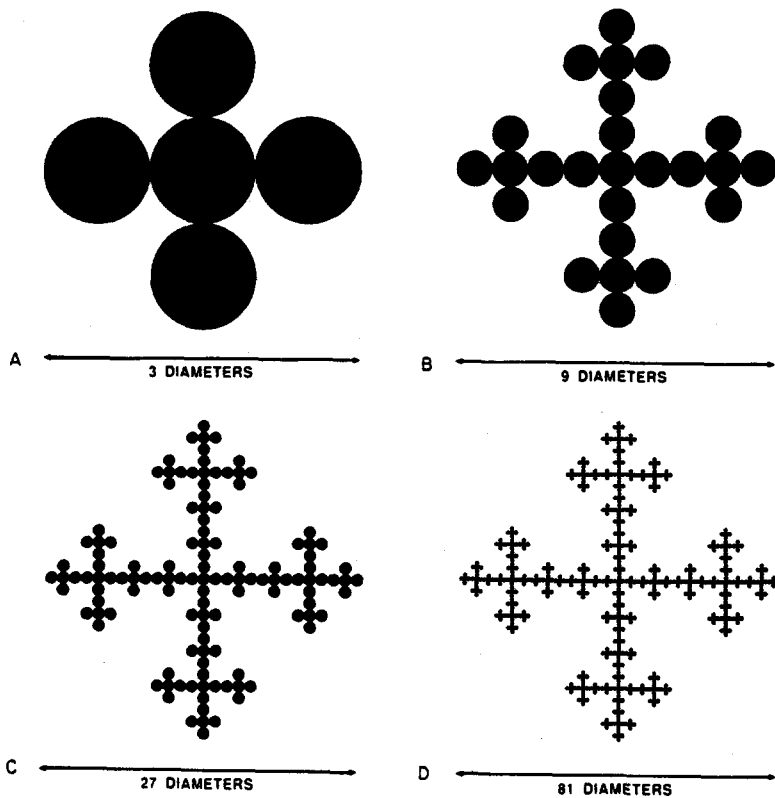


Fig. 2. Four stages in the construction of self-similar fractals with a dimensionality (D) of $\log(5)/\log(3)$.

Ordinary Euclidean objects obey a similar relationship where the exponent D in equation (3) is the Euclidean dimensionality (d) of the object. Structures that can be described by equation (3) are often referred to as mass fractals. Many of the unique physical (and chemical) properties of fractals can be understood in terms of equation (3) and it provides the basis for many practical ways of measuring the fractal dimensionality.

Fractal structures exist in a Euclidean space (the embedding space) with a dimensionality d. The most important examples are $d = 2$ (surfaces and interfaces) and $d = 3$ (ordinary three dimensional space). The volume of the embedding space "occupied" by the fractal is given by

$$V \sim L^d \quad (4)$$

so that the mean density $\rho(L)$ is given by

$$\rho(L) \sim L^{(D-d)} \sim M^{(D-d)/D}. \quad (5)$$

One of the most important characteristics of self-similar fractals is that their density measured in the Euclidean embedding space becomes smaller and smaller as they grow larger and larger or are examined on successively larger and larger length scales.

In real physical systems the fractal scaling does not extend over an infinite range of length scales and the mean density ρ is related to the range of length scales λ over which fractal scaling is found by

$$\rho(\lambda) \sim \lambda^{(D-d)}. \quad (6)$$

Here $\lambda = L_2/L_1$ where L_2 and L_1 are the long and short cut-off lengths respectively for the fractal scaling regime.

Most fractals of importance in physics and chemistry differ from the examples shown in Figures 1 and 2. They are not exactly self similar; instead they are random structures that exhibit self similarity only in a statistical sense. Such random structures can be described by their density-density correlation functions $C^n(r_1, r_2 \dots r_n)$. Here $C^n(r_1, r_2 \dots r_n)$ is given by

$$C^n(r_1, r_2 \dots r_n) = \langle \rho(r_0)\rho(r_0+r_1) \dots \rho(r_0+r_n) \rangle \quad (7)$$

averaged over all possible origins (r_0). In many cases the correlation function is also averaged over all orientations and over an ensemble of realizations. In equation (7) $\rho(r)$ is the density at position r . For a statistically self-similar fractal the correlation functions have a homogeneous power law form

$$C^n(\lambda r_1, \lambda r_2 \dots \lambda r_n) = \lambda^{-n\alpha} C^n(r_1, r_2 \dots r_n). \quad (8)$$

The exponent α_n in equation (8) is given by $\alpha_n = d - D_n$. For statistically self-similar fractals the dimensionalities D_n are all equal and are equal to the all-purpose fractal dimensionality. In real systems equation (8) is obeyed over only a limited range of length scales ($L_1 \leq r \leq L_2$). For example in the case of a polymer molecule the range of length scales over which fractal scaling is observed ranges (at most) from the size of a monomer to the overall size (spatial extent) of the molecule. For relatively stiff polymer molecules the range of length scales over which geometric scaling is observed ranges from the persistence length to the overall size of the molecule and this range may be much smaller.

Figure 3 shows two (finite) percolation clusters⁹⁻¹⁴ generated on a square lattice. Percolation is an important model for a wide variety of phenomena. A percolation cluster can be constructed by randomly selecting unoccupied sites on a lattice of size (spatial extent) L and occupying them until a fraction p have been filled. If the clusters are identified as sites connected by nearest neighbor occupancy, then for small values of p the system will contain mainly isolated sites with a small number of larger clusters ("lattice animals") whose populations decrease rapidly (almost exponentially) with their size. As the occupation probability is increased, the number of large clusters grow until one of the clusters extends across the entire lattice. For $L \rightarrow \infty$ this happens when p reaches a critical value of p_c called the site percolation probability. At $p = p_c$ this spanning cluster occupies only a negligible fraction of the occupied sites. All of the other occupied sites belong to smaller non-spanning clusters that have a characteristic power law distribution.^{13,14}

$$N_s \sim s^{-\tau} \quad (9)$$

where N_s is the number of clusters containing s sites.

The clusters shown in Figure 3 were not obtained by randomly selecting a fraction p_c of the sites on a very large square lattice. Instead, they were grown using the algorithm of Leath¹⁵ and Alexandrowicz¹⁶ in which the sites on the perimeter of a growing cluster are randomly occupied with probability p_c or permanently blocked with probability $(1-p_c)$.

The behavior of a percolating system near the percolation threshold can be characterized in terms of a variety of critical exponents ($p = p_c$ is a critical point). For example, the probability $P(p)$ that a site on the lattice will belong to the infinite spanning cluster is given by

$$P(p) \sim (p-p_c)^\beta \quad (p>p_c). \quad (10)$$

Near to the percolation threshold the system can also be characterized by a correlation length ξ . For $p>p_c$ ξ corresponds to the distance at which the power law density correlations that characterize the fractal geometry of the infinite cluster on short length scales cross over to a constant value on long length scales. The length ξ is related to the occupation probability p by

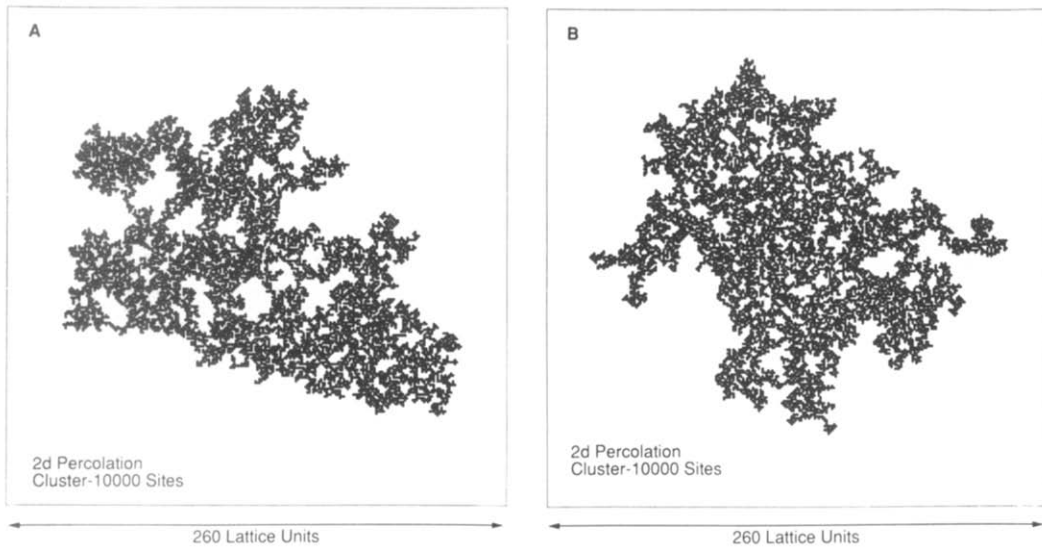


Fig. 3. Two percolation clusters grown on a square lattice using the Leath-Alexandrowicz^{15,16} algorithm. A site percolation threshold probability of 0.592746²⁰ was used to generate these small clusters.

$$\xi \sim (p - p_c)^{-\nu}. \quad (11)$$

It follows from this that the mean density of the infinite cluster is given by

$$P(p) \sim \xi^{(D-d)} \quad (12)$$

so that $\beta = \nu(d-D)$ and

$$D = d - \beta/\nu. \quad (13)$$

The exponents β and ν are believed to be known exactly for $d = 2$ ($\nu = 4/3$, $\beta = 5/36$)¹⁷⁻¹⁹ so that $D = 91/48 \approx 1.8958\dots$. The fractal dimensionality D and the exponents β and ν are universal quantities that depend on the dimensionality of the embedding space or lattice (d) but do not depend on the lattice structure or the rules used to determine how the occupied sites are joined to form clusters. The percolation threshold probability, on the other hand, is not a universal quantity (its value is sensitive to model details). For the case of site percolation on a square lattice the value of p_c (0.5927460 ± 0.0000005) is known very accurately from computer simulations.²⁰ The value of p_c is 0.311605 ± 0.000010 for site percolation on a cubic lattice.²⁰ If instead of filling sites on a square lattice the bonds connecting nearest neighbor nodes are randomly "filled", a continuous network is formed when a fraction $p_c = 1/2$ of the possible bonds has been established. This model is referred to as bond percolation on a square lattice. The fractal dimensionality for clusters generated by this model is also $91/48$.

Characterization of Self-Similar Fractals

There are many ways of measuring the all-purpose fractal dimensionality (D) of self-similar fractals. For structures that have been constructed using a systematic hierarchical procedure (such as those shown in Figure 1 and 2) D is known exactly. For random fractals (such as the percolation clusters shown in Figure 3) generated using simple algorithms we often have an exact (but frequently non-rigorous) value for the fractal dimensionality. However, in other cases (such as diffusion-limited aggregation or DLA²¹) there are no exact theoretical results

despite the fact that the models are often very simple and may have been the subject of intense theoretical investigation. In these cases we must resort to the numerical analysis of computer generated structures. In experimental systems the basic data are often available in the form of digitized micrographs of the structures. These images may be analyzed in the same way as the results of computer simulations.

We are frequently concerned with structures that grow in mass with increasing time or that contain many realizations of the same process with different characteristic sizes. In these cases we can employ equation (3) directly to measure the fractal dimensionality. One of the most frequently used methods is to measure the dependence of the radius of gyration, R_g , on the size (mass) s of the growing objects. The fractal dimensionality $D\beta$ is then obtained from the power law relationship between R_g and s

$$\langle R_g \rangle \sim s^\beta. \quad (14)$$

The corresponding fractal dimensionality is given by $D\beta = 1/\beta$. The symbol $\langle \rangle$ in equation (14) is used to indicate averaging over a large number of samples. In most of our equations this symbol is omitted unless we wish to emphasize the need to average over a large number of realizations. However, it should be noted that in most cases extensive averaging is required to reduce statistical uncertainties to reasonably small levels.

According to equation (14) a plot of $\ln(R_g)$ against $\ln(s)$ for a fractal structure should give a straight line with a slope of β or $1/D\beta$. This method can be used to measure the fractal dimensionality but it is an approach that can easily be misused. A much better way of displaying the results of an experiment or simulation is to plot $\ln(s^{-1/D} R_g)$ vs $\ln(s)$. Here β^* is an estimate or a theoretical value for the exponent β or $1/D\beta$. Figure 4 shows the results of doing this for the two percolation clusters using the theoretical value for β^* (48/91). For both clusters quite large fluctuations about the "expected" behavior can be seen and the dependence of R_g on s is quite different for the two clusters. These fluctuations and differences are an important characteristic of statistically self-similar fractals which have important implications for their properties. These fluctuations are related to the lacunarity³ of the fractals and can be used to obtain a more complete characterization of their geometries. If the dependence of R_g on s is averaged over a large number of samples, the fluctuations in Figure 4 will be removed and a smooth curve will be seen.

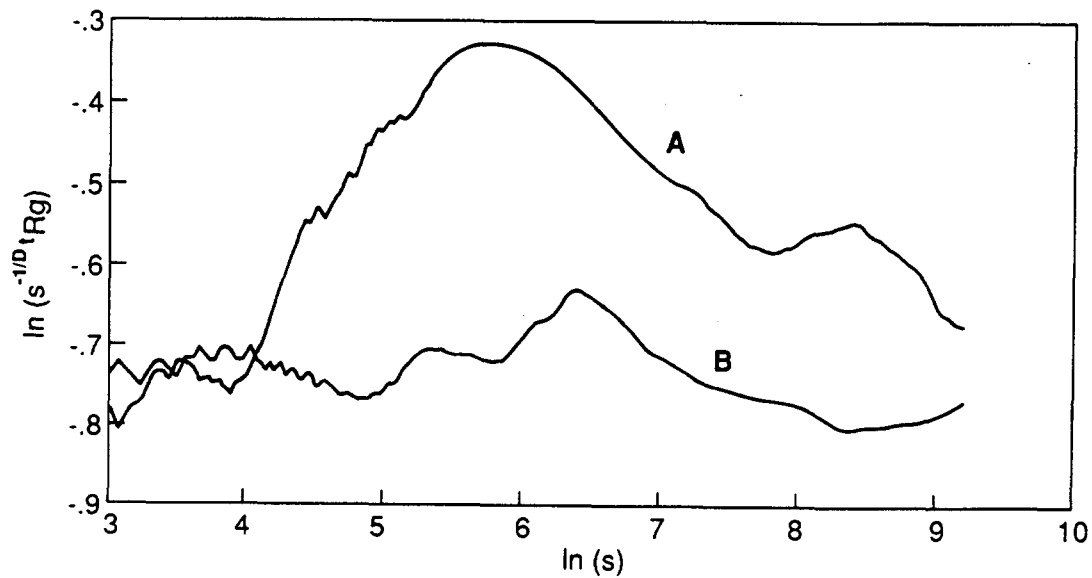


Fig. 4. Dependence of $\ln(s^{-1/D} R_g)$ on $\ln(s)$ obtained from the two clusters shown in Figure 3. Here D is the theoretical fractal dimensionality of 91/48.

After the fluctuations have been removed by averaging, another problem may be revealed. The averaged curve corresponding to those shown in Figure 4 may not be a horizontal straight line. This is a consequence of "corrections" to the asymptotic scaling relationship between R_g and s . In general, the power law relationships that described the structures of random fractals are accurate only in the asymptotic (large length scale) limit (i.e., $L_2/L_1 \rightarrow \infty$). In this event equation (14) should be replaced by

$$\langle R_g \rangle \sim s^\beta \quad (s \rightarrow \infty). \quad (15)$$

In many cases the corrections to the asymptotic power law form also have a power law form and the dependence of R_g on s may be written as

$$R_g \sim s^\beta (1 + As^{-\gamma} + Bs^{-\delta}). \quad (16)$$

In other cases more serious (logarithmic) corrections may be found and the dependence of R_g on s may be represented more accurately by

$$R_g \sim s^\beta (\log(s))^\gamma. \quad (17)$$

Such logarithmic corrections are often found for systems at their critical dimensionality (d_c).

In most cases a detailed theoretical understanding is needed to obtain the proper form for the corrections to scaling. However, in some favorable cases the leading corrections can be obtained from accurate experiments or large scale simulations. In a few simple cases (such as a random walk on a simple lattice) there are no corrections to the asymptotic scaling behavior.

If sufficient data are evaluated to reduce the statistical uncertainties, it is useful to explore the dependence of D_{eff} (the effective fractal dimensionality obtained from the dependence of R_g on s over a limited range of sizes or length scales) on s to obtain an estimate of the magnitude of the corrections to scaling. In favorable cases, it may be possible to fit the dependence of R_g on s by a two term power law

$$R_g \sim s^\beta (1 + As^{-\gamma}). \quad (18)$$

Uncertainties due to corrections to scaling can be reduced by extending the simulation or experiments to a larger range of length scales or by reducing statistical uncertainties by using a large number of samples and carrying out a systematic series analysis²²⁻²⁴ based on equation (18) or a more general form for the corrections to scaling (equation (16) for example).

A particularly revealing way of presenting the dependence of R_g on s is to display the dependence of the effective value of $\beta(s)$ on $\log(s)$. The effective exponent $\beta(s)$ is defined as

$$\beta(s) = \frac{d\ln(R_g(s))}{d\ln(s)} \quad (19)$$

and is measured by least square fitting a straight line to the coordinates $(\ln(s'), \ln(R_g(s')))$ over a small range of cluster sizes ($s_1 < s' < s_2$ where $s = (s_1 s_2)^{1/2}$). A large amount of data is required to reduce the statistical uncertainties to low enough levels to use this method. The reward is that it is possible to assess if $\beta(s)$ has approached sufficiently close to its asymptotic ($s \rightarrow \infty$) value or is still changing as the system size, s , is increasing.

For structures that have grown from a particular position (seed or nucleation site) it is often convenient to measure the mass, $M(\ell)$ contained within a distance, ℓ , measured from that position. For a self-similar fractal find that

$$M(\ell) \sim \ell^\gamma \quad (20)$$

and the fractal dimensionality D_γ is equal to γ . Again, equation (20) is expected to be a precise description of the dependence of M on ℓ only in the asymptotic limit $\ell \rightarrow \infty$ for a large ensemble of samples. For structures generated by computer simulations, the dependence of $M(\ell)$ on ℓ must be measured over the broadest possible range of length scales using many realizations of the model. Corrections to equation (20) similar in form to those given in equations (16) and (17) can then be explored systematically in order to obtain a more reliable estimate of the asymptotic value for γ or to assess if a reliable value can be obtained. Results obtained from experiments should be subject to a similar analysis. In this case there are additional uncertainties since a change in the effective value of γ with increasing ℓ may be a consequence of changes in the physical and chemical behavior as well as corrections to scaling resulting from the finite system size. The mean density $\rho(\ell)$ for distances in the range ℓ to $\ell + \delta\ell$ from the seed or nucleation site, could also be measured as a function of ℓ leading to the power law

$$\rho(\ell) \sim \ell^{-\delta} \quad (21)$$

and the corresponding fractal dimensionality $D_\delta = d - \delta$ where d is the Euclidean dimensionality of the embedding space.

The correlation functions $C^n(r_1, r_2, \dots, r_n)$ (equation (7)); particularly the two point density-density correlation function $C(r)$ given by

$$C(r) = \langle\langle \rho(r_0) \rho(r_0 + r) \rangle\rangle_{|r| = r} \quad (22)$$

are often used to measure the fractal dimensionality of structures generated by experiments and computer simulations. Here the symbol $\langle\langle \dots \rangle\rangle$ is used to indicate averaging over all orientations as well as over all origins (r_0). For a fractal structure $C(r)$ has the homogeneous form

$$C(r) \sim r^{-\alpha} \quad (23)$$

where the exponent α is given by $\alpha = d - D_\alpha$ (The quantity $d - D$ is often referred to as the "codimensionality"). In practice, equation (23) is obeyed over only a limited range of length scales between an inner and outer cut-off length (in the case of a colloidal aggregate, for example, these cut-off lengths would correspond approximately to the size of the particles and the overall size of the aggregate providing that processes such as collapse under gravity and thermal fluctuations²⁵ did not further limit the range of length scales over which fractal scaling could be observed. Equation (22) can also be written as

$$C(r) = \langle \rho(r) \rangle \quad (24)$$

where the averaging is over all possible origins in the sample that are occupied ($\rho(r_0) \neq 0$) by the sample. For a sufficiently "large" sample, this averaging may be sufficient to obtain a reliable estimate of the fractal dimensionality (i.e., we may average over a large number of regions in a large sample instead of over a large number of relatively small samples). For an image consisting of pixels that are either "on" or "off" ($\rho = 1$ or 0), $C(r)$ is the "on" pixel density at a distance r from an occupied "origin" pixel in the image averaged over all "on" pixels (origins) in the entire structure. If this quantity is calculated in a "brute force" fashion, the distances between all pairs of "on" pixels must be obtained. In practice, the effort can be reduced by selecting a number of pixels at random and averaging the density of "on" pixels, $\rho(r)$, at a distance r from these randomly selected (occupied or "on") pixels and obtaining $C(r)$ from equation (24). Care must be taken in calculating the density

$\rho(r)$. If $\rho(r)$ is obtained by dividing the number of occupied pixels, $N(r)\delta r$ with centers at distances in the range $r-\delta r/2$ to $r+\delta r/2$ from the center of the origin pixel by the volume in an annulus with inner and outer radii of $r-\delta r/2$ and $r+\delta r/2$, unwanted "oscillations" will be seen in the correlation function. Instead, $N(r)\delta r$ must be divided by $N_0(r)\delta r$ (the total number of pixels with centers in the range $r-\delta r/2$ to $r+\delta r/2$ from the center of a reference pixel). Alternatively, Fourier transformation methods can be used. The digitized image is Fourier transformed. The magnitude of the transformation is then obtained and an inverse transformation is carried out. The resulting pattern is then radially averaged to obtain the two point correlation function.²⁶ Because of the efficiency of fast Fourier transformation, this can be a very effective procedure (particularly if D is relatively large and there is a large number of "on" pixels). This method has been used to calculate the density-density correlation function for random dendrites in NbGe₂ thin films.²⁷

For structures of finite size the two point density-density correlation function will depend on the overall size of the structure described by a characteristic length R as well as the internal length r . In this case the correlation function can be written as $C(r,R)$. The function $C(r,R)$ represents the density-density correlation function averaged over a large number of structures of the same size or characteristic length R . If large clusters are (on average) related to small clusters by a change of length scale, it is natural to assume that $C(r,R)$ is a homogeneous function of its arguments so that

$$C(\lambda r, \lambda R) = \lambda^{-\alpha} C(r, R). \quad (25)$$

Taking a value of $1/R$ for λ we have

$$C(r/R, 1) = R^\alpha C(r, R) \quad (26)$$

or

$$C(r, R) = R^{-\alpha} f(r/R). \quad (27)$$

According to this scaling assumption the density-density correlation function for systems of different sizes (R) can be expressed in terms of the scaling form given in equation (27). The function $f(x)$ is called the scaling function and the exponent α is a scaling exponent. If equation (27) provides a valid description of the geometric scaling properties, then plots of $R^\alpha C(r, R)$ vs r/R for structures of different sizes will fall on a common curve (the scaling function $f(x)$). This is illustrated for clusters generated using a three dimensional off-lattice model for diffusion limited cluster-cluster aggregation in Figure 5. This is a simple but quite realistic model for the fast, irreversible aggregation of small particles to form large aggregates or flocs²⁸⁻³¹ that have a fractal dimensionality of about 1.80. Figure 5a shows the two point density-density correlation functions for clusters of five different sizes (100, 300, 1000, 3000 and 10,000 particles). In this case it is more convenient to select clusters of a particular size (number of particles, s) rather than a particular value (or small range of values) of the characteristic length R . Since s and R are related by $\langle R \rangle \sim s^{1/D}$ for fractal objects equation (27) can be written as

$$C(r, s) = s^{-\alpha/D} f(r/s^{1/D}) \quad (28a)$$

or

$$C(r) = s^{(D-d)/D} f(r/s^{1/D}). \quad (28b)$$

In Figure 5 plots of $\ln[s^{(d-D)/D} C(r)]$ vs $\ln(s^{-1/D} r)$ are shown for the five different cluster sizes. The fact that these curves overlap almost perfectly confirms the simple scaling assumption. This shows that both the internal density correlations and the global scaling properties of the cluster (such as the dependence of the radius of gyration on its mass) can be described in terms of the same fractal dimensionality. The scaling collapse shown in Figure 5b provides a more convincing demonstration of the self-similar geometry of these simulated aggregates and a more reliable way of estimating D than attempting to find the slope $d(\log(C(r)))/d(\log(r))$ over an intermediate range of length scales. (In practice the range of length scales over which $\log(C(r))$ is linearly related

to $\log(r)$ may be quite small.)

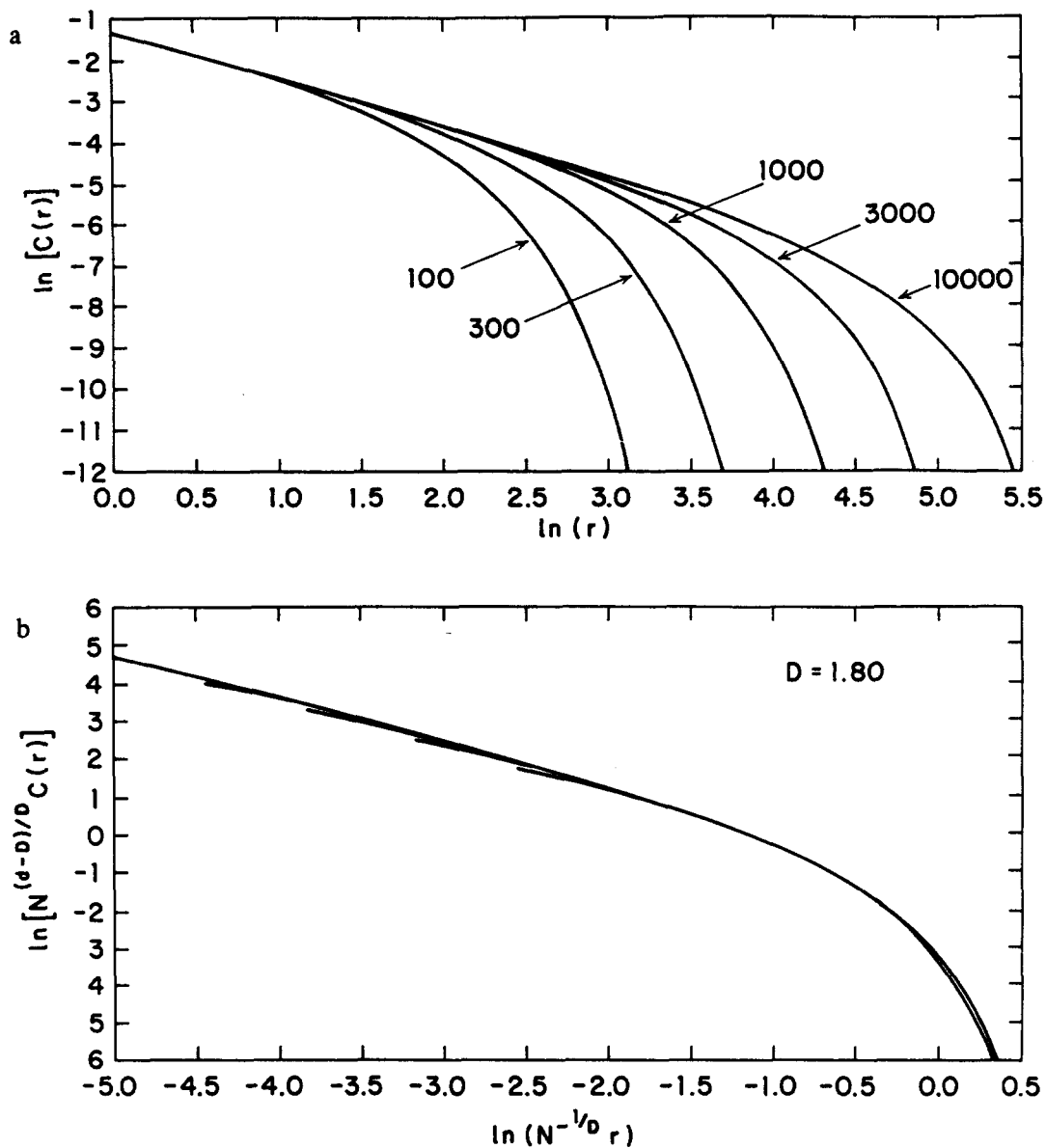


Fig. 5. Scaling of the two point density-density correlation functions for fractal aggregates of different sizes (N or s). Figure 5a shows the correlation functions obtained from 10^4 100 particle clusters, 10^3 300 particle clusters, 10^2 1000 particle clusters, 39 3000 particle clusters and 13 10,000 particle clusters generated using a three-dimensional off-lattice cluster-cluster aggregation model. Figure 5b shows how these correlation functions can be scaled onto a single curve, using the scaling form given in equation (28b).

Most determinations of the fractal dimensionalities in real microscopic systems are based on light, x-ray or neutron scattering experiments.³²⁻⁴⁷ The scattering structure factor $S(k)$ is determined by the two point density-density correlation function $C(r)$ and has the power law form

$$S(k) \sim k^{-D}. \quad (29)$$

Here k is the wave vector ($k = 4\pi \sin(\Theta/2)/\lambda$) where λ is the wavelength and Θ is the scattering angle. It follows from this that the scattered intensity $I(k)$ at wave vector k is given by

$$I(k) \sim k^{-D}. \quad (30)$$

In principle, D can be determined from the dependence of the scattered intensity on k . In practice, $I(k)$ exhibits the power law form given in equation (30) over only a limited range of wave vectors. The interpretation of small angle scattering experiments can be quite difficult and care must be taken to include appropriate corrections for finite size effects, short range correlations and instrumental effects.^{32,43} Care must also be taken to distinguish between the effects of a fractal internal structure and a power law size distribution.⁴⁵⁻⁴⁷

Figure 6 shows some scattering results obtained from both light scattering and small angle x-ray scattering experiments on colloidal silica (Ludox®) aggregates. This figure shows a power law dependence of the scattering intensity on the wave vector over more than two orders of magnitude in k (or length scale). However, it should be noted that the intensity scale for the x-ray scattering measurement has been shifted arbitrarily with respect to the intensity scale of the light scattering experiments to give an overall linear behavior in the log-log plot shown in Figure 6. The slope of -2.1 corresponds to a fractal dimensionality of 2.1. The slope of -4.0 at large k values (small length scales) arises from Porod⁴⁸ scattering from the relatively smooth surfaces of the individual particles. These experiments were carried out under slow aggregation conditions⁴⁹ and the fractal dimensionality of 2.1 agrees well with that obtained from simple models for reaction-limited (slow) cluster-cluster aggregation.⁵⁰⁻⁵⁴ However, the aggregation of colloidal silica is a complex chemical process and this agreement may be, to some extent, fortuitous. Other systems more nearly satisfy the conditions implicitly assumed in the reaction-limited cluster-cluster aggregation model and provide more complete realizations of this scenario.⁴²

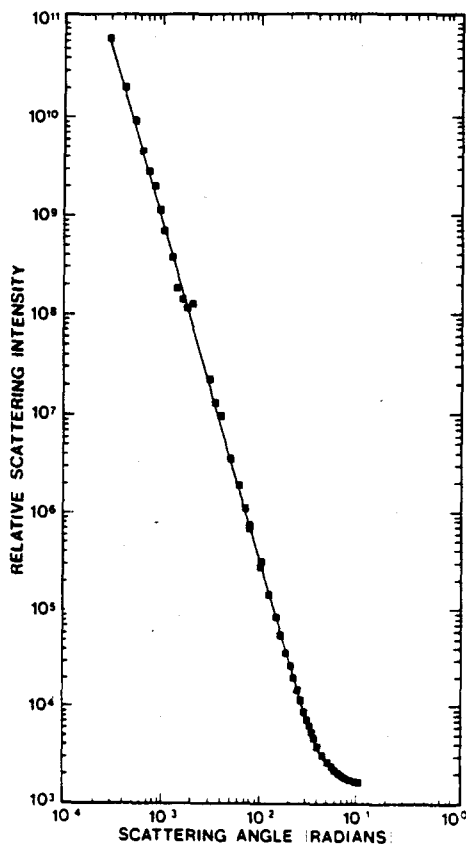


Fig. 6. Light scattering and small angle x-ray scattering data obtained from colloidal silica aggregates formed under slow aggregation conditions. Here results have been combined from both methods to illustrate fractal scaling over at least two decades of length scales. These results are taken from ref. 38 (Schaefer, Martin, Wiltzius and Cannell, *Phys. Rev. Lett.* 52, 2371 (1984)).

Many systems of importance in solid state physics and chemistry have an internal structure that is uniform on all but quite small length scales but are bounded by an irregular surface that (over some range of length scales) can be described as a self-similar fractal. Such structures are called surface fractals to distinguish them from structures such as those shown in Figures 2 and 3 in which the mass and surface exhibit the same fractal scaling behavior. For surface fractals the scattering intensity is given by

$$I(k) \sim k^{D_s - 6} \quad (31)$$

where D_s is the fractal dimensionality of the surface. For the case of a smooth surface ($D_s = 2$) equation (31) gives the classical Porod⁴⁸ scattering law.⁴⁸ Figure 7 shows the small angle x-ray scattering obtained from Beulah lignite coal.^{55,56} The dependence of $\log(I(k))$ on k is linear over approximately two decades in k (two decades in length scale). Bale et al.^{55,56} interpret this in terms of scattering from fractal pore surfaces in the coal. The slope of -3.48 ± 0.005 in Figure 7 corresponds to a fractal dimensionality of $D_s = 2.52 \pm 0.05$. Similar power law scattering was found for other coals. A variety of other examples of small angle x-ray scattering by mass and surface fractals can be found in Reference 34. Since the exponent describing the dependence of $I(k)$ on k lies in the range 0-3 for mass fractals and 3-4 for surface fractals, these two cases can easily be distinguished.

Another method commonly used to measure the fractal dimensionality of digitized images or computer generated objects is called box counting. The object is covered by a series of grids with grid elements of size ϵ and the number of occupied grid elements (boxes), $N(\epsilon)$, is counted. The procedure is repeated for a range of grid or box sizes ϵ . For a self-similar fractal the dependence of $N(\epsilon)$ on ϵ is given by

$$N(\epsilon) \sim \epsilon^{-D_\epsilon} \quad (32)$$

and an estimate of the fractal dimensionality can be obtained plotting $\log(N(\epsilon))$ against $\ln(\epsilon)$. The slope of this curve is $-D_\epsilon$ from which an effective value for D_ϵ can be obtained for the range of length scales measured. In

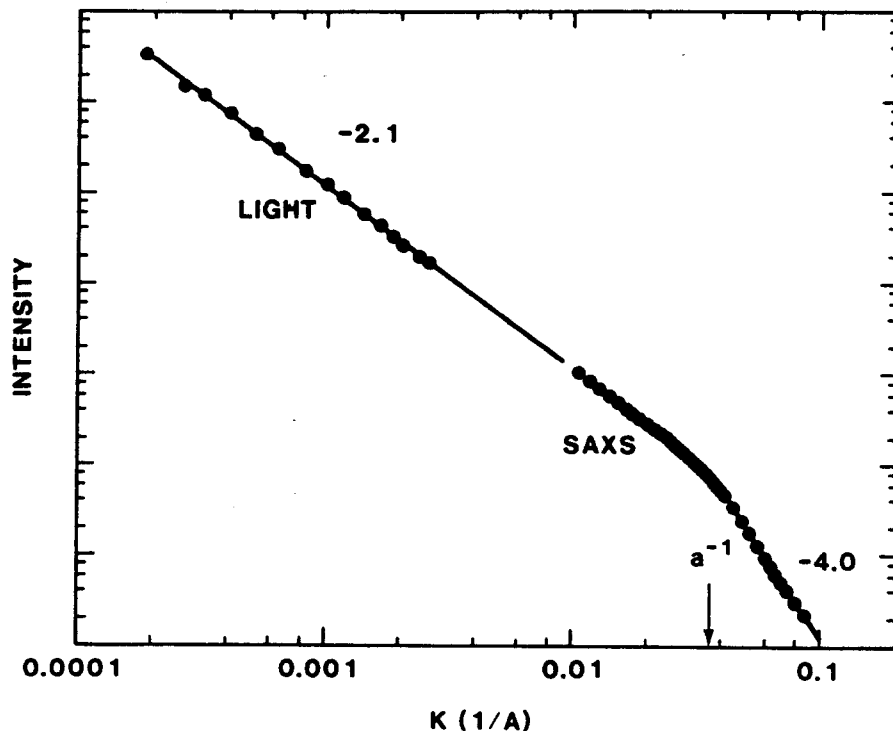


Fig. 7. Small angle x-ray scattering from Beulah lignite coal. These data were taken from reference 55 (Bale, Carlson, Kalliat and Schmidt, in *The Chemistry of Low Rank Coal*, H. H. Schobé, ed., ACS Symposium Series No. 264, American Chemical Society, Washington, D. C., 1984, p. 79. Here q is equivalent to wave vector k .

practice, this method is subject to substantial corrections that must be carefully taken into account to obtain reliable results.

In some cases a generalization⁵¹ of the "box counting" method (equation (4)) has been used to characterize fractals generated by either experiments or computer simulations. The fractal is covered by grids of size ϵ and the fraction of the mass $P_i(\epsilon)$ contained in each of the grid elements is measured. The partition function Z_q is defined by

$$Z_q(\epsilon) = \sum_i (P_i(\epsilon))^q \quad (33)$$

is measured for some particular q and the fractal dimensionality D_q is given by

$$D_q = \frac{1}{q-1} \left[\frac{d \log Z_q(\epsilon)}{d \log(\epsilon)} \right] \quad (34)$$

over a suitable range of length scales (ϵ). If the same value is obtained for the fractal dimensionality D_q for different values of q , then this is taken as evidence of self-similarity.⁵²⁻⁵⁴

In theoretical work the quantitative D_q are frequently defined as

$$D_q = \left(\frac{1}{q-1} \right) \lim_{\epsilon \rightarrow 0} [\log Z_q(\epsilon) / \log(\epsilon)] \quad (35)$$

However, for real structures the limit $\epsilon \rightarrow 0$ (or $L/\epsilon \rightarrow \infty$ where L is the system size or upper cut-off length) cannot be attained so we resort to equation (34) instead of equation (35).

Systems in which the quantities D_q are q dependent have been called geometric multifractals (the concept of multifractality is discussed briefly below and literature references provided for a more detailed study) by Tel and Vicsek.⁵⁵⁻⁵⁷ Mass multifractality and the role played by finite resolution (a finite range of length scales) in the measurement of D_q for real systems⁵⁸ is still a controversial subject that involves subtleties⁵⁹ that are beyond the scope of this review.

Fractal geometry can frequently be used to obtain a more simple and intuitive understanding of physical phenomena than that obtained from alternative approaches. The applications of self-similar fractal geometry can be facilitated by a few simple rules or ideas, some of which are given below.

1. Two fractals with dimensionalities D_1 and D_2 can be placed together in the same region of space without contacting each other (except by "accident") if $D_1 + D_2 < d$ where d is the dimensionality of the embedding space or lattice. For example, two random walks ($D_1 = 2, D_2 = 2$) will not intersect in a space of dimensionality $d > 4$. For this reason $d = 4$ is the critical dimensionality for self-avoiding walks. For $d > d_c = 4$ the fractal dimensionality of both random walks and self-avoiding random walks is 2. If the fractals are following trajectories with a fractal dimensionality D_t , then they will be mutually transparent (will not contact except by accident) if $d > D_1 + D_2 + D_t$. For this reason fractals with $D < 2$ are asymptotically transparent in three dimensional space (they are not intersected by photons or electrons ($D = 0$) following linear or ballistic ($D_t = 1$) paths). If $D > 2$ they will be asymptotically opaque.
2. The projection of a D dimensional fractal of mass M or characteristic size R onto a d dimensional space will have a fractal dimension of D if $D < d$. In this event the "area" (measure) of the projection will be proportional to the mass (measure) of the fractal. If $D > d$, the projection will compactly cover the space onto which it is projected and the "area" of projection will be proportional to $M^{d/D}$ (or R^d).
3. A d_1 dimensional "cross section" of a D dimensional fractal in a d_2 dimensional space will have a fractal dimension of $D + d_1 - d_2$.
4. The intersection of two fractals with dimensionalities D_1 and D_2 in a d dimensional space is a fractal with a dimensionality of $D_1 + D_2 - d$ (rule 1 follows from this).

5. The union of two fractals with dimensionalities D_1 and D_2 is $\max(D_1, D_2)$.
6. The product of two fractals with dimensionalities D_1 and D_2 has a dimensionality of $D_1 + D_2$. For example, the region swept out by a D_1 dimensional fractal following a trajectory with dimensionality D_2 is a fractal with a dimensionality of $D_1 + D_2$.
7. The distribution of unoccupied "holes" in a random fractal can be expressed in terms of a power law distribution ($N_L \sim L^{-\theta}$) where L is the characteristic length associated with the holes and $N_L \delta L$ is number of holes with lengths in the range L to $L + \delta L$. The exponent θ is equal to $D + 1$. If the size of the holes is expressed in terms of their volume (number of occupied sites, s , in a lattice model) then $N_s \sim s^{-\tau}$ and the exponent τ is given by $\tau = (d+D)/d$.

These rules are exact only in the limit $L/\epsilon \rightarrow \infty$ so that there may be important "finite size" corrections in real systems.

Self-Affine Fractals

An example of a self-affine fractal^{3,66} is shown in Figure 8. This fractal is constructed in much the same way as the Cantor set shown in Figure 1. This fractal can be rescaled by a self-affine transformation in which the length scale is changed by a factor of 5 in the x direction and a factor of 3 in the y direction. This prefractal can be extended to infinitesimally small length scales by continuing the systematic decimation process shown in Figures 8a, 8b, 8c and 8d. The fractal can also be extended to infinitely long length scales by assembling six patterns to form a larger structure, etc. If we attempt to measure the fractal dimensionality of the patterns shown in Figure 8 using the methods described above, confusing results will be obtained. For example, we could argue that each time the mass of the fractal is increased by a factor of 6 its volume in the embedding space is increased by a factor of 15 so that its density, ρ , decreases by a factor of 6/15. Consequently, from equation (5) we would conclude that $(D-d)/D = \log(6/15)/\log(6)$ or $D = 1.32328\dots$. Alternatively, the box counting method (equation (32)) could be used. In the limit $\epsilon \rightarrow \infty$ the system would look like a Cantor set with a dimensionality of $\log(3)/\log(5)$ or $D = 0.68260\dots$. In the limit $\epsilon \rightarrow 0$ the structure appears to be the product of a line and a Cantor set with a dimensionality of $1 + \log(3)/\log(5)$ or $1.68260\dots$. The structure generated by the process shown in Figure 8 could also be considered to be the product of two Cantor sets with dimensionalities $D_1 = \log(2)/\log(3)$ and $D_2 = \log(3)/\log(5)$ and according to rule 6 (see above) its fractal dimensionality is $D_2 + D_1$ or $1.31189\dots$. Another approach might be to attempt to measure the fractal dimensionality D_β from the dependence of $\log(R_g)$ on $\log(s)$. The radius of gyration will be dominated by the longest distances and in the limit $s \rightarrow 0$ $R_g \sim s^{v_{||}}$ where $v_{||} = \log(5)/\log(6)$ so that a value of $\log(6)/\log(5)$ or $1.11328\dots$ would be obtained. The failure of the methods that work so well for self-similar fractals to give consistent results in this case is a consequence of the fact that we have not correctly identified the fractal in Figure 8 as a self-affine fractal. In general, much more care is required to characterize self-affine fractals. For regular hierarchical fractals such as that shown in Figure 8 this is not a problem since the transformation that rescales the fractal pattern is known. However, for random fractals generated by natural processes it is more difficult to measure their geometric scaling properties.

A second example of a regular, hierarchical self-affine fractal is shown in Figure 9. Here we start by forming a small cross with a length of $5 d_0$ and a width of $3 d_0$ from discs with a diameter of d_0 (Figure 9a). In the next stage seven of these crosses are used to form a larger pattern with a length of $25 d_0$ and a width of $9 d_0$. In the n th stage the pattern contains 7^n discs and has a length (L) of 5^n and a width (w) of 3^n (Figures 9c and 9d). Consequently, the length and width of the pattern are related to its size (s) (number of discs) by

$$L \sim s^{v_{||}} \quad (36a)$$

$$w \sim s^{v_{\perp}} \quad (36b)$$

where $v_{||} = \log(5)/\log(7)$ and $v_{\perp} = \log(3)/\log(7)$.

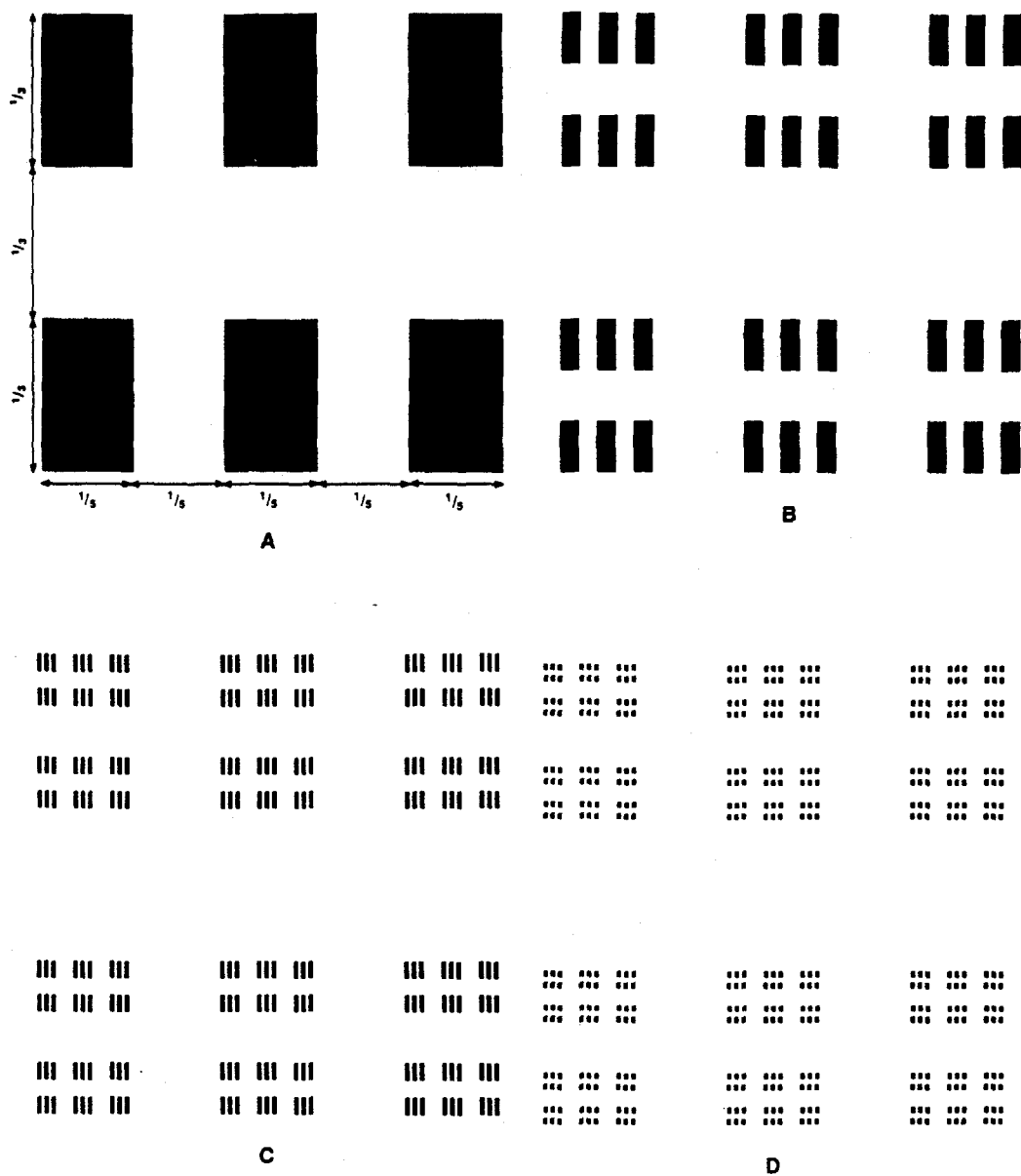


Fig. 8. Four stages in the construction of a self-affine fractal. The structure is not fully resolved in the fourth stage prefractal shown in Figure 8d.

Many measurements lead to results that can be represented as a single valued function of one or more variables. For example, this function might be the height ($h(x,y)$) of a surface at different positions (x,y) projected onto an underlying plane or it might be the porosity (or conductivity or other quantity) as a function of depth measured in an oil well or it might be the volume of water flowing in a river as a function of time. In these and many other examples the function $f(x)$ can be described in terms of self-affine fractal geometry. A simple deterministic self-affine fractal of this type is shown in Figure 10. The generator (Figure 10a) consists of four line segments of equal length. If each of these segments is replaced by the generator, the prefractal shown in

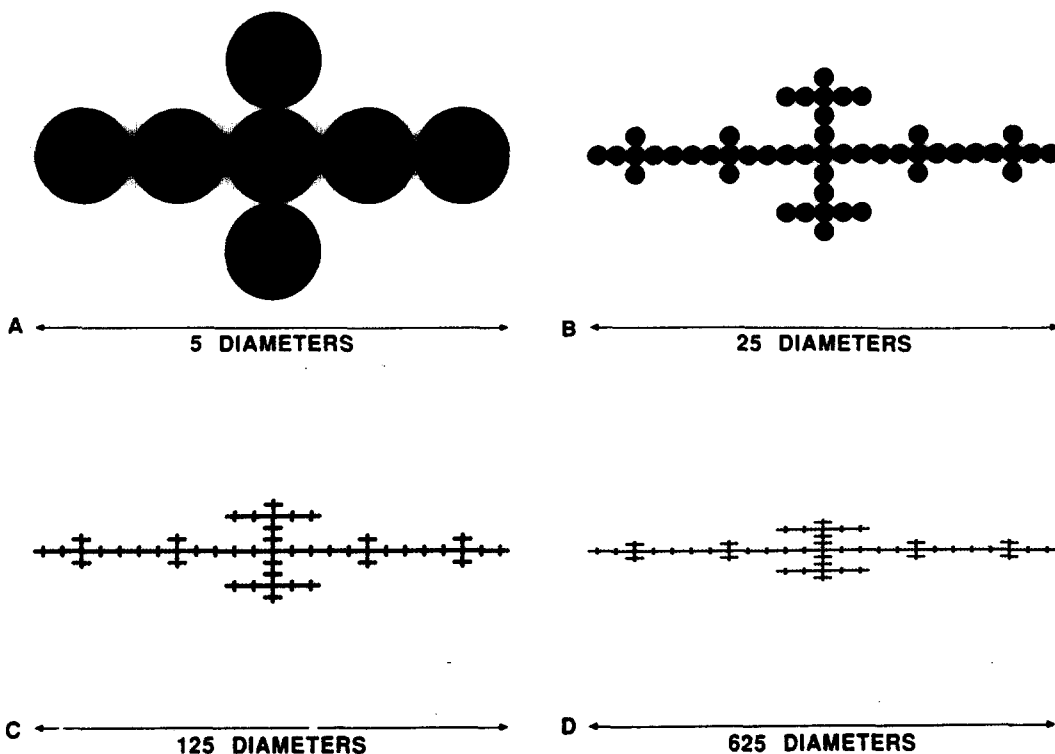


Fig. 9. Four stages in the construction of a simple deterministic self-affine fractal. In Figure 9a seven discs have been joined to form a small cross. Figures 9b, 9c and 9d show the next three stages containing 49, 343 and 2401 (7^2 , 7^3 and 7^4) particles respectively.

Figure 10b is obtained. In the next stage the structure shown in Figure 10c is generated, etc. The self-affine structure can also be extended to infinitesimally small length scales by replacing each line segment by an appropriately scaled version of the generator, etc. After an infinite number of generations a self-affine fractal curve will have been generated. This self-affine fractal can be rescaled onto itself by a change of length scales of 2^n in the y direction and 4^n in the x direction. This fractal curve is much too regular to be of use in describing most systems of interest in chemistry and physics. A much more important paradigm in this context is the Brownian process $B(t)$ that describes the distance moved by a Brownian particle in a time t . The Brownian process is invariant to a change in the time scale by a factor of b ($b>0$) combined with a simultaneous change in the distance scale by a factor of $b^{1/2}$. It is well known that the statistical properties of $B(t)$ and $b^{-1/2} B(bt)$ are equivalent. Since $B(t)$ and t rescale with different exponents, $B(t)$ is not self-similar but is a self-affine fractal. Figure 11 shows a discretized version of the Brownian process; ($B(t)$ is advanced by ± 1 , selected randomly, each time t is increased by 1). Figure 11 shows different lengths of the same curve with vertical scales proportional to the square root of the horizontal (time) scale. The observation that the four rescaled curves in Figures 11a, 11b, 11c and 11d look "similar" illustrates the self-affine scaling. If the fractal dimensionality of a non-discretized Brownian process that is self-affine on all length scales is measured using the box counting method (equation (32)) the result $D_E = 1.5$ will be obtained for $\epsilon \rightarrow 0$ and $D_E = 1$ for $\epsilon \rightarrow \infty$. The results obtained for $\epsilon \rightarrow 0$ and $\epsilon \rightarrow \infty$ are referred to as the local (D_L) and global (D_G) fractal dimensionalities respectively. The crossover between these two regimes occurs at a time t_c that is given by $|B(t+t_c) - B(t)| \approx t_c$. For time intervals (t) much greater than t_c $D_E \rightarrow 1$ and for time intervals much shorter than t_c $D_E \rightarrow D_L$.

A generalization of the Brownian^{3,66} processes $B_H(t)$ that can be rescaled by the transformation $B_H(t) \rightarrow b^{-H} B_H(bt)$ has played an important role in fractal geometry and has many important applications in physics,

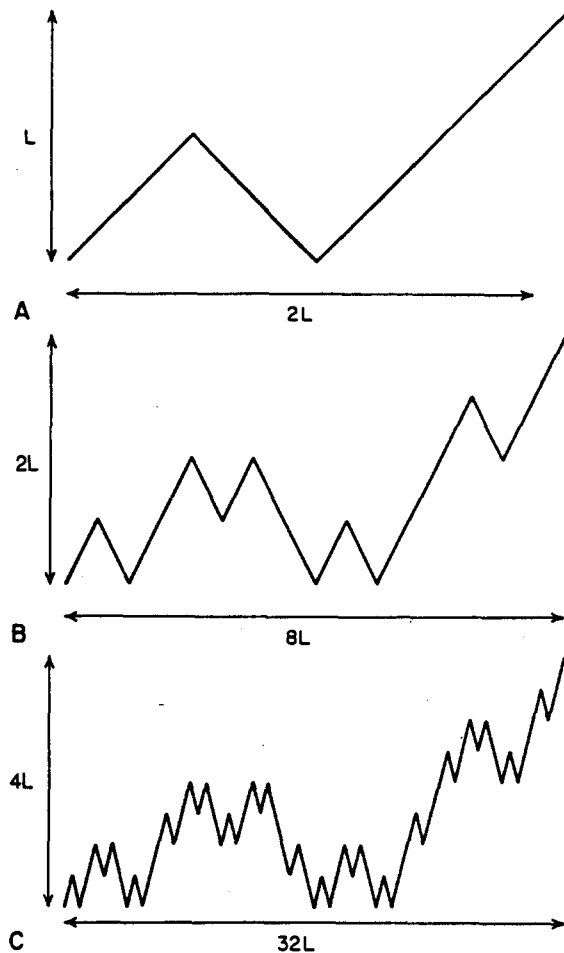


Fig. 10. An example of the generation of a self-affine fractal. Part A shows the generator of the fractal. This generator consists of 4 line segments of equal length. To generate Part B each of the line segments is replaced by a replica of the generator. This process is repeated to obtain the prefractal shown in Part C. The construction process can be extended to infinitesimally small length scales by replacing each line segment in the generator by an appropriately scaled version of the generator, etc.

chemistry and other areas. The exponent H that characterizes the generalized Brownian process is frequently called the Hurst exponent in recognition of Hurst's pioneering work on the water level statistics in the Nile river.^{67,68} Since the Brownian process is generated by a sequence of random additions, it follows (from the central limit theorem) that the increments $B_H(t_1) - B_H(t_2)$ will have a Gaussian distribution. In general, more than one exponent may be needed to describe self-affine fractals that depend on more than one coordinate. For example, a surface roughened by grinding in one direction might exhibit different fractal scaling behavior in the directions parallel and perpendicular to the grinding direction. Similarly, the spatial variation of properties in an oil field might be different in the horizontal and vertical directions.

There are many ways in which the scaling properties of this type of random self-affine fractals can be measured. In many cases the self-affine fractal is not a physical object but a time record obtained from some measured quantity such as the wave height at some position in the ocean.⁵ The exponent H describing a self-affine fractal time record $Y(t)$ or a fractal structure that can be represented by a random self-affine fractal curve can be measured using the difference correlation function $C_d(t)$ defined by

$$C_d(t) = \langle |Y(t+t_0) - Y(t_0)| \rangle \quad (37)$$

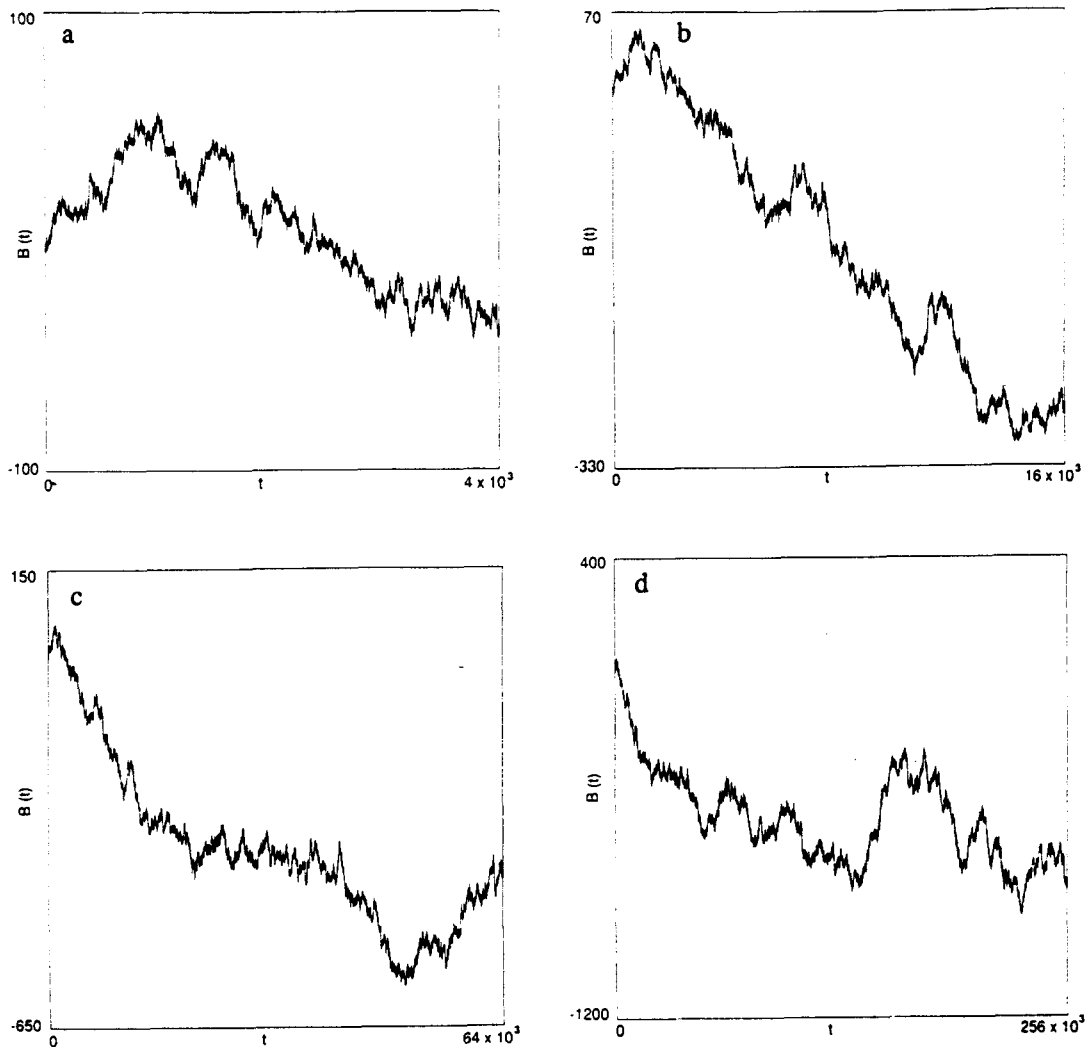


Fig. 11. Four sections of the same (discretized) Brownian process each starting at the point ($t = 0, B(t) = 0$). In Figure 11a the vertical scale is 100 units and the horizontal scale is 4×10^3 units. In each successive figure (11b, 11c and 11d) the horizontal length scale is increased by a factor of 4 and the vertical scale by a factor of 2. The Brownian process is a quintessential random self-affine fractal.

where the averaging is over all reference times t_0 . If $Y(t)$ is a self-affine fractal

$$C_d(t) \sim t^H \quad (38)$$

and this provides a convenient way of measuring H . Other correlation functions⁶⁹ such as

$$C_d^2(t) = \langle (Y(t+t_0) - Y(t_0))^2 \rangle \quad (39)$$

can be used to determine H . In this case H is measured via the relationship

$$C_d^2(t) \sim t^{2H} \quad (40)$$

It follows from equations (38) and (40) that a horizontal cross section (a cross section through $Y(t)$ at a constant value of Y) will intersect the curve $Y(t)$ at n values of t where n is related to the interval ($\tau = t_2 - t_1$) of the cross section by

$$n(\tau) \sim \tau^{(1-H)}. \quad (41)$$

This implies that points of intersection lie on a self-similar fractal subset with a fractal dimensionality given by

$$D = d_S - H \quad (42)$$

where d_S is the Euclidean dimensionality of the space of the independent variables. This provides a practical way of measuring H via the fractal dimensionality of the horizontal intersection.

It appears that many systems can be described quite well as uniform objects with a self-affine fractal surface. The scattering behavior of these objects is different from that of a surface fractal with a self-similar surface. On long length scales a self-affine surface appears to be smooth and horizontal scattering at wave vectors corresponding to these length scales will give the familiar Porod k^{-4} scattering behavior.⁴⁸ On short length scales the surface will appear to be rough and "vertical". Wong⁷⁰ has shown that for a d dimensional structure with a Hurst exponent H the small angle scattering intensity can be represented as

$$I(k) \sim Ak^{-(d+H)} + Bk^{-(d+1)} + \dots. \quad (43)$$

On long length scales ($k \rightarrow 0$) the second term will dominate and the Porod scattering law is again obtained. On short length scales the first term will dominate and the scattering exponent has a value of $-(d+H)$ or $-(3+H)$ for $d = 3$. This is a consequence of the crossover in the box counting dimensionality D_E from its global value of $d-1$ to its local value of $d-H$. If the local value for D_E is substituted for D_S in equation (31) that describes scattering by a self-similar surface fractal, the result

$$I(k) \sim k^{3-H-6} \sim k^{-(H+3)} \quad (44)$$

is obtained. This result is in accord with that obtained by Wong. Alexander⁷¹ has argued that the crossover length characterizing the crossover from local to global behavior will, in most cases, be shorter than physical length scales so that only scattering characteristic of the global structure will be seen (i.e., only k^{-4} Porod scattering will be seen). However, it appears that scattering from self-affine rough surfaces that can be interpreted in terms of equation (44) is quite common.

The above discussion suggests that self-affine fractal surfaces can be thought of as having the properties of a self-similar fractal on short length scales and the properties of smooth surfaces on long length scales. While this picture may sometimes lead to correct predictions, the true self-affine nature of the transformation that rescales these fractals must always be kept in mind and care must be taken to distinguish between self-similar and self-affine fractals if serious error in the interpretation of the results of experiments and simulations is to be avoided.

It can be very difficult to distinguish between self-similar and self-affine surfaces on the basis of scattering experiments alone. In practice the distinction is often based on information concerning the processes that generated the fractal. For example, if a surface is produced by depositing material on an initially smooth surface or by tensile stress (fracture) then the direction normal to the initially smooth surface or parallel to the stress direction is obviously distinguished from other directions in space. Under these conditions it seems reasonable to suppose that the surface might be self-affine. On the Earth's surface the difference between the horizontal and vertical directions are clearly important (particularly on long length scales) and mountain ranges can be represented quite well by self-affine fractals.³ On the other hand, if the rough surface is a result of an isotropic, homogeneous process such as percolation, then a self-similar geometry is expected. On the basis of these ideas it

seems that the rough surfaces of most dense objects should be self-affine.

An approach known as R/S analysis (rescaled range analysis) was developed by Hurst in connection with his studies of the Nile River.^{67,68} Here it is assumed that the signal $Y(t)$ can be represented by discrete random increments δy in Y at uniform intervals of length δt (in practice even a continuous signal must be discretized in order to analyze it). The signal $Y(t)$ over the interval $\tau = n\delta t$ can be represented by the quantity

$$X(\tau) = \sum_{m=1}^n [\delta y(m\delta t) - \langle \delta y \rangle_\tau] \quad (45)$$

The range $R(\tau)$ is the difference between the maximum and minimum values of $X(\tau)$ over the interval $\tau(n\delta t)$. It is clear that for a self-affine fractal

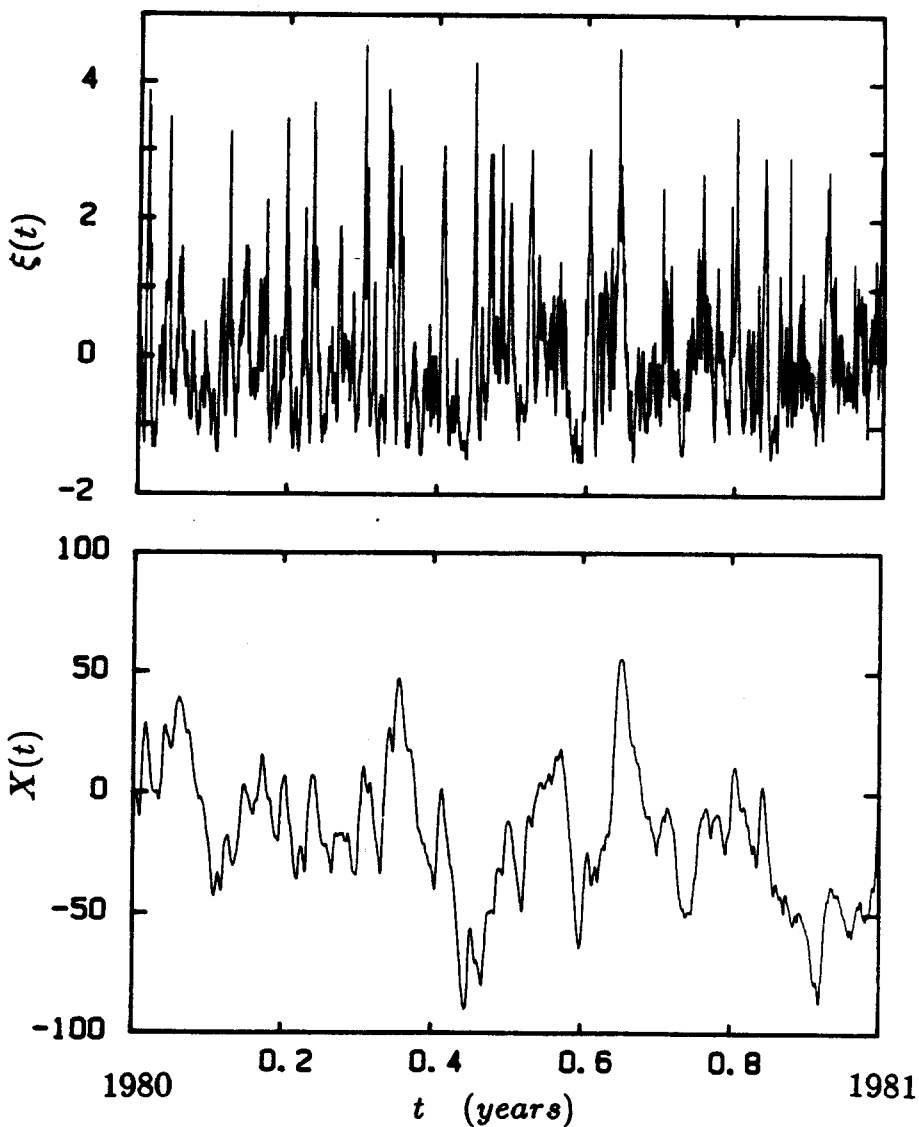


Fig. 12. The top part shows the normalized (to a zero mean value), seasonally adjusted wave height ($\xi(t)$) measured as a function of time at Tromsøflaket. The bottom figure shows the cumulative sum $X(t) = \sum \xi(m\tau)$, $m = 1 \rightarrow t/\tau$ as a function of time. This figure is taken from reference 78 (Froyland, Feder and Jossang, to be published. See also reference 5).

$$\langle R(\tau) \rangle \sim \tau^H. \quad (46)$$

The standard deviation ($S(\tau)$) in the increments $\delta y(\tau)$ over the interval τ is given by

$$(S(\tau))^2 = 1/n \sum_{m=1}^n (\delta y(m\delta t) - \langle \delta y \rangle)^2 \quad (47)$$

Hurst found empirically that the rescaled range ($R(\tau)/S(\tau)$) satisfied the relationship

$$(R/S) \sim (\tau/2)^H \quad (48)$$

and the exponent H can be determined from the dependence of (R/S) on τ . Self-affine fractal geometry and R/S analysis have been further developed and applied extensively to problems in geophysics and hydrology by Mandelbrot and Wallis.⁷²⁻⁷⁷ The exponent H is the Hurst exponent for the accumulated deviation of $\delta y(t)$ from its mean value. A rough surface could be represented in terms of an array of equal sized horizontal elements (the local height). The increments δy would then be the differences or step heights between adjacent elements and the Hurst exponent obtained from an analysis of the accumulated step height deviations would be the Hurst exponent for the surface.

A particularly clear exposition has recently been given by Feder.⁵ One of the applications discussed by Feder is the analysis of wave heights at Tromsøflaket (an area near Tromsø, Norway in the Norwegian Sea). Here the maximum wave height measured during a three hour interval plays the role of the random increment δy . Figure 12 shows the (seasonably adjusted) wave heights ($\delta y(t)$) and the sum $X(t)$ during a period of one year. It should be noted that the mean wave height has been subtracted from the wave heights shown in Figure 12. The result of an R/S analysis was carried out using data obtained over a three year period. The results indicate that the wave heights are persistently correlated ($H > 1/2$) for short time intervals (less than about 10 days) but are uncorrelated ($H \approx 1/2$) at longer time intervals. The increments $\delta y(t)$ can represent a wide variety of

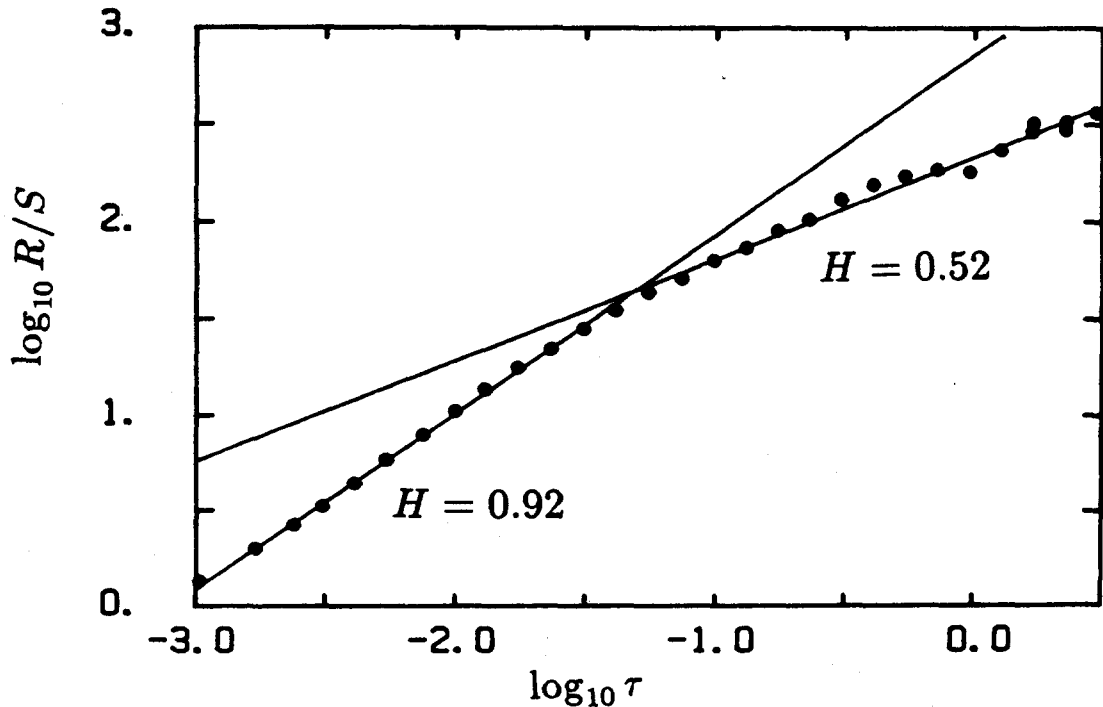


Fig. 13. Results obtained from an R/S analysis of the wave height record shown in Figure 12. This figure was taken from reference 78 (Froyland, Feder and Jossang) to be published. (See also reference 5).

measurements (the width of tree rings, step heights in a surface, records from oil well logs, rainfall and river discharges, to name just a few). For this reason self-affine fractal geometry finds broad applications in statistical analysis.

Recently, Dubuc⁷⁹ et al. have carried out a sobering assessment of some of the methods used to characterize self-affine fractals (they used Weierstrauss-Mandelbrot functions,⁸⁰ Kiesswetter functions⁸¹ and fractal Brownian motion^{3,82}). However, two of the three methods investigated by Dubuc et al. do not seem to be appropriate for self-affine curves. They are based on box counting or covering methods and are sensitive to the crossover behavior discussed above. It is not surprising that these methods give values for the fractal dimensionality (local fractal dimensionality, $\epsilon \rightarrow 0$) that are too low. The third method explored by Dubuc et al. is based on the power spectrum of $Y(t)$ that can be obtained by fast Fourier transformation. For a self-affine fractal the power spectrum $P(\omega)$ has the form

$$P(\omega) \sim \omega^{-\beta} \quad (49)$$

where $\beta = 2H+1$ or $H = (\beta-1)/2$. This approach was the only one tested by Dubuc et al. that I would recommend for self-affine fractals. Dubuc et al. present a new way for measuring the local fractal dimensionality of profiles (D_L) and hence the Hurst exponent via the relationship

$$H = d_S + 1 - D_L = d - D_L \quad (50)$$

or $H = 2 - D_L$ for $d_S = 1$. This method appears to work very well for the examples they have tested.

Fat Fractals

The most familiar fractals are self-similar fractals that in the asymptotic limit in which fractal scaling extends to infinitesimally small length scales have a mass or volume of zero. Physical approximations to these fractals are wispy, tenuous structures whose mean density $\rho(L)$ decreases as their mass increases according to equation (5). Fractal scaling is also found for structures that occupy a finite fraction of their embedding space (or lattice). Such fractals are often called "fat fractals" to distinguish them from the more familiar "thin" fractals described above. A simple example^{83,84} can be obtained by modifying the procedure used to construct the Cantor set shown in Figure 1. Now instead of removing the middle $1/3$ of each line in the n th stage of the generation process the fraction removed is $(1/3)^n$. Using this procedure the fraction of the length remaining converges to a finite value as $n \rightarrow \infty$ and the set generated by this method has a Hausdorff-Besicovitch dimension of 1. However, fat fractals such as this can be described in terms of non-Euclidean geometric scaling relationships. For example, we could imagine filling all of the holes with a size less than ϵ . For the ordinary triadic Cantor set shown in Figure 1 the total filled length (or measure) $\mu(\epsilon)$ increases by a factor of $3/2$ each time that ϵ increases by a factor of 3 and the growth of $\mu(\epsilon)$ with increasing ϵ can be described by an exponent ϕ given by

$$\phi = \log(3/2)/\log(3) = 0.36907\dots \quad (51)$$

This exponent is equal to $1-D$ and in general for a self-similar fractal in a d dimensional embedding space $\phi = d-D$. For a fat fractal the relationship between $\mu(\epsilon)$ and (ϵ) is given by

$$\mu(\epsilon) = \mu_0 + k\epsilon^\phi. \quad (52)$$

We could also think of thickening or fattening the fractal by a distance ϵ and measuring the volume $V(\epsilon)$ as a function of ϵ . A fractal dimension D_x (called the exterior capacity dimension⁸⁵) can then be defined as

$$D_x = \lim_{\epsilon \rightarrow 0} \ln V(\epsilon) / \ln(\epsilon) \quad (53)$$

In practice it is often not possible to approach the limit $\epsilon \rightarrow 0$ and an effective value for D_x can be obtained by measuring the dependence of $V(\epsilon)$ on ϵ over a limited range of length scales. For ordinary, self-similar fractals the volume $V(\epsilon)$ is related (within a factor of order unity) to the volume of the $N(\epsilon)$ boxes of size ϵ required to cover the fractal so that (from equation (30))

$$V(\epsilon) \approx N(\epsilon) \epsilon^d \sim \epsilon^{d-D} \quad (54)$$

so that $D_x = d - D$.

A third procedure would be to cover the fractal with a grid with elements of size ϵ and measure the number $N'(\epsilon)$ of those elements that were partially filled. The fractal dimension D_y can then be defined by

$$D_y = N'(\epsilon) \sim \epsilon^{-D_y}. \quad (55)$$

For self-similar fractals the values for the fractal dimensionality obtained from these procedures are all directly related to the all-purpose fractal dimensionality D . However, for fat fractals different results can be obtained and it is important to define precisely which fractal dimensionality (or dimensionalities) is being used to characterize the fractal.

Subfractals

Subfractals are structures that are not themselves fractals but have associated with them some structure that is fractal. An example based on the Cantor set in Figure 1 is shown in Figure 14.^{3,86} Starting with a diagonal line of slope 1 on the interval (0-1) the middle third is replaced by a horizontal line segment and the other two thirds are replaced by lines with slopes of 3/2 (Figure 14a). In the next stage of construction each of the segments with slopes of 3/2 is replaced by two segments with slopes of $(3/2)^2$ and a central segment of zero slope (Figure 14b) in the asymptotic limit. The curve generated by this process is horizontal in the gaps of the Cantor set in Figure 1 and vertical in the regions occupied by the Cantor set (Cantor "dust"). The total length of both the vertical and horizontal segments is 1. This curve is neither a self-similar nor self-affine fractal (though it can be mapped onto a part of itself after an appropriate affine transformation in which the height is increased by a factor of 2 and the length by a factor of 3).

The curve shown in Figure 14 is known as a "Devil's staircase".³ It represents the integral of the mass of a "Cantor bar" as a function of distance. The Cantor bar is constructed in a fashion similar to that used to construct the Cantor set shown in Figure 1. However, each time a line segment of length L is replaced by two segments of length $L/3$ (with the middle third missing) the mass density in the two remaining thirds is increased by a factor of 3/2 so that the total mass is conserved. This means that at the n th stage in the iteration process the line segments of length of $\ell = (1/3)^n$ have a mass (measure) of $\mu = (1/2)^n$. Consequently, the relationship between the length of a segment ℓ and its mass or measure μ is given by

$$\mu = \ell^\alpha \quad (56)$$

where α is an exponent known as the Lipschitz-Hölder exponent. This is a quantity that will be encountered again in the next section on fractal measures and multifractals. Because of its close relationship with the Cantor set and Cantor Bar there is a strong urge to classify the Devil's staircase (and other structures with similar properties) as a fractal and quantitatively characterize it by a fractal dimensionality. Pfeifer⁸⁶ has suggested that this can be done by considering the volume $V(r)$ surrounding the surface or curve that is inaccessible to balls of radius r . The dependence of $V(r)$ or r is then given by

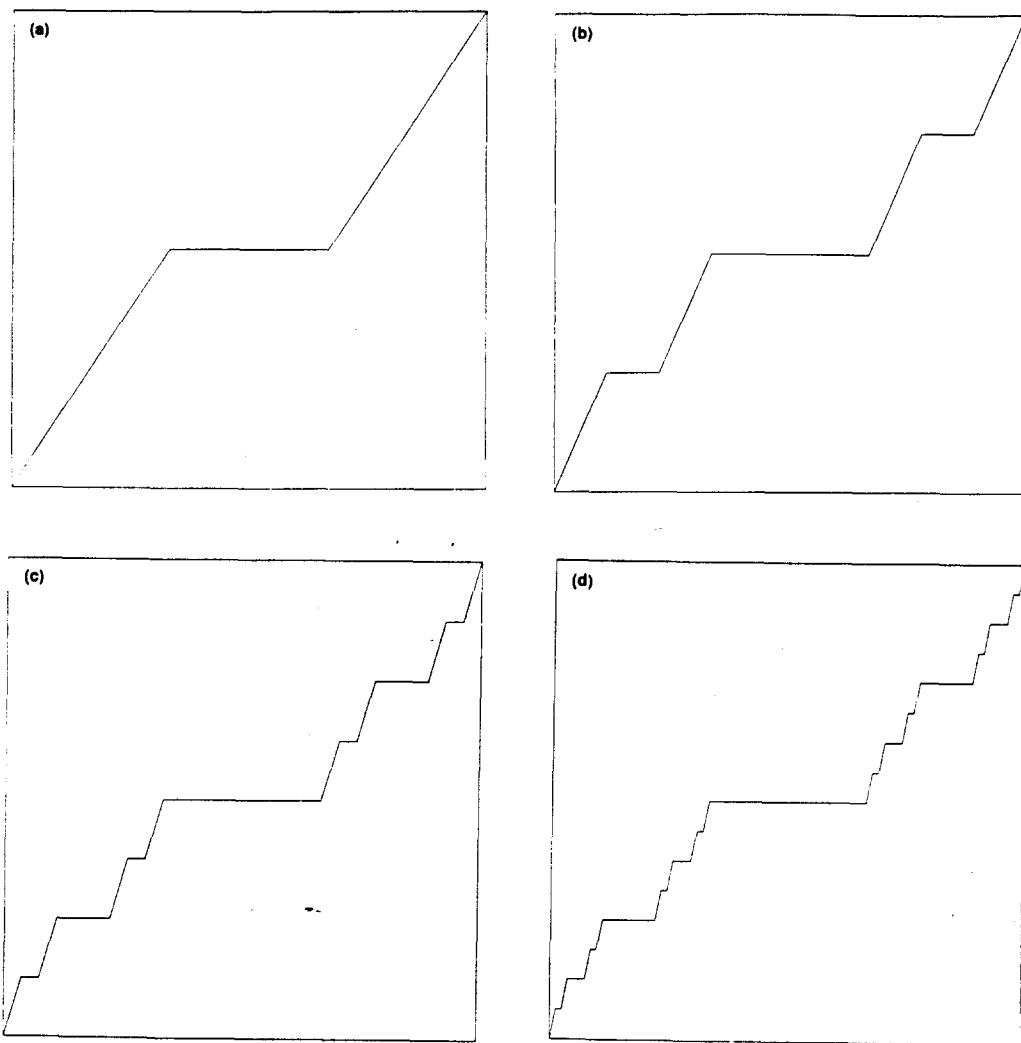


Fig. 14. Four stages in the construction of a subfractal. The construction process starts with a straight line from (0,0) to (1,1). At each stage in the construction process the middle third of each non-horizontal line segment is replaced by a horizontal line segment and the slopes of the remaining two thirds are increased by a factor of 3/2.

$$V(r) \sim r^{d-D_i} \quad (57)$$

where D_i is called the "irregularity dimensionality". For the Devil's staircase $D_i = \log(2)/\log(3)$ (the dimensionality of the corresponding Cantor set).

The Devil's staircase set illustrates why Mandelbrot has been reluctant to provide a concise mathematical definition of a fractal. It is intuitively a fractal yet according to one proposed definition of a fractal³ (a set for which the Hausdorff-Besicovitch dimensionality strictly exceeds the topological dimensionality (D_T)) it is not a fractal since $D_H = D_T = 1$. The intuitive idea that this is in some way a fractal is given substance by the idea of an irregularity dimensionality.

Fractal Measures and Multifractals

In many problems in physics and chemistry we are interested in how some quantity of interest
JPSSC 20:3-C

(concentration of reactant or product in a reaction, electric field, stress field, temperature, etc.) is distributed over a system of interest.⁸⁷ This distribution can be described in terms of a measure or measure density $\mu(x)$ that specifies the value of the intensive variable at the position x . The measure μ associated with some (not necessarily connected) region is equal to $\int \mu(x)dx$ where the integral is over all positions x in that region. For an asymptotic fractal the measure density can vary discontinuously on all length scales and the measure can be described in terms of the quantities $\mu(x, \epsilon)$ that specify the amount of "stuff" within a distance ϵ from x . So far, in this review, we have (implicitly) been concerned with uniform measures that are constant (within a factor or order unity) throughout the system. For example, we have assumed that the mass contained in a fractal (or non-fractal) structure is proportional to the volume that it displaces and that either quantity can be used to measure the fractal dimensionality. In many systems, however, the measure $\mu(x)$ (or $\mu(x, \epsilon)$) may be extremely non-uniform and it frequently happens that this measure can be described in terms of fractal scaling (even in cases where the system or "substrate" is Euclidean).⁸⁸

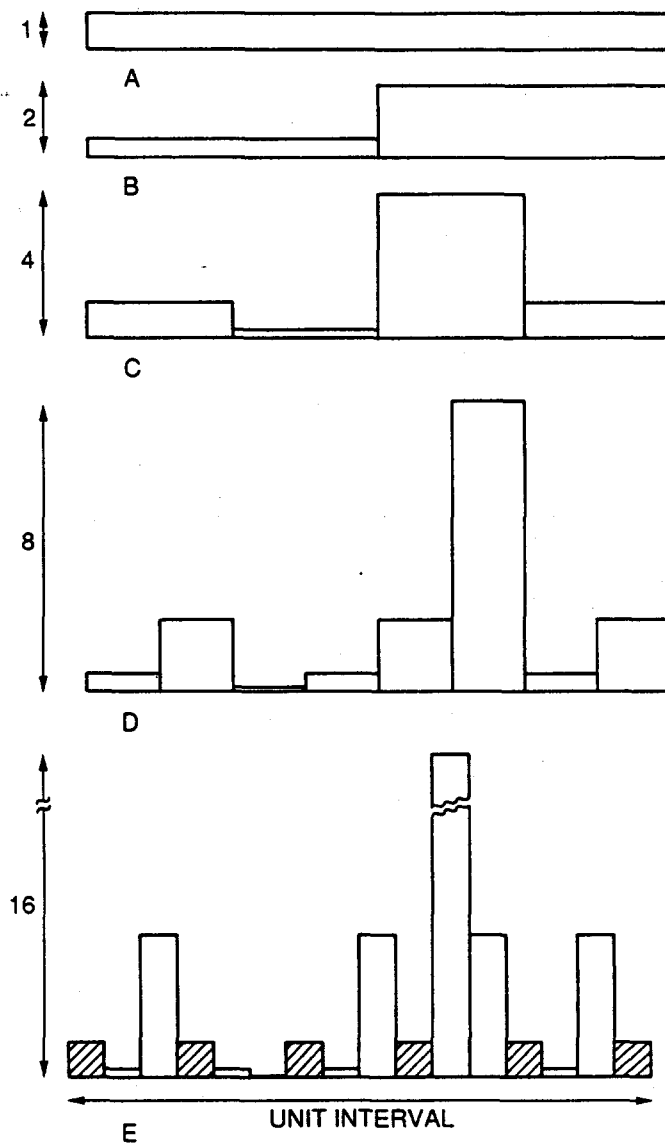


Fig. 15. Construction of a multiplicative multifractal measure on the unit interval. Figure 15e shows the fourth stage in the generation process (described in the text). The shaded regions, each of length $1/16$, have the same measure and constitute a subset of the line. In the asymptotic limit $n \rightarrow \infty$ (where n is the number of generations) those regions consisting of segments of length 2^{-n} that have the same measure are fractal subsets of the unit interval.

A simple example of the generation of a fractal measure on a Euclidean substrate is shown in Figure 15. Starting with a uniform measure ($\mu(x) = 1$ or $\mu(x,\epsilon) = \epsilon$) on a unit interval (Figure 15a) the interval is divided into two equal intervals and the measure associated with the right half is multiplied by 1/2 and that associated with the left half is multiplied by 2 (Figure 15b). In the next stage (Figure 15c) each of the intervals of length 1/2 is further divided into intervals of length 1/4 but now the right half is multiplied by 2 and the left half is multiplied by 1/2. As the process proceeds (Figure 15d) each interval is divided into halves. In the n th generation the measure in the right half is multiplied by 1/2 and the measure in the left half is multiplied by 2 if n is odd. Otherwise, the measure in the left half of each interval is multiplied by 2 and the measure in the right half is multiplied by 1/2. After a large number of generations ($n \rightarrow \infty$) we can examine those regions that have the same measure (same value for $\mu(x,\epsilon)$ where $\epsilon = 2^{-n}$). For example, after $n = 2m$ generations those regions with a measure density $\mu(x)$ of 1 or a measure $\mu(x, 2^{-n})$ of 2^{-n} (the subset with $\mu(x) = 1$) are quite uniformly distributed over the line and there are $n!/(m!m!)$ intervals each of length 2^{-n} that carry a measure density of 1 or a measure of 2^{-n} . The total length occupied by this subset ($n!/(2^n m!m!)$) decreases with increasing n more slowly than any power of n and it has a fractal dimensionality of 1. In general, the length occupied by the subset that carries a measure density of $(1/2)^{(n-j)}$ is given by

$$V(j) = 2^{-n} n! / ((n-j)! j!) \quad (58)$$

in the limit $n \rightarrow \infty$. The asymptotic form of Sterling's approximation ($\ln(n!) \rightarrow n \ln(n)$) can be used to determine the dependence $V(j)$ on j , i.e.

$$\ln(V(j)) \approx n \ln(n) - (n-j) \ln(n-j) - j \ln(j) - n \ln(2) \quad (59a)$$

or

$$\ln(V(j)) \approx (n-j) \ln(n/n-j) + j \ln(n/j) - n \ln(2) \quad (59b)$$

and the fractal dimension of this subset is given by

$$D(j) = \lim_{n \rightarrow \infty} \ln V(j) / \ln(\epsilon_n) = \lim_{n \rightarrow \infty} \ln(V(j)) / \ln(2^{-n}) \quad (60)$$

where $\epsilon(2^{-n})$ is the length over which the measure is constant. It follows from equations (59) and (60) that

$$D(j) = [\zeta \ln(\zeta) + (1-\zeta) \ln(1-\zeta)] / \ln(1/2) \quad (61)$$

where $\zeta = j/n$. This means that in the limit $n \rightarrow \infty$ the hierarchical, multiplicative procedure illustrated in Figure 15 divides the line into an infinite number of interpenetrating fractal subsets each having its own fractal dimensionality given by equation (61). To obtain equation (61) a "short-cut" has been taken by assuming that each of the subsets labeled by j (in the limit $n \rightarrow \infty$) has a fractal spatial distribution and then calculating $D(j)$ from equation (60). This assumption is not necessarily true. For example, if the line segments of size ϵ were scrambled randomly or if they were placed in order of decreasing ζ from right to left then these subsets clearly would not be fractal. A rigorous proof of equation (61) would require a detailed analysis of the spatial distribution of each of the subsets.

Systems like this with a fractal measure $\mu(x)$ are often called multifractals since an infinite number (continuous distribution) of fractal dimensions are needed to fully characterize the measure in the asymptotic ($n \rightarrow \infty$) limit.

In the limit $n \rightarrow \infty$ it is more useful to obtain the fractal dimensionality for a new subdivision of the line consisting of all of those subsets for which the quantity ζ in equation (61) lies in the range ζ to $\zeta + \delta\zeta$. The

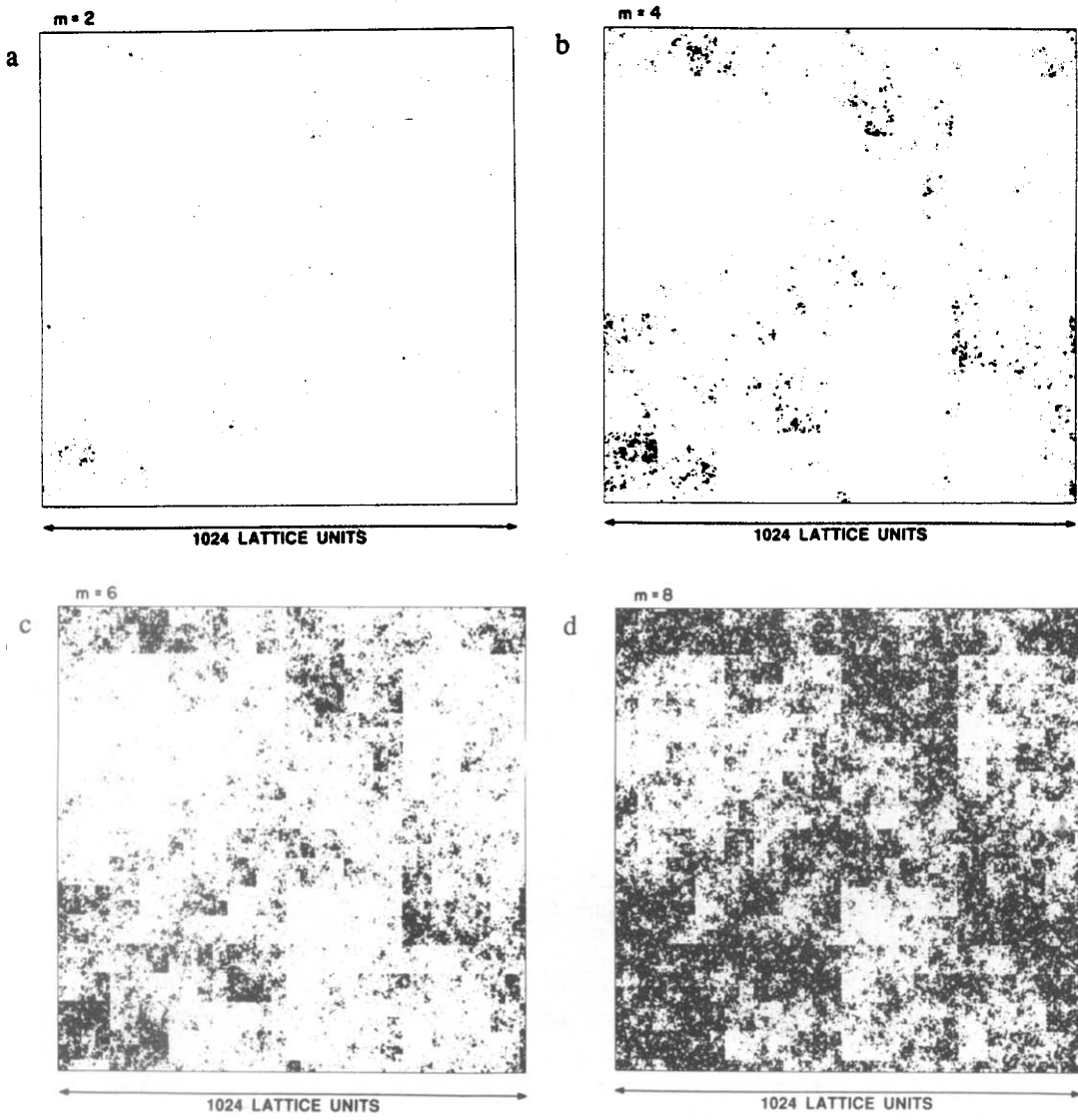
volume occupied by this new subset can be obtained from equation (59) and is given by

$$\ln(V(\zeta)) = -n[\zeta \ln(\zeta) + (1-\zeta) \ln(1-\zeta)] - n \ln(2) + \delta\zeta \ln n \quad (62)$$

and from this it follows that the fractal dimensionality for this subset is also given by equation (61). In the limit $n \rightarrow \infty$ the last term in equation (62) becomes negligible compared to the first two terms. A similar procedure can be used to subdivide a plane (cube) into quadrants (octants) etc. In this case the fractal dimensionality of the subsets is given by

$$D(\zeta) = D(j) = \frac{d[\zeta \ln(\zeta) + (1-\zeta) \ln(1-\zeta)]}{\ln(1/2)} \quad (63)$$

where d is the Euclidean dimensionality of the substrate. An example is shown in Figure 16. In this case²⁹ measurement of the fractal dimensionalities of the subsets (via their two point density-density correlation functions) gives results that are consistent with equation (63).



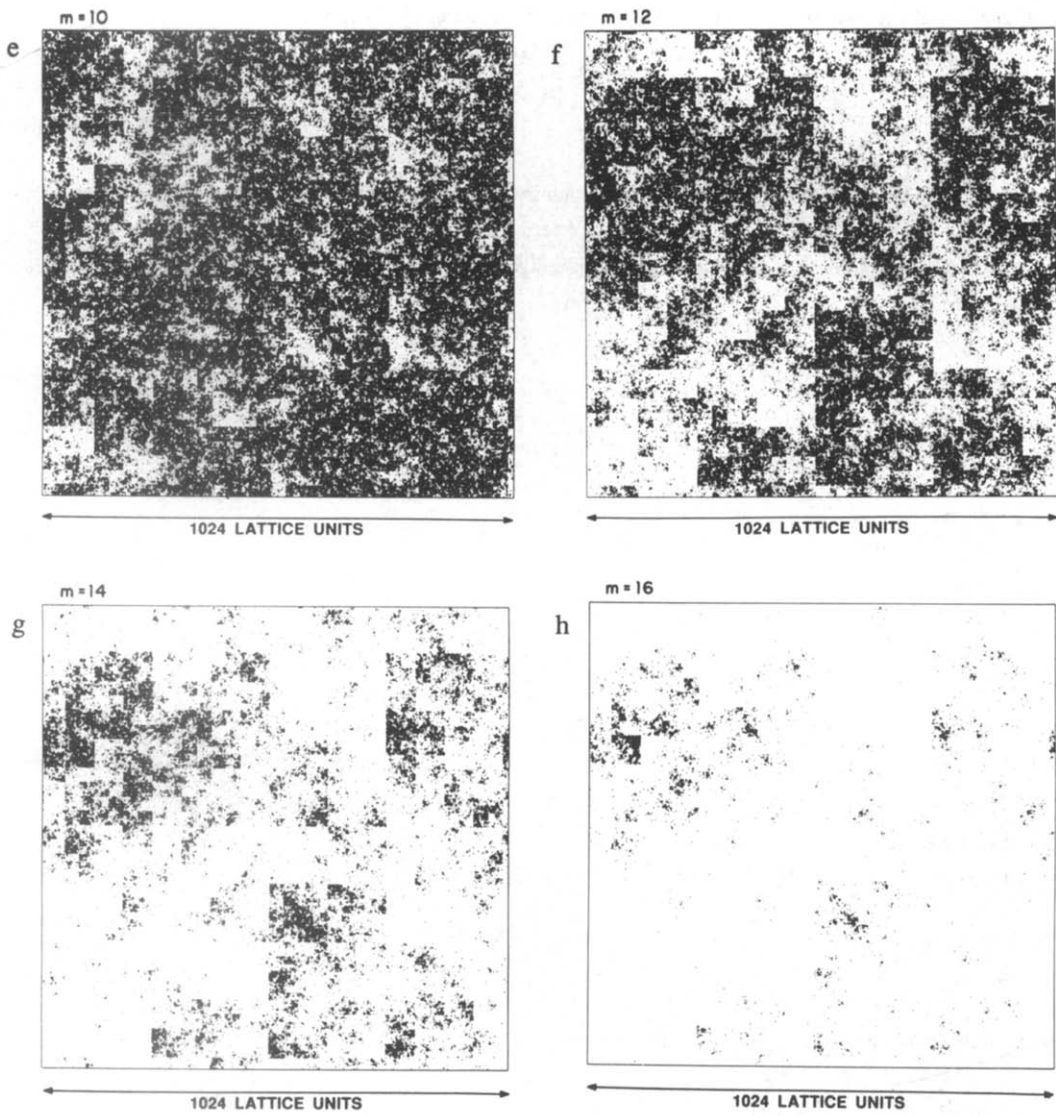


Fig. 16. Division of a plane into interpenetrating fractal subsets. At the first stage in the construction process the plane is divided into four quadrants and an integer. I_j is added to all of the sites in the j th quadrant. The quantities I_j are selected from the integers 0, 1, 1, 2 randomly excluding multiple selection. At the next stage this process is repeated for all of the quadrants to generate 16 subquadrants. After n stages an integer ranging from 0 to 2^n is associated with each position on the plane. Figure 16 shows the results starting with a $2^{10} \times 2^{10}$ (1024×1024) lattice after the 10th generation. In Figures 16a-16h the location of those sites for which the integer (n) has values of 2, 4, 6, 8, 10, 12, 14 and 16 are shown. If a measure $\mu(i,j) = n(i,j)$ is associated with each site then a multiplicative measure will have been defined on the lattice and in the limit $n \rightarrow \infty$ this measure will be a multifractal measure that can be subdivided into fractal subsets that are distinguished by the Holder exponents (α).

It is apparent from these examples that the multifractal measure can be characterized by the function $D(\zeta)$ where ζ covers the interval $0 \leq \zeta \leq 1$. However, it is important to recognize that the procedure illustrated in Figure 15 does not preserve the normalization of the measure $\mu(x)$. A normalized measure $\mu'(x)$ can be obtained from

$$\mu'(x) = \mu(x)/\int \mu(x) dx . \quad (64)$$

In practice it is not convenient to use the quantity ζ to identify the subsets on the multifractal measure. Instead, the dependence of the normalized measure, $\mu'(\zeta, \epsilon_n)$, on the length ϵ is used to identify that part of the measure

with a fractal dimensionality of $D(\zeta)$. Here $\mu'(\zeta, \varepsilon_n)$ is the value of that part of the measure associated with the index ζ that is uniform over a distance of ε . A new index α (equation (54)) defined as

$$\alpha(\zeta) = \lim_{\varepsilon \rightarrow 0} \frac{d \log(\mu'(\zeta, \varepsilon))}{d \log(\varepsilon)} \quad (65)$$

is used to identify the subsets of the measure. The quantity $\alpha(\zeta)$ is known as the Lipshitz-Holder exponent⁵ or the strength of the singularity⁹⁰ of the subset characterized by ζ . A normalized measure can be generated automatically by using weights of $2(1-a)$ and $2a$ instead of 2 and $1/2$ in Figure 14. In that case the quantity $\mu'(\zeta, \varepsilon)$ is given by

$$\mu'(\zeta, \varepsilon_n) = (2a)^n \zeta (2(1-a))^n (1-\zeta)_n^2 \quad (66)$$

and

$$\varepsilon = \varepsilon_n = 2^{-n} \quad (67)$$

so that $\alpha(\zeta)$ is given by

$$\alpha(\zeta) = - \frac{\xi \log(a) + (1-\xi) \log(1-a)}{\log(2)} \quad (68)$$

The fractal dimensionality $D(\zeta)$ of this subset is usually represented by $f(\alpha)$ (i.e., $f(\alpha(\zeta))$).

Several methods have been developed for the characterization of fractal and non-fractal structures with fractal measures. For example, the partition function $Z(q)$ (equation (33)) can be used in conjunction with equation (34) to calculate the quantities D_q . Now $Z(q)$ is defined as

$$Z_q(\varepsilon) = \sum_i (\mu_i(\varepsilon))^q \quad (69)$$

where $\mu_i(\varepsilon)$ is the integral of $\mu_i(x)$ over the i th region of size ε ($\mu(x_i, \varepsilon)$) and the measure is normalized

$$\int \mu(x) dx = 1 \quad (70)$$

For a multifractal system the dependence of Z_q on L and ε can be written as

$$Z_q \sim (L/\varepsilon)^{-\tau(q)}. \quad (71)$$

From equation (34) it follows that the dependence of Z_q on L/ε is also given by

$$Z_q \sim (L/\varepsilon)^{(q-1)D_q} \quad (72)$$

so that the exponents $\tau(q)$ and D_q are related by

$$\tau(q) = (q-1)D_q. \quad (73)$$

The partition function, Z_q , can also be written in terms of its fractal subsets as

$$Z_q = \int d\alpha \rho(\alpha) (L/\varepsilon)^{f(\alpha)-q\alpha} \quad (74)$$

where $\rho(\alpha)$ is a finite density coefficient. In the limit $(L/\epsilon) \rightarrow \infty$ only the subset (s) for which $f(\alpha)-q\alpha$ is a maximum dominate Z_q . For a particular value of q this dominating contribution will come from the subsets labelled by the index $\alpha(q)$ defined by

$$\frac{d}{d\alpha}(q\alpha-f(\alpha))|_{\alpha=\alpha(q)}=0 \quad (75a)$$

or

$$\frac{d}{d\alpha}[f(\alpha(q))] = q. \quad (75b)$$

Consequently, equation (74) can be replaced by

$$Z_q \sim (L/\epsilon)f(\alpha(q))-q\alpha(q). \quad (76)$$

A comparison of equations (71) and (76) leads to the result

$$\tau(q) = q\alpha(q) - f(\alpha(q)) \quad (77a)$$

or

$$f(\alpha(q)) = q\alpha(q) - \tau(q) \quad (77b)$$

so that

$$\alpha(q) = \frac{d}{dq}(\tau(q)) \quad (78)$$

This means that $\alpha(q)$ can be obtained by measuring the quantities $\tau(q)$ or D_q as a function of q . $\alpha(q)$ is then obtained from equation (78) and then $f(\alpha)$ ($f(\alpha(q))$) is obtained from equation (77). These results were originally obtained by Halsey et al.⁹⁰ In most simulations either the system size L or the "resolution" ϵ is fixed. For structures grown on a lattice the lattice provides a natural value for ϵ (the size of a single lattice site) and it is convenient to measure Z_q as a function of L and replace (L/ϵ) by L in equation (71) (and also in equations 72, 74, and 76). Similarly, in an experiment on a growing structure instrument resolution or a physical cut-off length might provide a natural value for ϵ . For experiments or simulations carried out in a system with a fixed size or a physically imposed upper cut-off length, it would be natural to measure $f(\alpha)$ by examining the dependence of Z_q (ϵ, L) on ϵ .

The procedure described above always leads to a smooth convex $f(\alpha)$ curve. Unfortunately the effective $f(\alpha)$ curve obtained in this fashion does not reveal the quality of the data on which it is based. The determination of $\tau(q)$ or D_q is subject to the same sort of uncertainties (finite size effects and statistical uncertainties) as is any scaling exponent or fractal dimensionality.

An alternative procedure^{91,92} is based on the histogram of the normalized measure $\mu_i(\epsilon)$ for systems of different sizes (L) with a fixed value for ϵ . This histogram can be represented by the quantity $N(\chi)$ where $N\chi\delta\chi$ is the number of regions of size ϵ for which $\ln(\mu(\epsilon))$ lies in the range $\chi \rightarrow \chi + \delta\chi$. For a multifractal measure the histogram $N(\chi)$ (the normalized histogram) can be represented by the scaling form

$$\frac{\ln[N(\chi)\ln(L)]}{\ln(L)} = g[\chi/\ln(L)] \quad (79)$$

The asymptotic ($L \rightarrow \infty$) value of argument, x , of the function $g(x)$ in equation (79) is $-\alpha$ where α is the

Lipshitz-Holder exponent and the asymptotic value of the right hand side of equation (79) is the fractal dimensionality of the subset labeled by the index χ . It follows that the function $g(x)$ and $f(\alpha)$ are related by

$$g(x) = f(-\alpha). \quad (80)$$

At present we have much less experience characterizing multifractals than "simple" fractals. In many other cases the approach to the asymptotic ($L \rightarrow \infty$ or $\epsilon \rightarrow 0$) limit appears to be unusually slow. Reliable methods for measuring the $f(\alpha)$ curve have not yet been established. This is an active area of research.^{90,93-97}

The appealing physical picture of the $f(\alpha)$ curve or spectrum proposed by Halsey et al. in which the multifractal measure is interpreted in terms of an infinite family of interpenetrating fractal sets each having its own scaling index (α) and fractal dimensionality $f(\alpha)$ has been challenged.⁹⁸ It is apparent that this interpretation is not universally applicable but in many cases it provides a valuable framework for interpreting the results of experiments and simulations.⁹⁹ If the $f(\alpha)$ curve is obtained by averaging data from a large number of samples, negative values of f may be seen for some values of α , the values of α for which $f(\alpha) < 0$ are not found in an infinite system ($L/\epsilon \rightarrow \infty$), but some of the members of an ensemble of finite systems do contain regions in which these values of α occur. The negative portions of $f(\alpha)$ describe how rapidly the subsets characterized by the corresponding values of α become depopulated as the system size increases. They measure the degree of emptiness of empty sets.¹⁰⁰

APPLICATION TO SIMULATION RESULTS

Fractal geometry has been applied extensively to results obtained from computer simulations that are intended to model natural processes. Although applications to experimental observations are ultimately much more important there are several reasons for first considering the role of fractal geometry in helping to understand and summarize the results of computer simulations.

1. At this stage computer simulation results are more extensive.
2. In many cases higher quality data is available.
3. In experimental work ambiguities may arise because the dominant physical processes may change with length scales. In many cases the physical details of the processes involved in experiments are poorly controlled and understood. For this reason computer simulations are often the preferred means of testing theoretical ideas and new approaches to data analysis.
4. It is generally much easier to change and control "conditions" in a simulation than an experiment.
5. Computer simulations are often less expensive and require less planning and preparation.

Growth Models

Simple (computer) models have been used for more than thirty years in an attempt to develop a better understanding of the formation of disorderly patterns. Almost invariably these models lead to the formation of patterns that can be described in terms of fractal geometry. This provides a partial answer to the question "why are fractal structures so common in nature". A deeper, more fundamental answer to this question may come from concepts such as self-organized criticality.¹⁰¹⁻¹⁰⁹ Interest in this area grew rapidly following the introduction of the diffusion-limited aggregation model by Witten and Sander²¹ in 1981. In the intervening years significant advances have been made towards the goal of developing a sound theoretical understanding of these models,¹¹⁰⁻¹²⁰ but this goal remains elusive even for very simple models such as DLA. Despite the fact that these models themselves are not fully understood, they do provide a basis for understanding and describing a broad range of processes.

Cluster Growth Models

The Eden Model

Perhaps the most simple and best understood non-equilibrium growth model is that developed by Eden¹²¹ to simulate the growth of cell colonies. In this model cells in the cell colony are represented by filled sites on a lattice and the growth process is represented by randomly selecting and filling unoccupied sites on the colony perimeter with a probability proportional to the number of occupied nearest neighbors. In most cases the simulation is started with a single occupied lattice site that is called the "seed" or "growth site". A simplified version of this model in which unoccupied perimeter sites (vacant sites with one or more occupied nearest neighbors) are randomly fitted with equal probability (independent of the number of nearest neighbors) has become more popular than the original Eden model. This version is sometimes called the "Physicist's Eden model". A third version of the Eden model (refs. 122 and 123) has recently been introduced in which occupied surface sites (occupied sites with one or more unoccupied nearest neighbors) are selected at random and one of their unoccupied nearest neighbors is randomly selected and filled. This model seems to reduce the surprisingly large corrections to the asymptotic scaling properties associated with this model. The structures formed by the Eden models are completely dense (small holes are formed near to the outer surface but they rapidly become filled). Figure 17 shows a cluster of 2.5×10^6 sites grown using the simplified Eden model. Since the growth algorithm is very simple, much larger structures can quite easily be generated. As the cluster grows, it becomes completely filled and the fractal dimensionality of clusters generated by this model is equal to that of the embedding space or lattice ($D = d = 2$ in this case). The surface, on the other hand, has a much more interesting structure that can be described in terms of self-affine fractal geometry. Figure 18 shows a small portion of the surface of the cluster shown in Figure 17 (in the diagonal (1,1) direction). Although the cluster shown in Figure

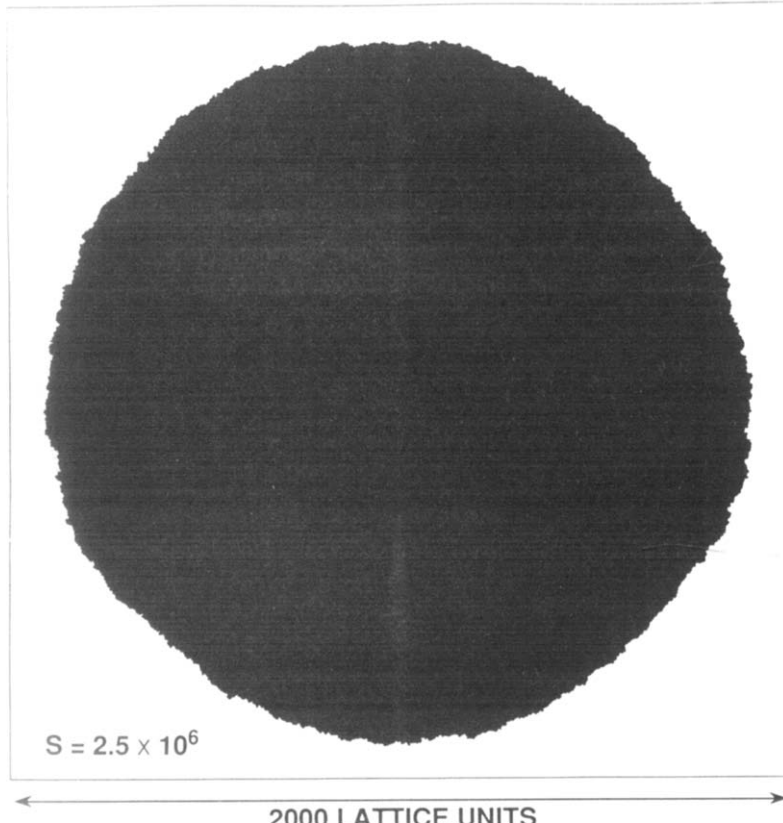


Fig. 17. A cluster of 2.5×10^6 sites grown on a square lattice using the simplified Eden model.

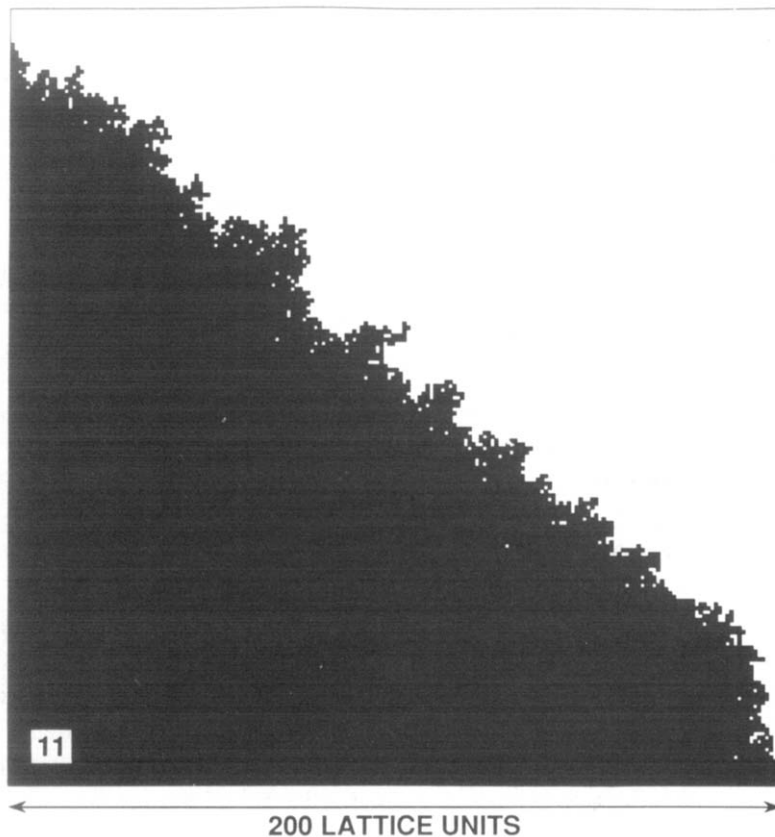


Fig. 18. A portion of the surface of the cluster in Figure 17 in the diagonal (1,1) direction. This figure shows the surface roughness and the presence of surrounded vacant sites near to the perimeter.

17 appears to have a circular shape with rough edges, the growth of the surface does not proceed at equal rates in all directions. The growth in the direction of the lattice axes is faster by a factor of about 1.025 than in the diagonal directions.¹²⁴⁻¹²⁷

Instead of occupying the sites on the perimeter of the growing clusters one at a time, a fraction f of the sites could be selected randomly and occupied simultaneously. The Eden model then corresponds to the limit $f \rightarrow 0$.

Richardson¹²⁸ found a transition from a more or less circular shape to a diamond shape as f is increased from 0 to 1. A similar transition¹²⁹ can be observed if the fluctuations in the Eden growth process are reduced by "noise reduction".^{130,131} In the noise reduced Eden model an unoccupied perimeter site must be selected m times before the site is filled. The limit $m \rightarrow 1$ corresponds to the ordinary Eden model and the limit $m \rightarrow \infty$ corresponds to simultaneously filling all of the surface sites ($f \rightarrow 1$). Figure 19 shows a cluster of 50,000 occupied sites grown with a noise reduction parameter (m of 1000). Figure 20 shows the unoccupied perimeter sites for clusters of 8 sizes in the range 5×10^3 to 5×10^5 on a scale proportional to $s^{1/2}$ (where s is the number of occupied sites) for $m = 10$ and $m = 100$. It is apparent that the shapes of the clusters soon reach an asymptotic form intermediate between that of a circle and a diamond. Recently, interest in the Eden model has been concerned primarily with the surface roughness. This subject will be discussed in more detail later in this review.

Diffusion-Limited Aggregation

The development of diffusion-limited aggregation (DLA) was stimulated by the earlier work of Forrest and Witten¹³² on the aggregation of small metallic particles in a gas. This process produces tenuous aggregates that have a fractal structure. The measurement of a fractal dimensionality of 1.7-1.9 for iron particle aggregates

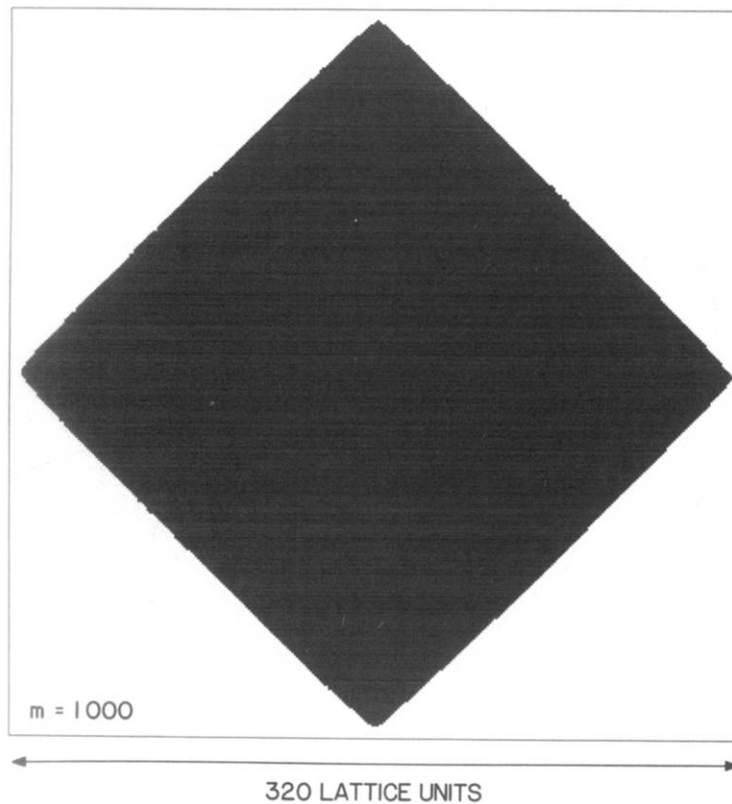


Fig. 19. A cluster of 50,000 sites grown on a square lattice using the noise reduced Eden model with a noise reduction parameter, m , of 1000.

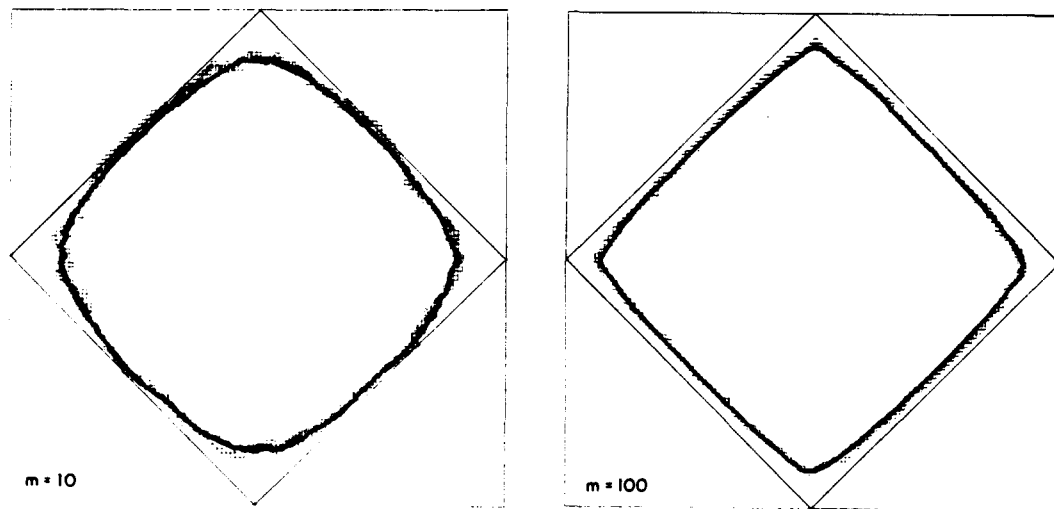


Fig. 20. Superposition of the unoccupied interface sites for Eden clusters containing 5000, 10,000, 20,000, 40,000, 80,000, 160,000, 320,000 and 500,000 occupied sites. The results obtained with a noise reduction parameter m of 10 and 100 are shown.

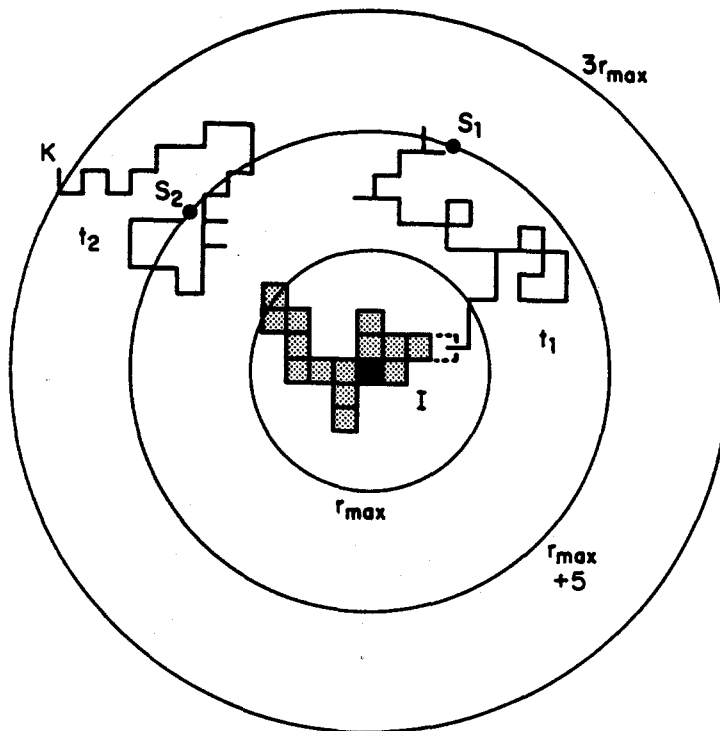


Fig. 21. An early stage in a square lattice model simulation of diffusion-limited aggregation. The original seed or growth site is shown in black and the other sites that are occupied at this stage are shaded. Two typical trajectories starting at random position on the launching circle are shown. Trajectory t_1 reaches an unoccupied surface site (growth site), which is indicated by dashed edges, and this site is occupied. Trajectory t_2 reaches the termination circle which in this case has a radius of $3 R_{\max}$ where R_{\max} is the maximum radius of the cluster. This trajectory will be terminated and a new trajectory started at a random position on the launching circle.

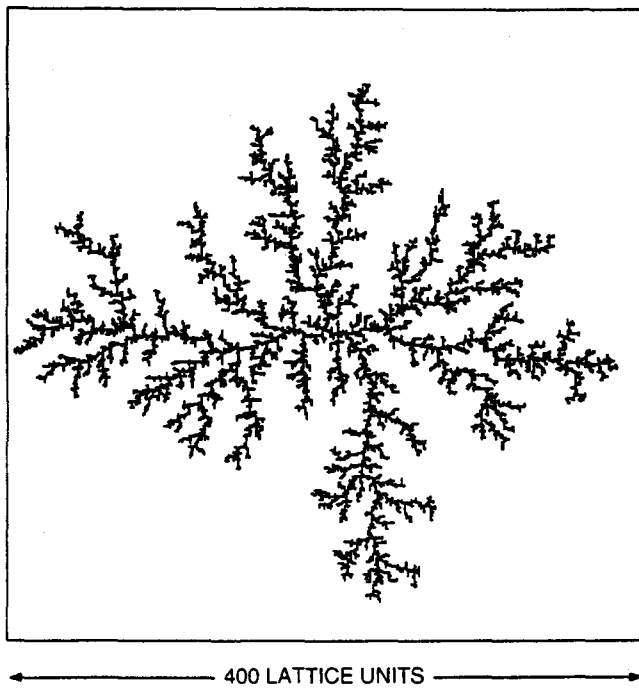


Fig. 22. A cluster of 10^4 sites grown on a square lattice using a diffusion-limited aggregation model that illustrated in Figure 21.

initiated the now quite extensive work on fractal aggregates.

In the diffusion-limited aggregation model of Witten and Sander²¹ particles are added, one at a time, to a growing cluster or aggregate of particles via random walk trajectories. Figure 21 illustrates a two dimensional version of this model carried out on a square lattice. At the stage of growth illustrated in Figure 21 a small cluster has already formed. The particles are imagined to have come from infinity but are actually launched from a random position on a circle which just encloses the cluster (in this case this launching circle has a radius of $r_{\max} + 5$ lattice units where r_{\max} is the maximum radius of the cluster measured from the original "seed" or growth site). Two typical random walk trajectories are shown in Figure 21. Trajectory t_1 eventually brings the random walker into an unoccupied perimeter site. At this stage this perimeter site is filled (growth occurs) and a new random walker is launched from the launching circle (whose radius increases as the cluster grows). Trajectory t_2 eventually moves the particle a long way from the cluster and this trajectory is terminated when it reaches the killing circle which has a radius of $3 r_{\max}$ in this simulation (this is satisfactory for small scale simulations but a more typical value for the radius of the killing circle in more recent large scale simulations is $100 r_{\max}$). The procedures described above and illustrated in Figure 21 are repeated many times until a large cluster has grown. Figure 22 shows a cluster of 10^4 particles generated using the model illustrated in Figure 21. The structure shown in Figure 22 does not closely resemble that of the iron particle aggregates¹³² and for this purpose the DLA model has been superceded by cluster-cluster aggregation models.^{29-31,133-139} The DLA model is, however, one of the most important models in statistical physics since it appears to provide a basis for understanding a broad range of processes including fluid-fluid displacement in porous media, dielectric breakdown, the growth of bacterial cell colonies, the dissolution of porous materials and random dendritic growth. Interest in the DLA model has also been maintained at a high level because it represents a major unsolved theoretical problem.

In the DLA model the random walkers are used to simulate a scalar field ϕ that obeys the Laplace equation

$$\nabla^2 \phi = 0. \quad (81)$$

For a random walk on a square lattice the probability that a random walker will visit a site at position (i,j) can be expressed in terms of the probabilities of visiting its nearest neighbors by

$$P(i,j) = 1/4 [P(i-1,j) + P(i+1,j) + P(i,j-1) + P(i,j+1)]. \quad (82)$$

Similarly, if a scalar field ϕ obeying the Laplace equation is discretized onto a square lattice, then $\phi(i,j)$ is given by

$$\phi(i,j) = 1/4 [\phi(i-1,j) + \phi(i+1,j) + \phi(i,j-1) + \phi(i,j+1)] \quad (83)$$

and the Laplace equation can be solved numerically using equation (83) with appropriate boundary conditions. In this case $\phi = 0$ for sites on the perimeter of the clusters (the random walks are terminated if they reach these sites) and $\phi = 1$ on some distant boundary that encloses the cluster. Consequently, the DLA model can be used to represent any random growth process in which the growth probabilities are controlled by a field obeying the Laplace equation. It is because of the central role of the Laplace equation in classical physics that DLA-like processes are important and ubiquitous.

During the past decade substantial advances have been made in the way DLA simulations are carried out.¹⁴⁰⁻¹⁴² The key to these advances is the recognition that if a random walker is enclosed in an empty region with a simple boundary (at the center of a circle or square, for example) the random walk within that region can be replaced by a single step to an appropriately selected position on that boundary. Figure 23 shows a cluster of 10^6 particles grown using a two dimensional off-lattice model. Using a large number (400) of off-lattice clusters of this size a fractal dimensionality of 1.715 ± 0.004 has been obtained from the dependence of the radius of gyration on the cluster size (equation (14)).

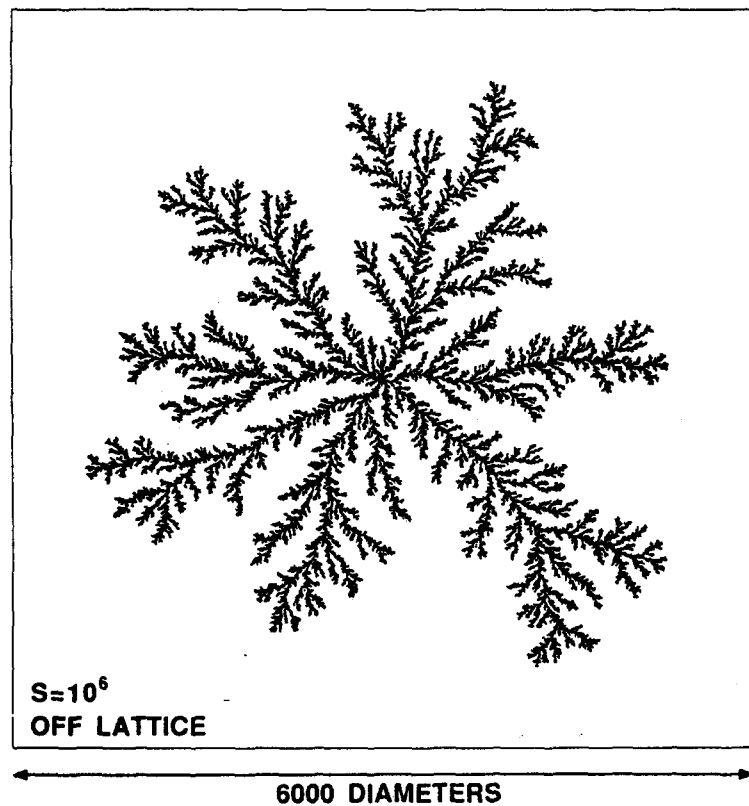


Fig. 23. A cluster of 10^6 particles (discs of equal size) grown using a two dimensional off-lattice version of the diffusion-limited aggregation model.

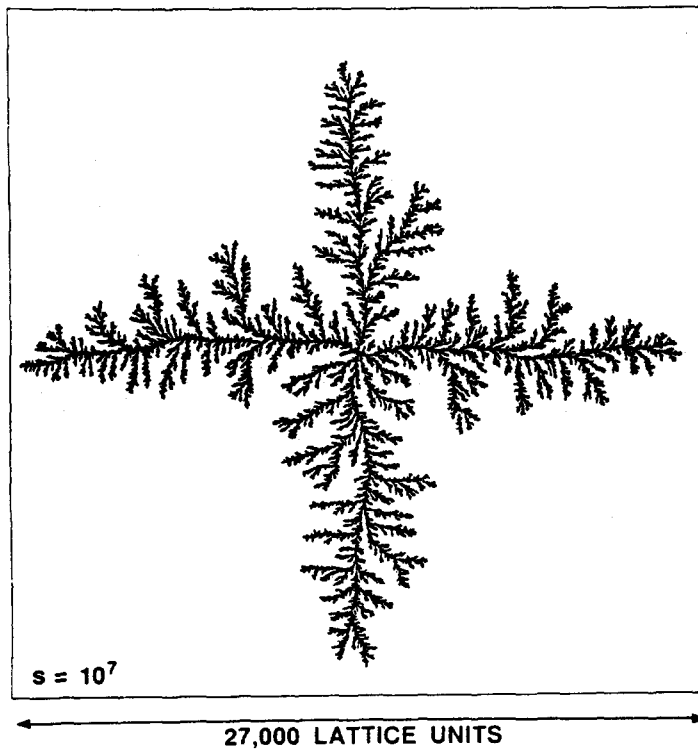


Fig. 24. A cluster of 10^7 sites grown on a square lattice using the diffusion-limited aggregation algorithm of Ball and Brady (ref. 141).

As in the case of the Eden model (see above) the anisotropy of the square lattice has a subtle effect on the overall geometry of small clusters. As the clusters grow in size the consequences of the lattice anisotropy become more apparent. While the cluster shown in Figure 22 quite closely resembles that shown in Figure 23, much larger square lattice DLA clusters have a distinctly cross-like shape. For example, Figure 24 shows a cluster of 10^7 sites generated using the square lattice algorithm of Ball and Brady.¹⁴¹ The effects of lattice anisotropy can be enhanced by noise reduction (see above). Figures 25a and 25b show clusters of 50,000 sites generated on a square lattice using noise reduction parameters (m) of 2 and 3 respectively. These clusters resemble quite closely the much larger cluster shown in Figure 24 that was grown without noise reduction. This observation has led to the idea that the asymptotic shape of square lattice DLA clusters is well represented by finite sized clusters grown with noise reduction. Figures 25c and 25d show 50,000 site clusters grown with larger noise reduction parameters. The overall shape of these clusters is believed to represent the asymptotic $s \rightarrow \infty$ shape of ordinary square lattice DLA clusters. From the dependence of the radius of gyration on the cluster size (equation 15) an effective fractal dimensionality, $D\beta$, much closer to 1.5 than the value of 1.71 found for off-lattice DLA is obtained from simulations carried out using large noise reduction parameters (m). Figure 26

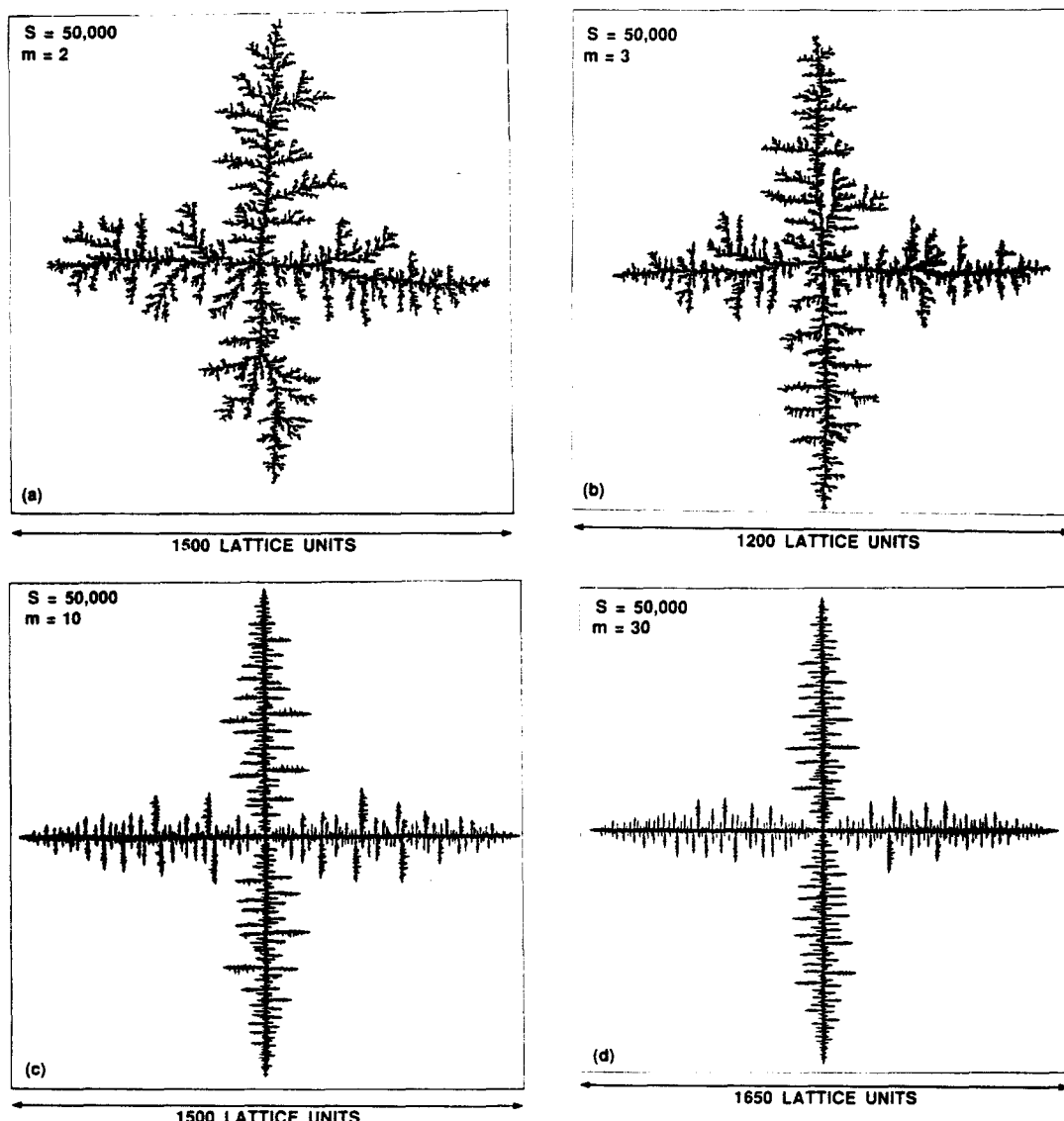


Fig. 25. Relatively small (50,000 site) square lattice DLA clusters grown with noise reduction parameters, m , of 2, 3, 10 and 30 in Figures 25a, 25b, 25c and 25d respectively.

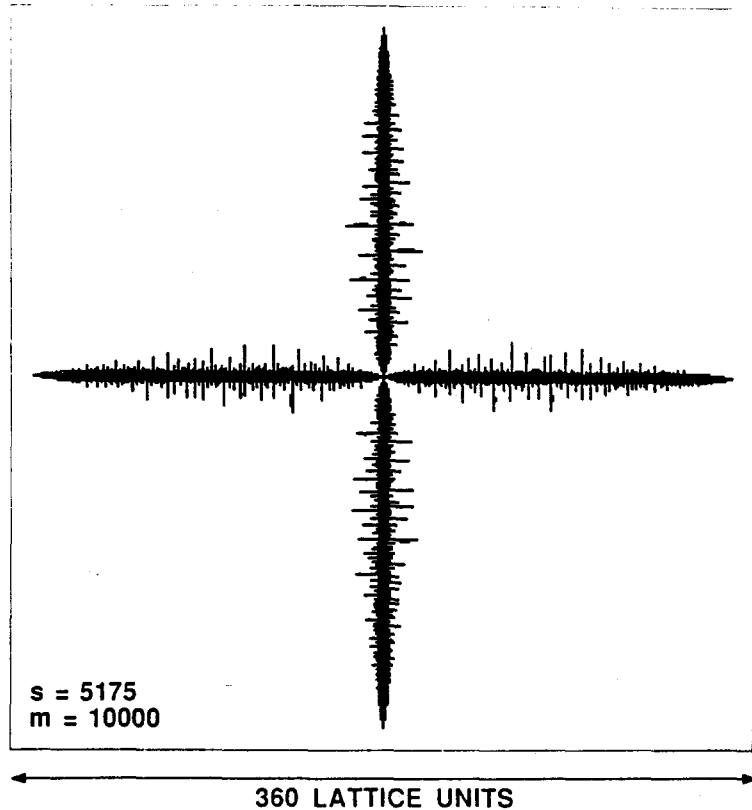


Fig. 26. A cluster of 5175 sites generated on a square lattice using a noise reduced DLA algorithm with a noise reduction parameter (m) of 10,000.

shows a smaller cluster grown with a much larger noise reduction parameter ($m = 10^4$). This cluster does not resemble those shown in Figures 25c and 25d. However, this is attributed to finite size effects and the cluster shown in Figure 26 is expected to evolve into a cluster with the overall shape of those shown in Figures 25c and 25d. A theoretical^{110,111} analysis of noise reduced DLA indicates that the cluster at first grows 4 dense arms that begin to branch when the cluster size reaches a magnitude proportional to $(\log(m))^3$. This prediction is in accord with computer simulation results.¹¹⁰ In Figure 26 the cluster is at a stage just after side branching has begun to occur.

While most diffusion-limited aggregation simulations have been concerned with growth from a single seed or growth site a variety of other boundary conditions have been investigated. One of the most important of these is growth from a flat substrate with periodic boundary conditions in the lateral direction (Figure 27).¹⁴³⁻¹⁴⁶ This might represent processes such as the injection of a low viscosity fluid into a high viscosity fluid along the edges of a Hele Shaw cell containing a porous medium¹⁴⁷ or it might represent a process such as electrodeposition of a metal such as zinc onto a long electrode in a pseudo two dimensional system.^{148,149} The growth of MnO₂ pseudo fossils in sandstone often appear to correspond to this process¹⁵⁰ but their exact origin is uncertain. The deposit generated in this fashion consists of a "forest" of "trees" that are not connected to each other. It is natural to investigate the size distribution of these trees. Racz and Vicsek¹⁵¹ suggested that the tree size distribution could be expressed in the form

$$N_s \sim s^{-\tau} f(s/s^*) \quad (84)$$

where s^* is a characteristic size corresponding to the size of the largest clusters (tree) in the system and $f(x)$ is a cut-off function with the characteristic $f(x) = \text{const.}$ for $x \ll 1$, $f(x) \ll 1$ for $x \gg 1$. Assuming that the deposit

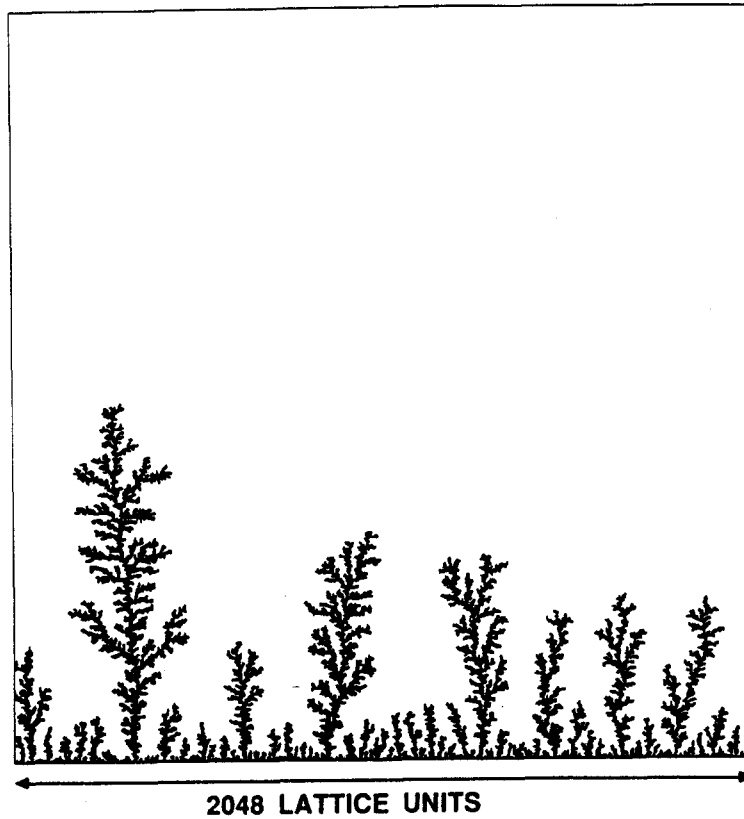


Fig. 27. A pattern generated by a two dimensional square lattice model simulation of diffusion-limited deposition onto a line. Periodic boundary conditions were used in the lateral direction.

shown in Figure 27 has a fractal structure with the same (homogeneous) density correlations as that associated with the structures shown in Figures 22 and 23 then the density profile $\rho(h)$ can be written as

$$\rho(h) = h^{-\alpha} f'(h/h^*) \quad (85)$$

where the exponent α is the codimensionality ($d-D$) and $f(x)$ is a cut-off function similar to the function $f(x)$ in equation (84). Here h^* is characteristic of the maximum height of the deposit. From equations (84) and (85) we can write two expressions for the total mass (M) contained within the deposit.

$$M \sim \int_0^\infty \rho(h) dh \sim h^{*(1-\alpha)} \quad (86)$$

$$M \sim \int_0^\infty s N_s ds \sim s^{*(2-d)} \quad (87)$$

It also follows from the assumption that the density correlation within the deposit can be described in terms of the fractal dimensionality D that $s^* \sim h^{*D}$. Consequently, we obtain from equations (86) and (87) the result

$$D(2-d) = 1+D-d \quad (88)$$

or

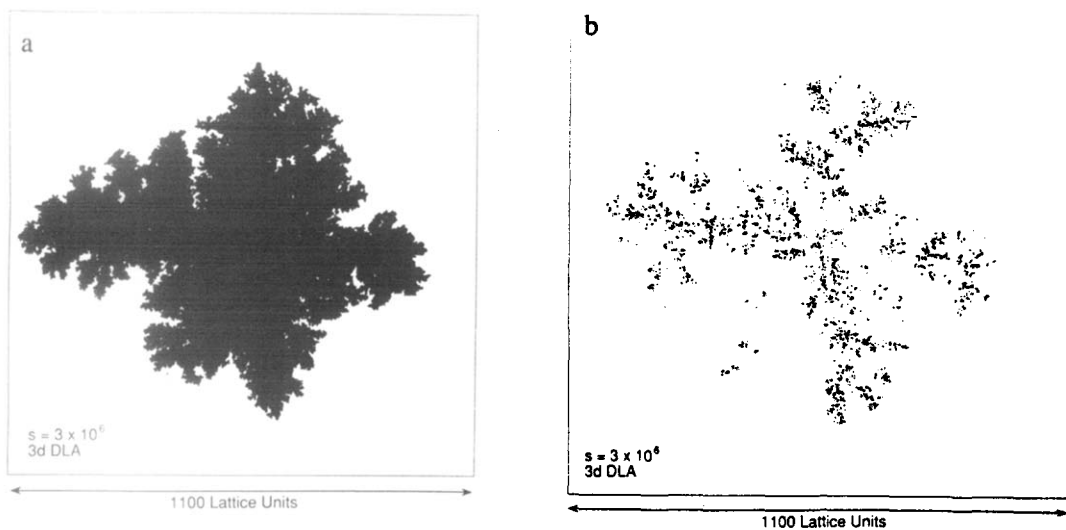


Fig. 28. A projection onto a plane (Figure 28a) and a cross section through the origin (Figure 28b) of a 3×10^6 site cubic lattice DLA cluster.

$$\tau = 1 + (d-1)/D \quad (89)$$

using the values obtained for $D\beta$ from large scale simulation results ($D\beta \approx 1.715$ for $d = 2$, $D\beta \approx 2.50$ for $d = 3$) for the fractal dimensionality D in equation (6) the values $\tau = 1.58$ for $d = 2$ and $\tau = 1.80$ for $d = 3$ are obtained. These results were obtained by Racz and Vicsek¹⁵¹ using essentially the same argument and are in quite good agreement with the results of later computer simulations.¹⁴⁴ However, it now appears that the structure of DLA clusters and deposits are more complex than that suggested by the ideas used to derive equation (89).^{146,152-154}

DLA simulations have also been carried out in spaces and lattices with Euclidean dimensionalities greater than 2.^{142,155,156} For example, Figures 28a and 28b show a projection and cross-section of a 3×10^6 site DLA cluster grown on a cubic lattice and Figure 29 shows a projection onto a plane of a 10^6 site cluster grown on a four dimensional hypercubic lattice. The effects of the lattice anisotropy are quite evident in these figures. Off-lattice and hypercubic lattice model simulations give values for the fractal dimensionality that are in quite good agreement with the predictions of non-rigorous mean field theories.^{117,157-160}

$$D = (d^2+1)/(d+1) \quad (90)$$

for $3 \leq d \leq 5$. However, the results for $d = 2$ ($D = 1.715 \pm 0.004$) are not consistent with equation (90). A constant (size independent) value of about 1.715 is obtained for clusters of sizes ranging from a few thousand to 10^6 for two dimensional off-lattice DLA. This appears to be by far the most reliable numerical result obtained for DLA and it appears most unlikely that the asymptotic value for $D\beta$ is given by equation (90) ($D\beta = 5/3$). In general, mean field theories for DLA are based on assumptions that are not readily justified. In addition, they do not lead to a satisfactory intuitive physical understanding of the DLA growth process.

A more promising theoretical approach is based on the idea that if the sites with the maximum growth are located on the periphery of the cluster (this is almost obviously true for DLA) then the fractal dimensionality can be calculated from the dependence of the maximum growth probability (P_{max}) on the cluster size.¹⁶¹ If P_{max} and the cluster size, s , are related by

$$P_{max} \sim s^\gamma \quad (91)$$

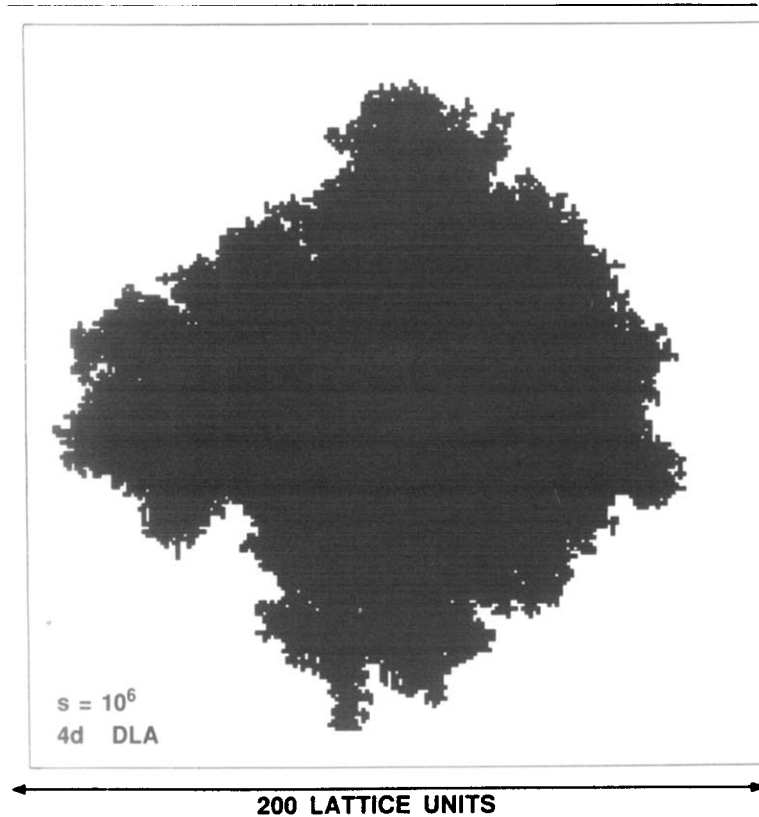


Fig. 29. A projection onto a plane of a 10^6 site DLA cluster grown on a four dimensional hypercubic lattice.

then it follows that

$$\frac{dR}{ds} \sim s^{-\gamma} \quad (92)$$

where R is the cluster radius. For a fractal cluster ($s \sim R^D$) equation (92) implies that

$$D = 1/(1-\gamma). \quad (93)$$

Turkevich and Sher^{113,162} suggested that the exponent γ could be obtained from the asymptotic shape of the cluster envelope. At the time the largest available square lattice DLA clusters consisting of about 10^5 sites had an overall "diamond"-like shape with a characteristic internal vertex angle of 90° . This led Turkevich and Sher to suggest that the asymptotic shape of lattice model DLA clusters reflected the structure of the lattice and that the exponent γ could be obtained by solving the Laplace equation for an absorbing boundary on a wedge with a characteristic angle (θ) determined by the lattice. With this boundary condition (and a fixed value for ϕ , the scalar field obeying the Laplace equation, at infinity) a standard conformal mapping analysis leads to the result

$$P(r) \sim r^{(x-1)} \quad (94)$$

and

$$x = \pi/(2\pi - \theta) \quad (94b)$$

where $P(r)$ is the gradient of the scalar field ϕ normal to the absorbing surface at a distance r from the wedge tip. It follows from equation (94) that the maximum growth probability is given by

$$P_{\max} = \frac{\epsilon}{\xi} r^{x-1} / \int r^{x-1} \quad (95a)$$

or

$$P_{\max} = (\epsilon/\xi)^x \quad (96)$$

where ϵ is the inner cut-off length and ξ is the size of the wedge. For the cluster growth problem the length ξ is proportional to the cluster radius R so that

$$P_{\max} \sim (\epsilon/R)^x. \quad (97a)$$

and

$$P_{\max} \sim s^{-x/D} \quad (97b)$$

so that the exponent γ in equation (91) has a value of x/D . Combining equations (93) and (94b) we have

$$D = 1/(1-x/D) \quad (98)$$

or

$$D = 1 + x = (3\pi - \theta)/(2\pi - \theta). \quad (99)$$

Equation (99) leads to the result $D = 5/3$ for $\theta = \pi/2$ (i.e., for a square lattice). This value for D is in quite good agreement with the effective value of $D\beta$ obtained for clusters containing about 10^5 sites. However, it is clear from Figure 24 that the basic assumption concerning the asymptotic shape of square lattice DLA clusters is not correct. It is now believed that the structure shown in Figure 25d represents the asymptotic form of square lattice DLA. This implies that the effective value for the angle θ in equation (99) is small but non-zero. Consequently, the theoretical approach outlined above indicates that the asymptotic ($s \rightarrow \infty$) fractal dimensionality for square lattice DLA is close to but larger than 1.50. This is consistent with the effective value for D obtained from square lattice DLA simulations carried out using the noise reduced DLA model. A similar but more cautious theoretical picture for square lattice DLA was developed simultaneously by Ball et al. Ball and his collaborators^{115,116} have used similar theoretical approaches to the shapes of DLA clusters (number of arms for which stable growth can occur) and the fractal dimensionality of off-lattice DLA. This work is beyond the scope of this review but it is interesting to note that the value for two dimensional off-lattice DLA obtained in this manner ($D = 1 + \sqrt{2}/2 = 1.707\dots$) is quite close to the value of 1.715 ± 0.004 obtained from large scale simulations and cannot be eliminated on the basis of these simulations.

Using conformal mapping, statistical arguments and scaling analysis a quite detailed description of noise reduced DLA has been obtained,¹¹⁰⁻¹¹¹ including the transition from compact to fractal growth, the shape of the cluster and the shapes of their tips. Unfortunately, it is not clear how this approach can be extended to the off-lattice, fluctuation dominated regime.

The realization that the growth probability distribution for DLA could be described in terms of a multifractal scaling picture^{87,114} led to considerable optimism that this might provide important new insights into the nature of DLA that could lead to a much better theoretical understanding. So far this optimism has not

been justified. While there is considerable interest in the growth probability distribution in DLA¹⁶⁹⁻¹⁷² much of this work has been focussed on the low probability part of the distribution that has little to do with the pattern formation process. While this work may be of importance from an intellectual point of view and may lead to understanding in other areas, it seems unlikely that it will contribute to a better understanding of the DLA growth process.

This summary does not by any means exhaust the theoretical approaches that have been applied to the DLA growth process. However, a more detailed discussion would also be beyond the scope of this review. Additional information can be found in the literature (references 173-177, for example).

In an important generalization of the DLA model^{178,179} the Laplace equation is solved numerically to obtain the local value of the potential ϕ or its gradient at the surface the growing cluster. To represent the growth process, unoccupied perimeter sites are selected randomly with probabilities P_i given by

$$P_i \sim (\phi_i)^\eta \quad (100)$$

or

$$P_i \sim n(\phi_i)^\eta \quad (101)$$

where n is the number of occupied nearest neighbors. Here P_i is the growth probability for the i th site and ϕ_i is the magnitude of the scalar field at this site. The discretized Laplace equation (equation 83) is solved subject to the boundary condition $\phi_j = 0$ for all of the occupied sites and $\phi = 1$ on some distant boundary enclosing the cluster. Since the Laplace equation must be solved after each growth event, this algorithm cannot compete with the DLA algorithm if the growth exponent η in equations (100) and (101) is 1. DLA-like algorithms (using random walkers) can also be used for small integer values of η .¹⁸⁰⁻¹⁸² However, for large η and non-integer values of η there are no practical DLA-like algorithms. These models are called "Laplacian growth" models or dielectric breakdown models. A more complete description of these models can be found in references 179, 180, 183, and 184. The local boundary conditions at the surface of the growing fractals are not the same in the standard DLA and dielectric breakdown models. This is not believed to influence the asymptotic scaling behavior, but it can have a large effect at the early stages of growth (particularly if large noise reduction parameters are used).^{185,186}

The growth probability exponent η in equations (100) and (101) does change the fractal scaling properties of the clusters generated by this model. The fractal dimensionality D changes continuously as η is changed. In the limit $\eta \rightarrow 0$ the Eden model ($D = 2$) is recovered and in the limit $\eta \rightarrow \infty$ the structure becomes linear. However, it is not known if D attains a value of 1 at a finite value of η or only in the limit $\eta \rightarrow \infty$.

Ballistic Growth and Deposition

In the ballistic aggregation model¹⁸⁷ particles are added, one at a time, to a growing cluster or aggregate of particles via randomly selected ballistic (linear) trajectories. The particles are added irreversibly at the position in which they first contact the growing cluster. Off-lattice, square lattice and semi-lattice (off-lattice trajectories with on-lattice growth) models have been developed. Figure 30 shows a cluster of 10,000 particles grown using a three dimensional off-lattice version of this model. Vold¹⁸⁷ carried out pioneering simulations using this model which indicated that the number of particles $N(\lambda)$ within a distance λ measured from the first particle ("seed" particle) in the cluster was given by

$$N(\lambda) \sim \lambda^{2.3} \quad (102)$$

This result could be interpreted in terms of a fractal dimension of 2.3 (compare with equation (20)). However, Sutherland¹⁸⁸ pointed out that the ballistic trajectories used by Vold were not properly selected from a random

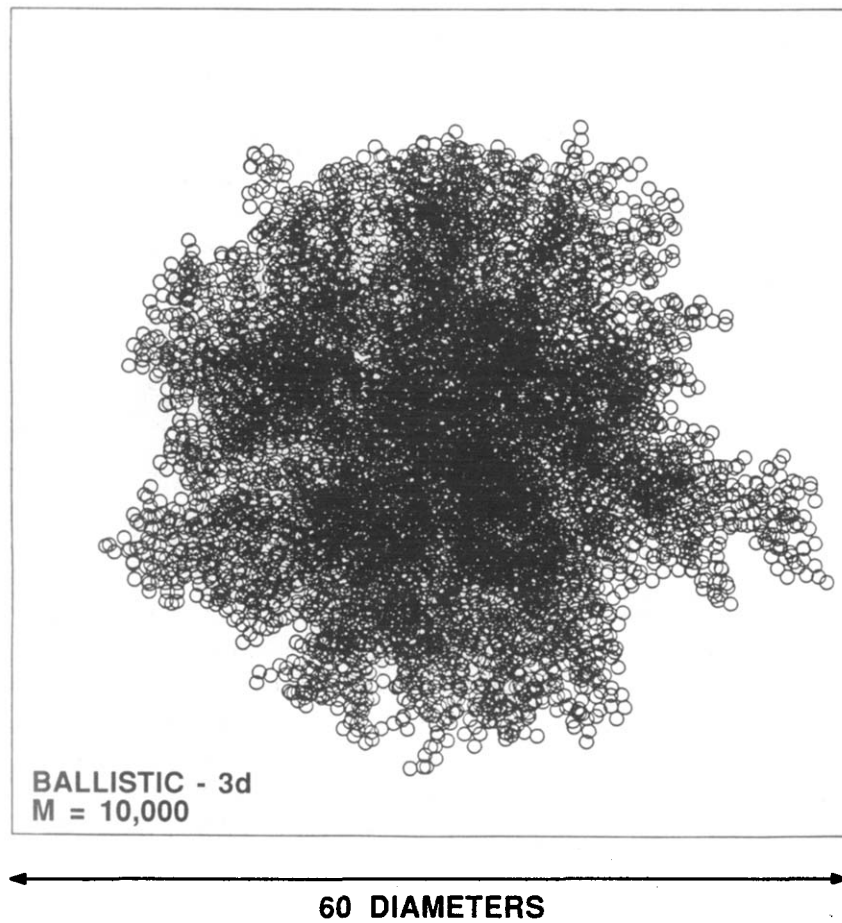


Fig. 30. A cluster of 10,000 particles generated using a three dimensional off-lattice ballistic aggregation model.

distribution and concluded on the basis of simulations carried out using up to 2000 particles that $D = d$ for $d = 2$ and 3. Despite the simplicity of this model, it is not easy to obtain accurate values for the asymptotic fractal-dimensionality because of surprisingly large corrections to scaling. It is only quite recently, on the basis of large scale simulations^{189,190} and theoretical arguments¹⁸⁹ that a consensus that $D = d$ for this model has developed. Two dimensional simulations have also been carried out in which a cluster is grown from a single growth site using randomly selected trajectories, all in the same direction. Quite striking fan-like patterns are generated.¹⁹⁰ Figures 31a and 31b show two of these fans generated using off-lattice and square lattice models that contain 2.5×10^5 particles or sites. These patterns have complex structures that appear to have a hierarchical character (the large fans seem to contain smaller fans). A quantitative description of these patterns has not been found.

Vold^{191,192} also developed a variety of ballistic deposition models to simulate sedimentation processes. Densities of 0.128 to 0.0146 were found for the deposition of anisometric particles with aspect ratios varying from 1-18. Much larger scale simulations give a density of about 0.146 for the deposition of spherical particles.¹⁹³

Figure 32 shows the results of a two dimensional simulation of ballistic deposition on a square lattice using vertical "particle" trajectories. The internal structure is complex (like that in the center of the "fans" shown in Figure 31) but is uniform on all but short length scales. The structure of the surface, on the other hand, shows roughness on all length scales and has the scaling properties of a self-affine fractal. This aspect of the ballistic deposition model will be described below in more detail.

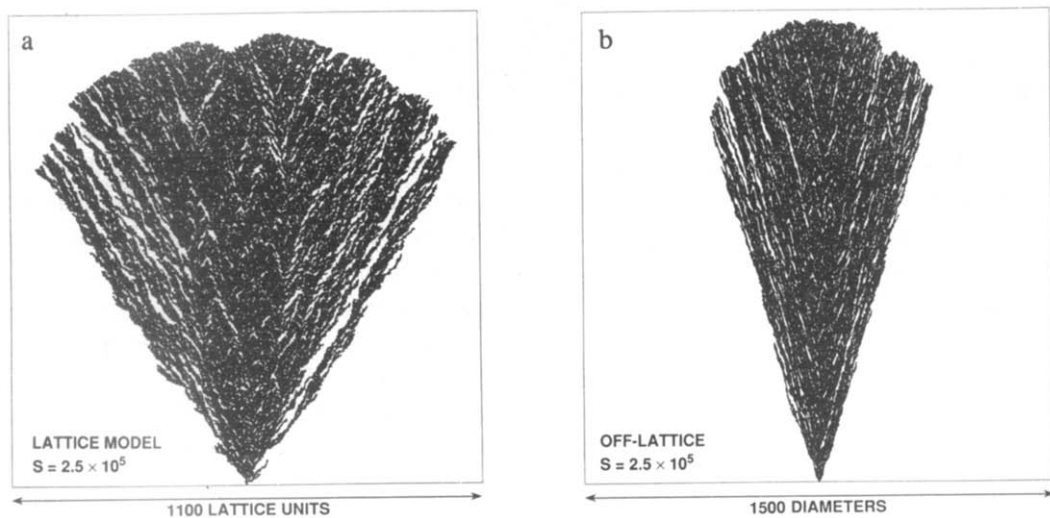


Fig. 31. Fan-like patterns generated by ballistic deposition. The structures are generated via a random ballistic deposition process with vertical particle trajectories starting at the top of these figures. Figure 31a and 31b show clusters of 2.5×10^5 sites or particles generated using square lattice and off-lattice models respectively. This figure illustrates that the characteristic "fan angle" is not a universal quantity.

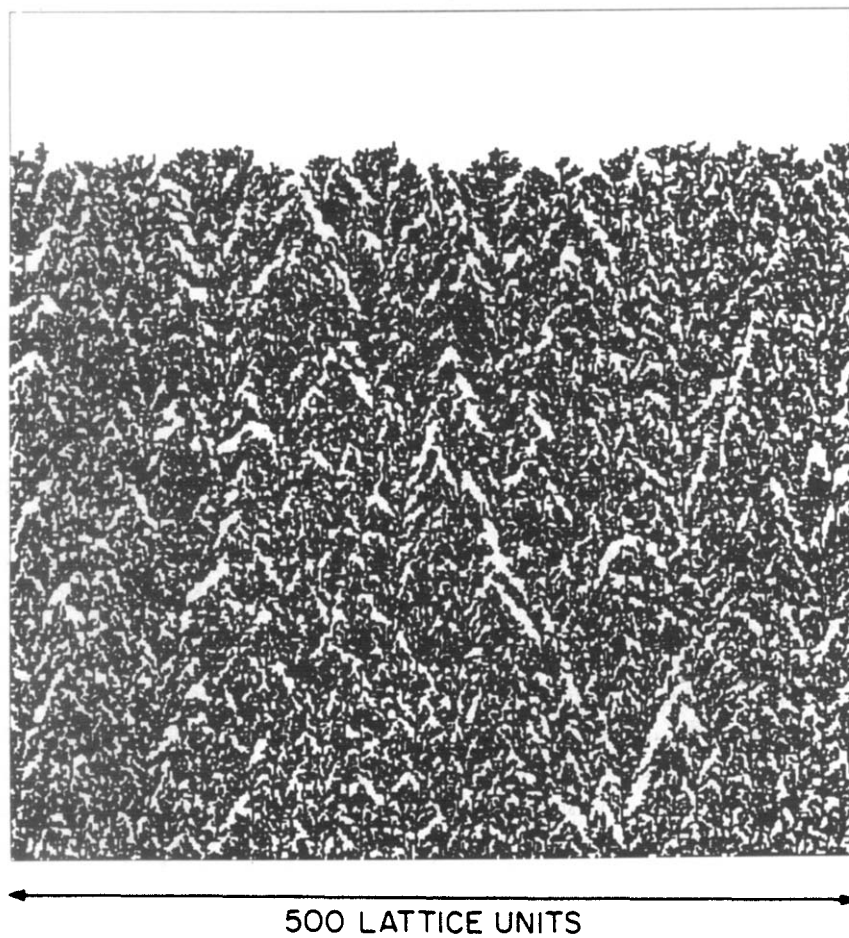


Fig. 32. The structure resulting from a two dimensional square lattice mode for ballistic deposition onto a substrate. In most simulations periodic boundary conditions are used in the lateral direction. Here a small portion of a deposit grown on a wide substrate is shown.

Percolation Fractals

The percolation model that has been briefly described in the introduction is one of the most important models in statistical physics. It has been used to represent a broad variety of structures including polymer gels, porous materials, ion exchange membranes, biological structures, composite materials and alloys and has been used to help understand a broad range of phenomena associated with these structures (conductivity and other transport processes, mechanical properties, dissolution, dielectric breakdown, the spreading of disease and fires to name just a few). A discussion of even a few of these applications would be beyond the scope of this review. The discussion in this section will be restricted to illustrating how fractal geometry can be used to describe the structures generated by this very simple model. This geometric description leads to a much better intuitive understanding of the nature of percolating systems and processes occurring in, on and around them. The concepts of fractal geometry can also be used in more rigorous fashion to obtain a deeper theoretical understanding of these structures and phenomena. In considering the physical and chemical properties of percolating systems, it is important to recognize that if a fraction $p \leq p_c$ of the sites on a lattice are filled, the total system will appear to be uniform on all but very short length scales. The holes in large clusters will be filled by smaller clusters so that the density-density correlation function $C(r)$ will be essentially independent of r . Consequently, the fractal nature of the system will not be revealed by experimental methods such as small angle scattering or image analysis of a cross-section through the system. To see the fractal nature of the large clusters they must be separated from each other and the small clusters or "labeled" in some way so that their internal connectivity is revealed. For example, in the case of a polymerizing system near to the gel point the gelation processes can be halted and the clusters can be separated by dilution. It may be possible to obtain information concerning the largest ("infinite") cluster properties such as conductivity and elasticity that do depend on connectivity. However, the close proximity of clusters of different sizes will, in many cases, obfuscate interpretation of the results.

Since fractal structures interact with their environment through their surfaces, considerable interest has developed in the characterization of the surface structure and the application of fractal geometry in areas such as catalysis, adsorption, electrochemistry and tribology.

Figure 33 shows a small "percolation cluster" of 8827 sites grown on a square lattice. For such a complex structure there is no unique definition of the surface. Figures 33b and 33c show two different "surfaces" of the percolation cluster. The surface shown in Figure 33b is known as the hull¹⁹⁴ of the percolation cluster. This hull can be found by starting a nearest neighbor (NN) walk at an occupied site with an extreme value for its x or y coordinate. The walk proceeds in clockwise direction and at each step the walk advances in the most counterclockwise direction possible. This process is like walking around the shore of a lake. The walk continues until it eventually returns to its origin and the sites visited by the walk constitutes the hull. The hull can also be defined as all of those occupied sites that are adjacent (NN or next nearest neighbors) to unoccupied sites that can be reached by paths consisting of NN or next nearest neighbor (NNN) steps between unoccupied sites starting from a position outside of the region occupied by the cluster. The perimeter shown in Figure 33b was obtained using both procedures. Although the hull of the small cluster shown in Figure 33b contains most of the sites in the entire cluster, the asymptotic fractal dimensionality of the hull is smaller than that of the cluster and in the limit $s \rightarrow \infty$ the hull occupies a negligible fraction of the cluster sites.

The surface shown in Figure 33c is the outer hull of the percolation cluster. This surface consists of all of those occupied sites that are adjacent (NN or NNN) to unoccupied sites that can be reached from "infinity" by paths consisting only of nearest neighbor steps between unoccupied sites. Figure 33d shows the paths consisting of nearest neighbor steps only and Figure 33e shows the paths consisting of NN and NNN steps. These are the paths used to find the external hull and the hull of the percolation clusters. Theoretical arguments¹⁹⁵⁻¹⁹⁷ indicate that the fractal dimensionality for the two dimensional percolation hull is equal to $7/4$ ($1+1/v$) and this result is consistent with those obtained from computer simulations.^{194,197,198} The outer hull has a much smaller fractal dimensionality¹⁹⁹ and a theoretical value of $4/3$ (v)¹⁹⁵⁻¹⁹⁷ has been established. These values

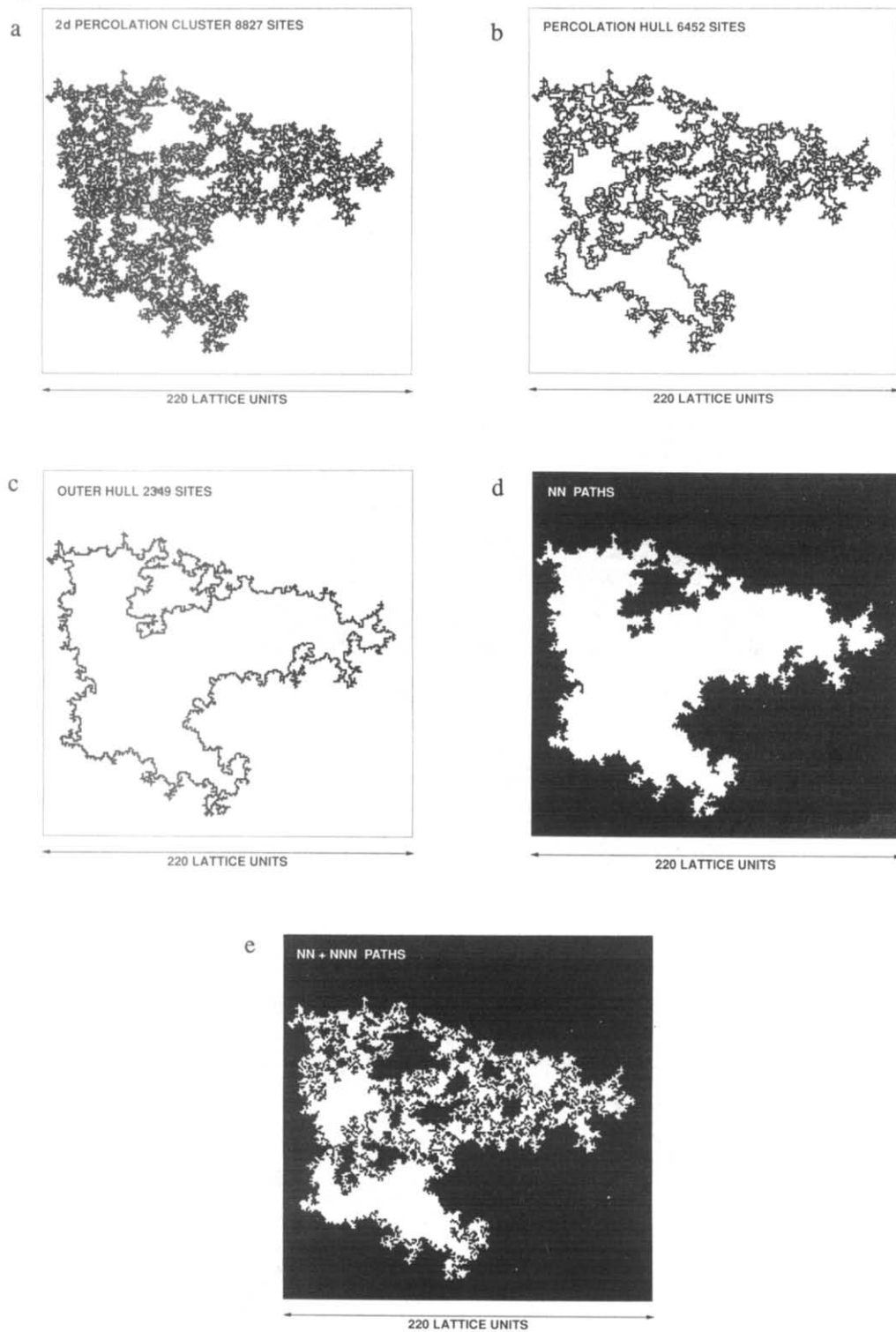


Fig. 33. Two of the many surfaces of a percolation cluster. Figure 33a shows the cluster itself. Figures 33b and 33c show the hull and outer hull of the cluster. Figures 33d and 33e show the NN and NN+NNN paths on unoccupied sites (starting from "infinity") that can be used to find the external hull and the hull respectively.

are regarded as being exact but non-rigorous.

Many other fractal subsets of the percolation cluster have been identified. These include the skeleton,²⁰⁰ the backbone²⁰¹ and the "singly connected" or "red" sites²⁰² (those sites that if removed would cut the cluster into two clusters). Identification of these fractal substructures and determination of their fractal properties plays an important role in the development of a better understanding of processes occurring on percolation fractals.

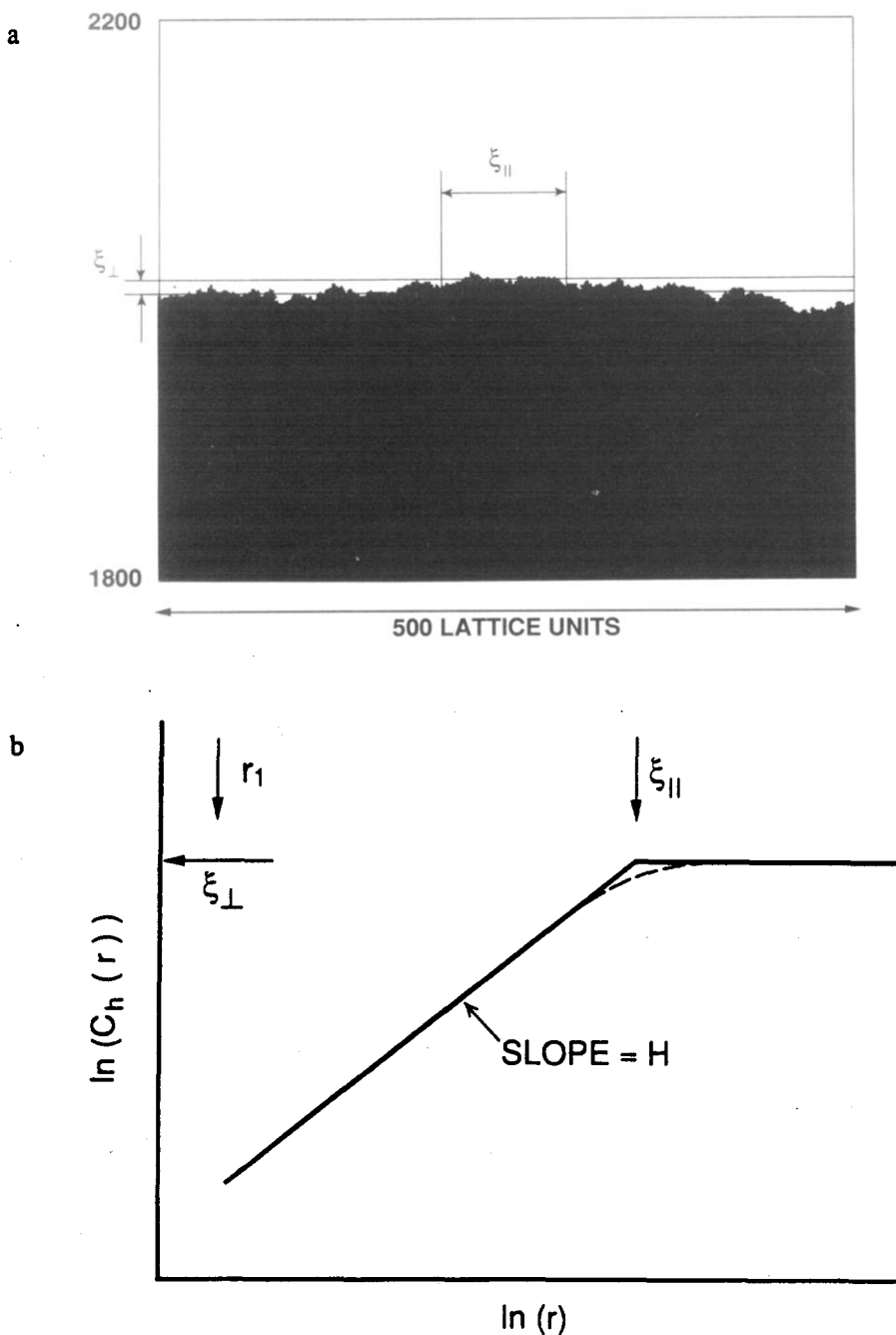


Fig. 34. Characterization of rough surfaces using the correlation lengths (ξ_{\parallel} and ξ_{\perp}) and the correlation function $C_h(r)$. Figure 34a illustrates the definitions of ξ_{\parallel} and ξ_{\perp} . Figure 34b shows a schematic representation of the height difference correlation function ($C_h(r)$) for a self-affine fractal surface. ξ_{\parallel} and ξ_{\perp} are the correlation lengths that limit the range of fractal scaling.

Models for the Growth of Rough Surfaces

Rough surfaces play a central role in many processes of importance in solid state physics and chemistry. Chemical reaction, phase transformation processes and transport processes frequently occur at rough surfaces or interfaces that can be described in terms of self-similar or self-affine fractal geometry. It appears that self-affine surfaces are much more common than self-similar surfaces. In many processes (erosion, deposition and wear, for example) an initially smooth surface evolves into a rough surface at a more or less constant rate. The growing surface roughness can frequently be described in terms of the correlation lengths $\xi_{||}$ and ξ_{\perp} (Figure 34a) parallel and perpendicular to the overall plane of the surface (parallel to the original substrate). The length ξ_{\perp} describes the amplitude of the surface roughness or the "thickness" of the surface. The length $\xi_{||}$ describes the lateral distance over which correlations in the deviation of the surface height ($h(x)$) from the average height $\langle h(x) \rangle$ persist.

The growth of these lengths is often algebraic

$$\xi_{\perp} \sim t^{\beta} \quad (103)$$

$$\xi_{||} \sim t^{1/z}. \quad (104)$$

For a self-affine surface the exponents β and $1/z$ are, in general, different and the correlation lengths ξ_{\perp} and $\xi_{||}$ are related by

$$\xi_{\perp} \sim \xi_{||}^{\alpha} \sim \xi_{||}^{\beta z} \quad (105)$$

where the exponent α is equivalent to the Hurst exponent (H). In some cases (such as a surface generated by ballistic deposition at grazing incidence) three correlation lengths (ξ_x , ξ_y and ξ_z) and three exponents (v_x , v_y and v_z) may be needed to describe the growth of the surface roughness.²⁰³

Surfaces of this type can be described in terms of the height difference correlation function $C_h(r)$ defined as

$$C_h(r) = \langle |h(x) - h(x+r)| \rangle |r| = r. \quad (106)$$

For a self-affine fractal this correlation function is expected to have the power law form

$$C_h(r) \sim r^H \quad (107)$$

for distances r that are larger than an inner cut-off length r_1 and smaller than the lateral correlation length $\xi_{||}$ (see Figure 34b). For surfaces that do not have single valued heights it is often sufficient to use the largest height at position x for $h(x)$ in the height difference correlation function. Very similar results can be obtained using other correlation functions like that given in equation (39).

For a system in which the lateral correlation length ($\xi_{||}$) is not confined to values smaller than L (as a result of finite size effects or physical processes) $\xi_{||}$ will grow according to equation (104) until the length L is approached. The dependence of the correlation length ξ_{\perp} (ξ) on L and t can then be represented by the scaling form²⁰⁴

$$\xi(L,t) \sim L^{\alpha} f(vL^{\alpha/\beta}) \quad (108)$$

$f(x) \rightarrow \text{const.}$ for large values of x , so that $\xi \sim L^{\alpha}$. In the limit $x \ll 1$ $f(x)$ increases as a power of x . For small

values of $x \xi_{\parallel} \ll L$ so that ξ should depend only on t and from this it follows that $f(x) \sim x^\beta$ and $\xi \sim t^\beta$ (equation (103)). These results are generally valid for the constant growth of a self-affine rough surface from an initially smooth planar surface.

Simple Models for the Growth of Self-Affine Rough Surfaces

A variety of simple models have been developed to simulate the growth of rough surfaces. Some of these models lead to the generation of "smooth" surfaces (smooth in the sense that the correlation length $\xi(\xi_{\perp})$ grows at most logarithmically with increasing time or height). However, most of these models lead to surfaces that can be described in terms of self-affine fractal geometry. The most extensively explored models are based on the Eden model and ballistic aggregation model for cluster growth described above. A simple two dimensional model for ballistic deposition is illustrated in Figure 35. In this model all of the sites in the lattice with a zero height (Y coordinate for $d = 2$ or Z coordinate for $d = 3$) are filled at the start of a simulation to represent a planar substrate. Columns of the lattice are then selected at random and if the i th column has been selected then the site in that column of the lattice at a height h'_i is given by

$$h'_i = \max(h_{i-1}, h_i+1, h_{i+1}) \quad (109)$$

is filled. This process is repeated many times to generate a deposit. For the three dimensional case (deposition onto a planar substrate) the height of the new site in the randomly selected columns with (lateral) coordinates (i,j) is given by

$$h'_{i,j} = \max(h_{i-1,j}, h_{i+1,j}, h_{i,j+1}, h_{i,j-1}, h_{i,j+1}) \quad (110)$$

This simple model generates structure which resemble those formed by processes such as sedimentation, vapor deposition onto cold surfaces²⁰⁵⁻²¹⁰ and the deposition of supercooled water droplets onto cables,²¹¹ airplane wings, etc.

Because of both the simplicity of these algorithms and their minimal storage requirements (only the maximum occupied heights or the height of the active zone in each column needs to be stored) quite large deposits can be generated (10^{10} or more sites on a conventional mainframe computer and as many as 10^{12} sites on special purpose computers²¹²). Part of a deposit generated by a relatively small scale two dimensional simulation is shown in Figure 32. The structures generated by these simple ballistic deposition models have quite low densities ($\rho \approx 0.467$ and 0.300 for the two dimensional and three dimensional lattice models with nearest neighbor sticking and $\rho \approx 0.357$ and 0.147 for the corresponding off-lattice models) but are uniform on all but quite small length scales. For porous structures such as these the "surface" can be defined in many ways. Here we focus attention on the "upper surface" consisting of the highest occupied site in each column. The surface width or thickness $\xi(\xi_{\perp})$ can then be defined as

$$\xi^2 = \frac{1}{N} \sum_{i=1}^N (h_i - \langle h_i \rangle)^2 \quad (111)$$

where N is the number of columns in the lattice. A similar quantity ξ_a (the width of the active zone) can be defined using the heights of the active zone sites instead of the maximum heights. The height of the active zone site in each column is the height at which a new site can be added. The quantities ξ and ξ_a are very closely related and serve equally well as a measurement of the perpendicular correlation length. The exponent β in equation (103) can be measured from the dependence of ξ or ξ_a on the mean deposit height, $\langle h \rangle$, or on the time, t (the average number of deposition events per column). The exponent α (the Hurst exponent) can be measured by growing the deposit in a channel or strip of width L with periodic boundary conditions. As the deposition

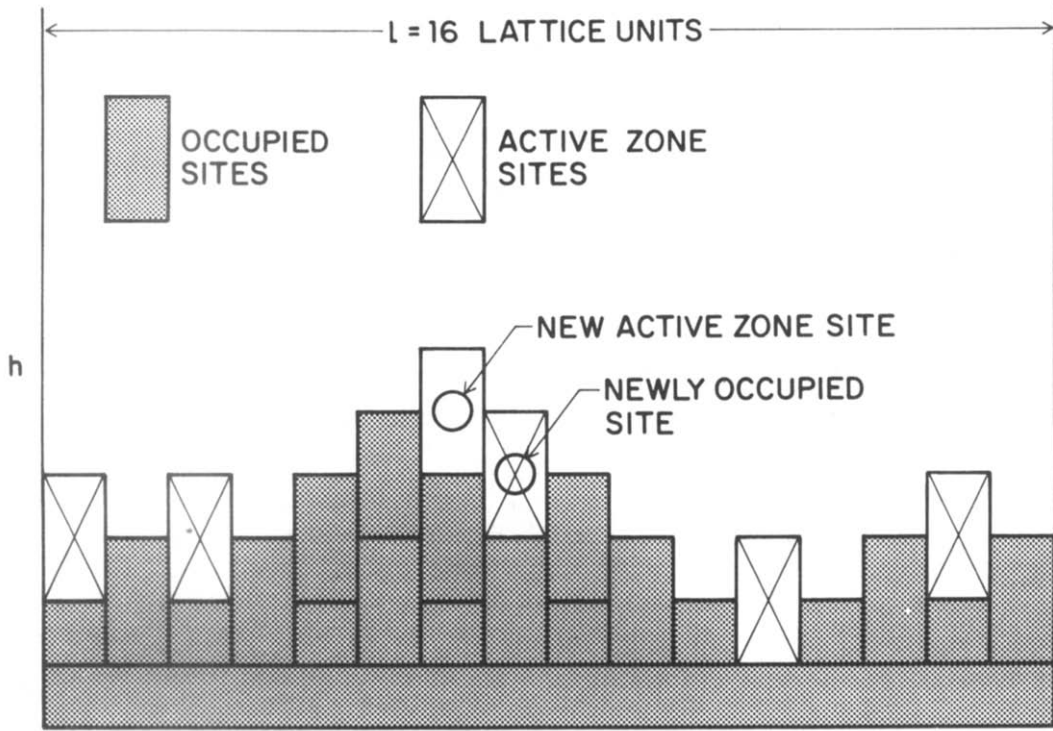


Fig. 35. The restricted step height ballistic deposition model.

process continues the horizontal correlation length ξ_{\parallel} grows until it reaches a value of L and then ceases growing. After this stage the perpendicular correlation length ξ_{\perp} (ξ) is measured and the dependence of ξ_{\perp} on ξ_{\parallel} can be obtained via dependence of ξ (or ξ_a) on L by carrying out a series of simulations using strips of different widths. These methods evaluate α and β separately by approaching limits $x \gg 1$ and $x \ll 1$ respectively where $x = t/L^{\alpha/\beta}$. An alternative (and quite satisfactory) approach would be to measure the dependence of ξ on t and L in the $x \approx 1$ regime. The exponents α and β could then be determined via a data collapse using the scaling form given in equation (108). Because of large corrections to scaling accurate measurement of the exponents α and β is difficult. In addition, the fluctuation in ξ becomes very large in the $x \gg 1$ limit for large values of L and statistical uncertainties are also quite large. Family and Vicsek²⁰⁴ obtained values of 0.42 ± 0.03 and 0.30 ± 0.03 for α and β respectively for two dimensional ballistic deposition. Values much closer to the theoretical values²¹³ of $1/2$ and $1/3$ have been obtained from larger scale simulations.²¹⁴ The effect of these corrections to scaling can be very much reduced by using the model illustrated in Figure (35). In the two dimensional version of this model the initial height is zero in odd numbered columns and 1 in even numbered columns. Growth is only allowed in minima sites (sites for which both nearest neighbor columns have a greater height). The minima sites are selected randomly and their heights are increased by two lattice units. In this way the height difference between adjacent columns is always ± 1 and the deposit is dense. Figures 36a and 36b show the dependence of ξ on L in the limit where $h \gg L^{\alpha/\beta}$ (or the argument, x , of the scaling function in equation (108) is much greater than 1) obtained from the two dimensional model illustrated in Figure 35 and the corresponding three dimensional model. Using these models the results $\alpha = 0.503 \pm 0.001$, $\beta = 0.300 \pm 0.012$ were obtained for $d = 2$ and $\alpha = 0.363 \pm 0.005$, $\beta = 0.230 \pm 0.001$ was obtained from the three dimensional model.²¹⁴ Here the uncertainties are the standard errors of least squares fits. This procedure ignores correlations between data points and underestimates the uncertainties for β . In addition, systematic errors (finite size effects) may be much larger than the statistical uncertainties despite the reduction of these uncertainties in the restricted step height model.

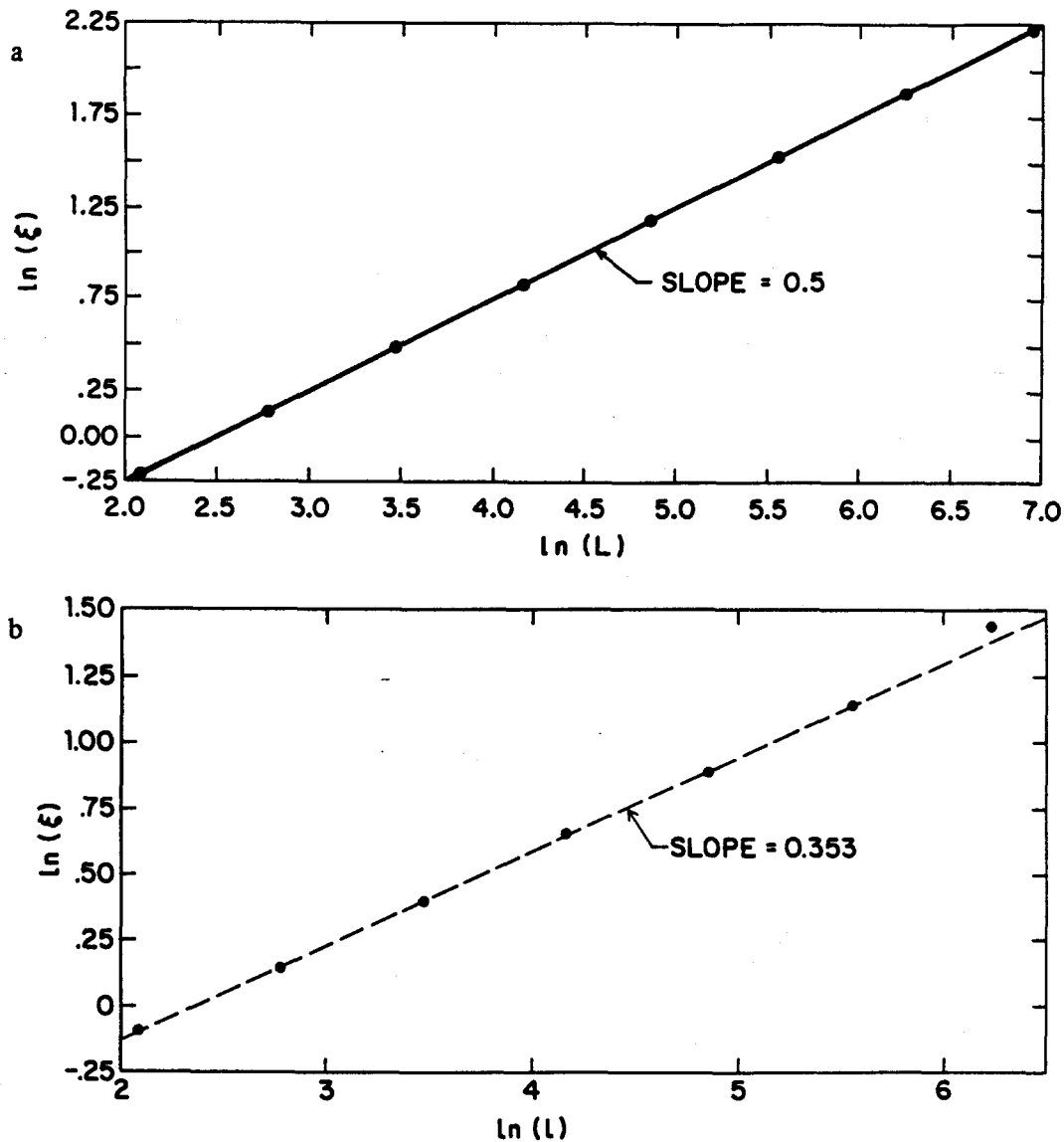


Fig. 36 Dependence of the surface thickness, ξ , on system width L for the two dimensional restricted step height models illustrated in Figure 35 (Figure 36a) and a corresponding three dimensional model (Figure 36b) in which step heights are restricted to ± 1 lattice units.

Using a quite similar model Kim and Kosterlitz²¹⁵ obtained the results $\beta = 0.332 \pm 0.005$, 0.250 ± 0.005 , 0.20 ± 0.01 and $\beta \approx 1/6$ for $d = 2, 3, 4$, and 5 respectively. Values of 0.5000 ± 0.0005 and 0.40 ± 0.01 were obtained for the exponent α for $d = 2$ and $d = 3$. The results from both of these ballistic deposition models and the model illustrated in Figure 35 satisfy the theoretical scaling relationship^{214,216,217}

$$\alpha + \alpha/\beta = 2 \quad (112)$$

quite well. Kim and Kosterlitz conjectured that $\beta = 1/(d+1)$ based on their simulation results. However, there are other conjectures²¹⁸ and at present there are no rigorous or exact results for $d > 2$.

Figure 37 shows cross sections parallel to the substrate through the rough surfaces generated by the three dimensional restricted step height model. These figures show the intersections of the surfaces with a plane at the

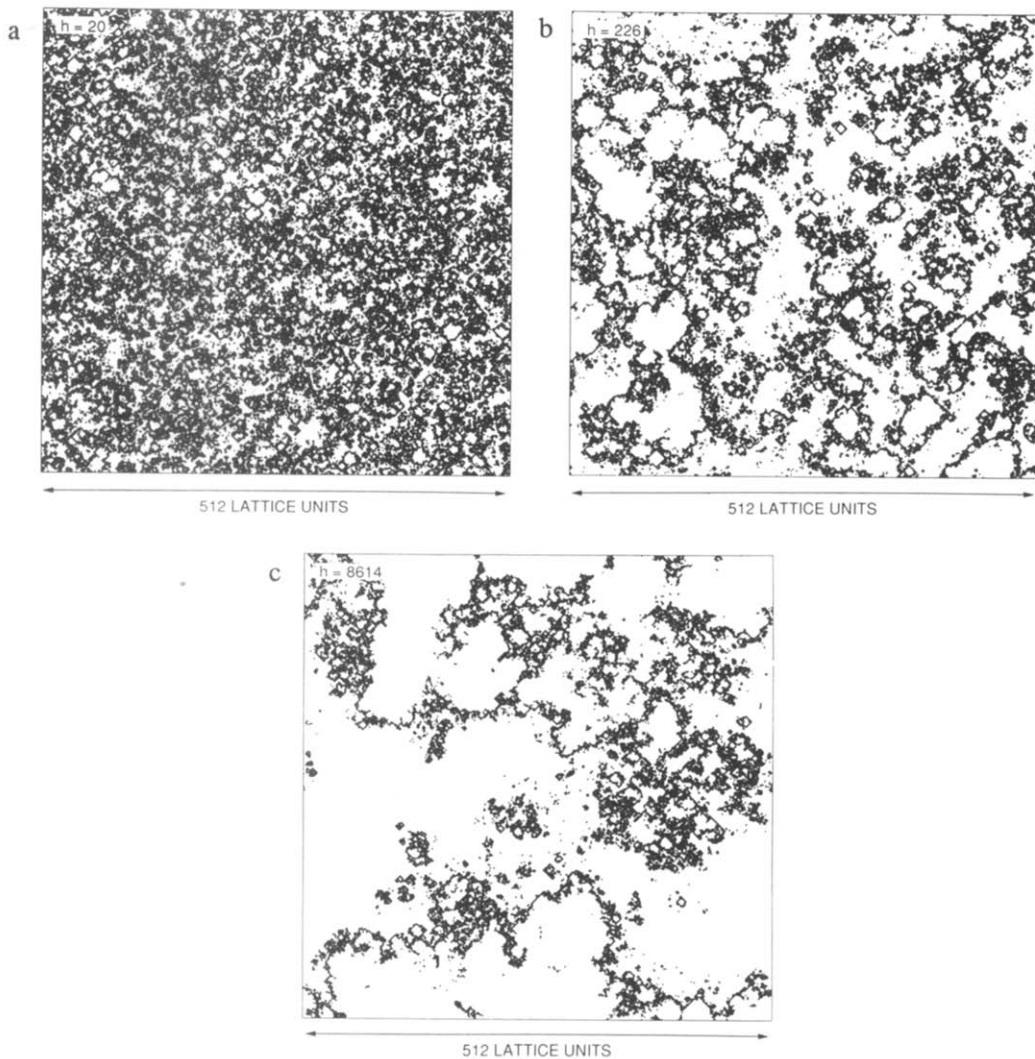


Fig. 37 Cross sections through the surfaces generated using a three dimensional ballistic deposition model in which the step heights in the surface are restricted to ± 1 lattice units. Here 3 cross sections are shown parallel to the substrate at the mean surface height. The mean surface heights are 20, 226 and 8614 lattice units in Figures 37a, 37b and 37c respectively.

mean surface height $\langle h \rangle$. Figures 37a, 37b and 37c show these intersections at stages where the deposit height had reached values of 20, 226 and 8614 lattice units respectively. Figure 38 shows the two point density-density correlation functions at more frequent intervals obtained from simulations similar to those shown in Figure 37. These correlation functions show a power law form ($C(r) \sim r^{-\alpha}$) on short length scales crossing over to a constant value at larger values of the distance r ($r > \xi_{||}$). The exponent α has a value of 0.34 corresponding to a fractal dimensionality D_α of 2.66. These results are consistent with the idea that the intersection of a self-affine fractal with a planar surface in the "parallel" direction should be a self-similar fractal with a fractal dimensionality of $d-H$ where H is the Hurst exponent. The value for $H(\alpha)$ obtained in this manner is in good agreement with that obtained more directly (see Figure 36). The results in Figure 38 suggest that the correlation function can be represented by the scaling form

$$C(r,t) \sim t^{-\beta} f(r/t^{\beta/\alpha}) \quad (113)$$

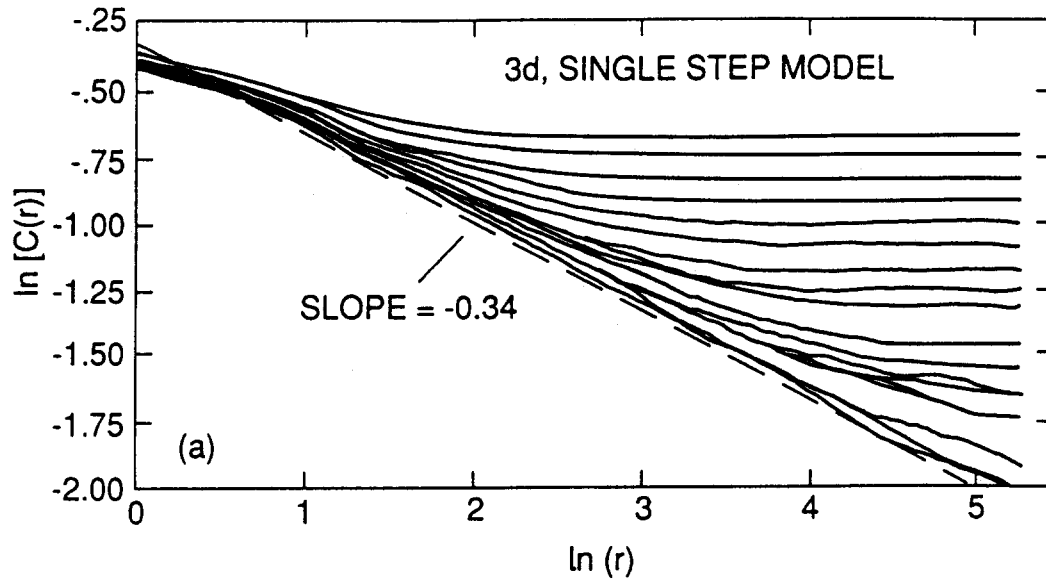


Fig. 38 Density-density correlation functions obtained from cross sections through the surfaces of deposits formed by a cubic lattice model for deposition onto a planar substrate. These results were obtained from a model in which the step heights in the surface were restricted to ± 1 lattice units. This figure was obtained from 2 simulations carried out using substrates of size 1024×1024 (LxL) lattice units. The density-density correlation functions $C(r)$ are shown for 18 mean height levels (times) in the range $20 \leq h \leq 19382$ lattice units ($10 \leq t \leq 9691$).

where the scaling function $f(x)$ has the form $f(x) \sim x^{-\alpha}$ for $x \ll 1$ (so that $C(r,t) \sim r^{-\alpha}$ for $r < \xi_{||}(t)$) and $f(x) = \text{const.}$ for $x \gg 1$ (so that $C(r,t) \sim t^{-\beta}$ for $r > \xi_{||}(t)$).

The ballistic deposition and Eden models appear to be very closely related. In both cases the interior structure is uniform on all but very short length scales and the dependence of the surface thickness ξ on L and t can be represented by the scaling form given in equation (108).^{122,123,204} Computer simulations indicate that, for $d = 2$, the exponents α and β have the same values for the Eden model as for the ballistic deposition model. Despite the simplicity of these models, it is very difficult to get good results for $d > 2$. Kertesz and Wolf^{219,220} suggest that there are two contributions to the surface thickness ξ an intrinsic width that depends on local structure of the growth or deposit and a long wavelength contribution described by equation (108). They suggest that equation (108) can be modified to give

$$\xi^2(L,t) = [aL^\alpha f(t/L^\alpha/\beta)]^2 + \omega^2 \quad (114)$$

where ω is the intrinsic width that is the major source of corrections to the scaling form given in equation (108). They found that the width ω can be controlled by a judicious use of noise reduction (see above). These simulation results suggest that the intrinsic width ω is proportional to $1/m$ where m is the noise reduction parameter. The amplitude, a , of the long wavelength fluctuations in equation (114) also depends on m but it appears to have an m independent part. Using noise reduction, Wolf and Kertesz obtained the results $\alpha = 0.33 \pm 0.01$, $\beta = 0.22 \pm 0.02$ for $d = 3$ and $\alpha = 0.24 \pm 0.02$, $\beta = 0.146 \pm 0.015$ for $d = 4$ from quite small scale simulations. This led them to suggest that the exponent α (the Hurst exponent) might have a value of $1/d$. If we assume the scaling relationship in equation (112) to be correct, then the Wolf/Kertesz conjecture for the Eden model is not consistent with the Kim/Kosterlitz conjecture for the ballistic deposition model $(1/d + (d+1))/d \neq 2$ except for $d = 2$). All of the numerical results are consistent with equation (112) that is believed to be correct for ballistic deposition and Eden growth models. Wolf and Kertesz^{219,220} obtained good results for the exponent β (0.33 ± 0.015) from quite small scale two dimensional simulations. The intrinsic width, ω , depends on model

details such as the local growth rules or step height restrictions. Equation (114) indicates why the magnitude of correction to scaling depends on such model details.

The growth of rough surfaces and interfaces such as those generated by the ballistic deposition and Eden models can be described by a Langevin equation for the evolution of the surface²¹³.

$$\frac{\partial h(x,t)}{\partial t} = V \nabla^2 h(x,t) + \lambda (\nabla h(x,t))^2 + \eta(x,t). \quad (115)$$

The first terms on the right hand side of equation (115) represent the effects of diffusion, restructuring and lateral growth and the last term represents the random deposition of material onto the surface. Here $\eta(x,t)$ is a random process that, in the most simple case, has a Gaussian distribution with no temporal or spatial correlations. The second term on the right hand side in equation (115) has quite different origins²²¹ in the ballistic deposition and Eden models. In the ballistic deposition model this term arises because the deposit density is smaller (and hence the rate of increase in the surface height is larger) as the angle of incidence increases^{193,222-224} from zero degrees (normal incidence). In the Eden model this term arises because there are more growth sites in an inclined surface than in a flat surface. (Growth at a constant velocity normal to an inclined surface increases the height more rapidly than growth at the same velocity normal to a horizontal surface). In the restricted step height model illustrated in Figure 36 the second (non-linear) term on the right hand side of equation (115) has yet another origin. In this case the density of growth sites decreases as the angle of inclination increases. Because the growth of both Eden and ballistic deposition model surfaces are described by the same equation (Burgers' equation²²⁵) they are expected to belong to the same universality class (i.e., all of the exponents associated with the evolution of the surface should be the same). This idea is consistent with all of the simulation results. Kardar, Parisi and Zhang²¹³ were able to solve equation (115) for the case $d = 2$ (1+1). (In processes such as this the system is often referred to as a 1+1 dimensional system or in general a $d+1$ dimensional system where d represents the dimensionality of the substrate). If this notation is used, as it is in reference 213, it must be remembered that d refers to the dimensionality of the substrate and $d+1$ to the dimensionality of the whole system). They found that $\alpha = 1/2$ and $\beta = 1/3$ for $d = 2$ (i.e., the 1+1 dimensional system). They conjectured that this result might be superuniversal (independent of d) but this is evidently not correct. At the time of writing this review no rigorous results are available from equation (104) for $d > 2$.

Many modifications of the basic ballistic deposition models have been explored to investigate processes such as vapor deposition onto a cold surface or to test theoretical ideas. In one of the most simple of these models the deposited particle is allowed to move "downhill" on the surface of the deposit until a local minimum is reached.²²⁶ Two equivalent two dimensional versions of this model are illustrated in Figure 39. These models generate deposits that have no voids and the deposit density does not depend on the angle of inclination of the substrate. Consequently, the term $\lambda(\nabla h(x,t))^2$ in Burgers' equation (equation (115)) disappears. For the case $d = 2$ this simplified Langevin equation gives the results $\alpha = 1/2$ and $\beta = 1/4$. These results are in excellent agreement with simulations.^{226,227} Edwards and Wilkinson²²⁸ described a detailed justification for the Langevin equation.

$$\frac{\partial h(x,t)}{\partial t} = V \nabla^2 h(x,t) + \eta(x,t) \quad (116)$$

(i.e., Burgers' equation without the non-linear terms) for three dimensional ballistic deposition with restructuring. They showed that equation (116) predicted that

$$\xi \sim (\log(t))^{1/2} \quad (t \ll L) \quad (117)$$

and

$$\xi \sim (\log(L))^{1/2} \quad (D \gg L) \quad (118)$$

that implies that the surface is not self-affine. This result has been confirmed using a three dimensional lattice model¹⁹³ similar to that illustrated in Figure 39a.

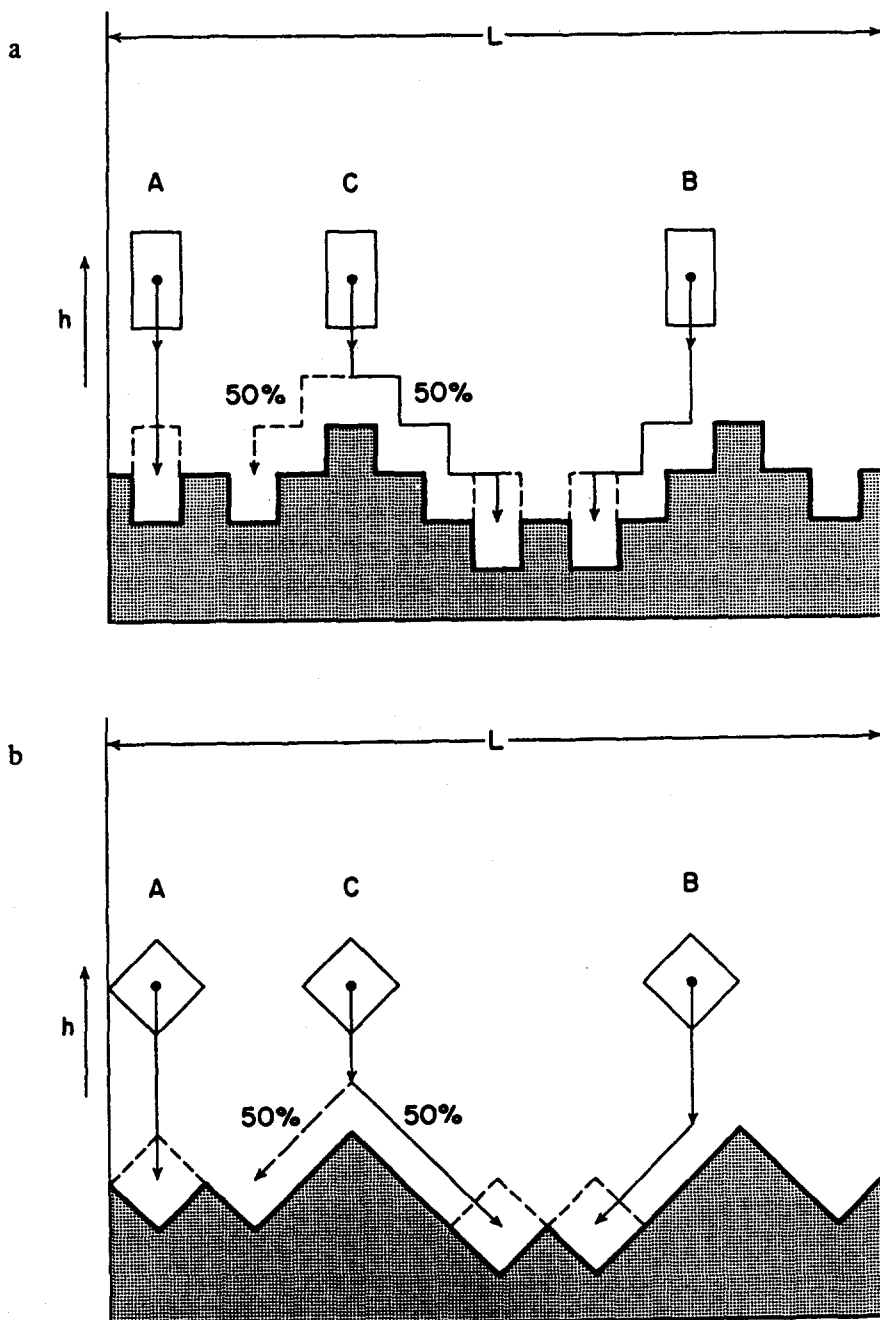
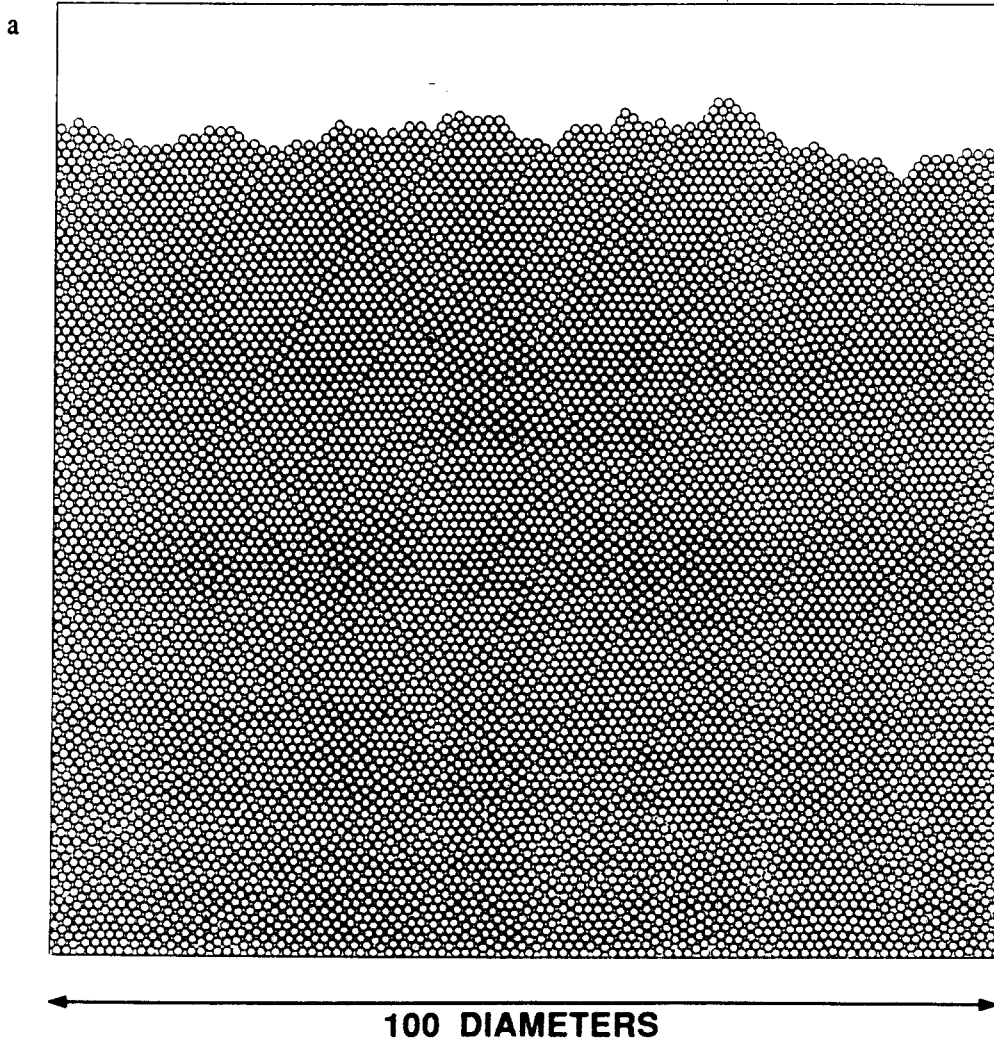


Fig. 39 Two models for ballistic deposition with restructuring. Figure 39a shows a model in which the initial substrate has heights of 1 in odd columns and 0 in even columns. After a particle has been added, it moves "down hill" on the surface (B) until it reaches a local minimum. The height is then increased by two lattice units. If the deposition occurs at a local maximum (C), the "particle" moves to the right or to the left with equal probability. If the particle is deposited in a local minimum (A), it remains there. Figure 39b shows an equivalent model.

In the case of off-lattice models for ballistic deposition with restructuring the deposit has a disordered structure (Figure 40). It appears that in this case the deposit density depends on the angle of incidence. If this is the case, then the Burger's equation will provide a more appropriate description of the evolution of the surface and this implies that the exponents with restructuring should be the same as those without restructuring. This idea is supported by computer simulations. The exponent β for the model illustrated in Figure 40 at first approaches an effective value of about 1/4 but its effective value increases to about 1/3 at larger heights.²²⁶ Similarly in three dimensional off-lattice simulations an effective value of about 0.22 is obtained for β .²²² These results indicate that in real systems in which restructuring is almost always present self-affine fractal surfaces are to be expected.

The disorderly structure shown in Figure 40a is uniform on all but very short length scales. Figure 40b shows the location of "defects" (discs that have other than 4 contacting neighbors) the defect density $\rho_d(h)$ at a distance h from the substrate can be described by the power law

$$\rho_d(h) \sim h^{-\alpha_d} \quad (119)$$



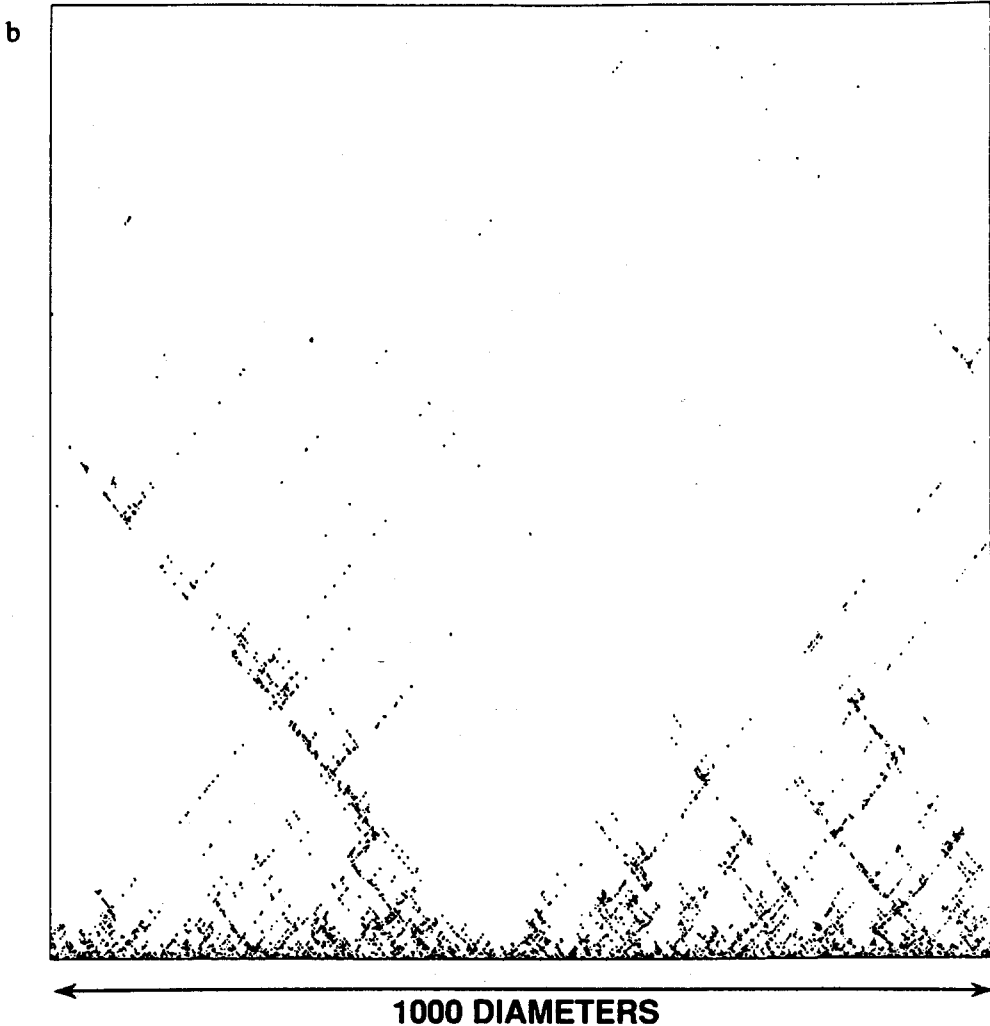


Fig. 40 The disordered structure generated by an off-lattice ballistic deposition model with restructuring. In this model particles (discs of identical size) move along a path of steepest descent to a local minimum after they first contact the surface of the growing deposit. Figure 40a shows the deposit structure and Figure 40b shows the location of "defects" in a much larger simulated disc packing.

where the exponent α_d has a value of about 1.92229 (the simulation results are consistent with an asymptotic value of 2.0) for large values of h . The pattern shown in Figure 40b suggests that the distribution of defects might be described in terms of fractal geometry. A fractal distribution of defects has been observed in other two dimensional disc packing problems.²³⁰

Pellegrini and Jullien²³¹ have investigated an interesting lattice model for ballistic deposition in which the non-linear term in the Burgers' equation is tuned via the fraction of "sticky" particles that do not undergo restructuring and the fraction of non-sticking particles that follow a path of steepest descent on the surface after the initial deposition event. For the 2(1+1) dimensional model the exponent α (H) is 1/2 for all values of c (the concentration of sticky particles) and the deposit density decreases smoothly with increasing c . In the case of the 3(2+1) and 4(3+1) dimensional models the effective value obtained for α (the Hurst exponent) changes abruptly at a "threshold" value c_s . This change in α is accompanied by a maximum in $d\rho/dc$ where ρ is the density and $(d\rho/dc)_{\max}$ at this maximum increases with increasing L (the system size) according to the power law

$$-(dp/dc)_{\max} \sim L^\mu \quad (120)$$

Using a simplified version of the model²³² in which only one stage of restructuring (transfer to the top of a nearest neighbor column) was allowed values of 0.0 ± 0.01 , 0.075 ± 0.03 and 0.25 ± 0.05 were obtained for the exponent μ in equation (120) for $d = 2(1+1)$, $3(2+1)$ and $4(3+1)$ respectively. For $d = 3$ the data were consistent with either a power law or logarithmic dependence of $(dp/dc)_{\max}$ on L . The "transition" occurs when the fraction of sticky particles (p) reaches a value near to the site percolation threshold probability for a $d-1$ dimensional lattice (≈ 0.5927 for $d = 3$ and about 0.3117 for $d = 4$). The simulations were not sufficient to unambiguously determine the nature of the transition for $d = 3(2+1)$ but this interesting study should stimulate more extensive work on this and related models.

Yan, Kessler and Sander²³³ have also used a model in which strength of the non-linear term in the Burgers' equation can be tuned via a parameter that controls the degree of surface diffusion. Although the numerical evidence for a phase transition in the $d = 3(2+1)$ does not appear to be as strong as that presented by Pellegrini and Jullien, Yan et al. interpret their simulation results in terms of a "phase transition" for both the $d = 3(2+1)$ and $d = 4(3+1)$ simulations.

On the other hand, direct numerical solution of the Burgers' equation²³⁴ does not provide evidence for a phase transition as the strength of the non-linear term is varied for the $d = 3$ case. This discrepancy may be a consequence of the discretization that is an inherent feature of the ballistic deposition lattice models. The effects of this discretization (if any) are not well understood. In any event the growth of rough surfaces in $2+1$ dimensions is an important theoretical problem with many possible applications. The possibility of an unexpected phase transition heightens interest in an area that was already undergoing rapid development.

Amar and Family²¹² have studied a surface growth model in which the "columns" of a lattice are selected at random. The height of the selected column is increased by one lattice unit if the total surface "area" would be decreased or preserved. If the surface area would be increased then the height of the selected column is increased with a probability given by

$$P(h_i \rightarrow h_i + 1) = e^{-k\Delta E_i}. \quad (121)$$

Here ΔE_i is the change in the surface area or energy. In addition, no height increment is allowed that would lead to a step in the surface with a height of greater than 1 lattice unit. In the limit $\Delta E = 0$ this model becomes equivalent to that of Kim and Kosterlitz.²¹⁵ For the $2+1$ ($d = 3$) dimensional case a "phase transition" is observed (at $k \approx 0.5$) as the parameter k is varied in equation (121). It has very recently been shown²³⁵⁻²³⁸ that in this model the magnitude of the non-linear term in the Burger's equation decreases as k increases from zero and changes sign (i.e., becomes zero) at $k \approx 0.5$. Consequently the behavior found by Amar and Family is not a phase transition between strong coupling and weak coupling regimes but is brought about by the disappearance of the second (non-linear) term on the r.h.s. of equation (115) at a unique value of the parameter k in equation (121).

Burgers' equation has been applied to a variety of problems other than the growth of interfaces. These include driven diffusion,²³⁹ the propagation of flame fronts^{240,241} and the growth of directed polymers.²⁴²

Other Models for the Growth of Rough Surfaces

In addition to the Eden and ballistic deposition models for surface growth, many other models for the formation of rough surfaces have been developed and in many cases they lead to the formation of fractal structures. In the solid-on-solid (SOS) model²⁴³⁻²⁵⁰ a surface or interface is represented on a lattice by the heights h_i associated with each of the lattice sites and the heights h_i can have any (integer) value from $-\infty$ to ∞ . The Hamiltonian for the surface is written in the form

$$H = \sum_{NN} |h_i - h_j| p \quad (122)$$

where the sum is over nearest neighbor pairs of sites. In a simulation the surface structure can be explored using standard Monte Carlo methods to minimize the free energy.^{251,252} In contrast to the Eden and ballistic deposition models, this is an equilibrium model. The surface roughness can be described in terms of the correlation function $C^2_h(r)$ (similar to $C^2_d(t)$ in equation (39) defined as

$$(C^2_h(r))^2 = \langle (h(r_0) - h(r_0+r))^2 \rangle_{|r|=r} . \quad (123)$$

This model has a transition (roughening transition) from a "smooth" surface at low temperatures ($T < TR$) to a rough surface at high temperatures. For the standard ($p = 1$ in equation (122)) two dimensional (1+1 dimensional) solid on solid model the transition temperature TR is at zero and the Hurst exponent describing the height correlations (equation (123)) is $1/2$.²⁴⁷⁻²⁴⁹ For the three (2+1) dimensional system the transition temperature is finite but the correlation function $C^2_h(r)$ has a logarithmic form so the surface is not fractal. Deposition and/or evaporation processes can be added to the basic solid on solid model to simulate surface growth processes. In this way it is possible to "interpolate" between the equilibrium solid on solid model and the completely non-equilibrium ballistic deposition model using a series of models that include both deposition and surface diffusion processes. A serious investigation of these models and the possible phase transition-like behavior associated with them is only just beginning. This should be an active area of research during the next few years.

The surface growth models described above can also be used or modified to simulate processes in which material is removed from an initially smooth or rough surface. In some of the growth models described above complex fractal patterns are formed because the most exposed parts of the surface (those that have grown the most) have the highest growth probabilities.²⁵³ Under these conditions a smooth surface is unstable with respect to roughening perturbations. If the process is inverted and the most exposed parts of the surface have the highest probability of being removed, then a smooth surface will be generated. This is the basis of processes such as electropolishing and the formation of smooth surfaces by various erosion processes.

If the Eden model is "reversed" to represent material removal, then this "anti-Eden" model is simply another (not necessarily identical) Eden model in which the identity of "phases" at the interface is exchanged.

In the case of the lattice models for ballistic deposition, the deposition process can be "reversed" by dropping "particles" at random down the columns of a lattice. When the particles enter an unoccupied site with one or more occupied nearest neighbors, one of these nearest neighbors is randomly selected and removed together with the incoming particle. For the case of a two dimensional system²⁵⁴ this model generates a self-affine "surface" with $\alpha = 1/2$ and $\beta = 1/4$. This model is very closely related to the deposition model investigated by Family²²⁷ in which a particle deposited in the i th column on the lattice is added to the column at position i , $i+1$ or $i-1$ that has the lowest height. Three dimensional simulations have not yet been carried out using these models but they probably give logarithmic behavior (non-fractal surfaces).

In the anti-DLA or diffusion-limited annihilation model^{255,256} sites are removed from the surface when they are entered by a random walker starting from "infinity" and a new random walker is launched from infinity after each such annihilation event. The surface generated by this model is quite smooth. For $d = 2$ (1+1) $\xi \sim \ln(L)^{1/2}$ (in the limit $h \gg L$) and for $d = 3$ the surface thickness (ξ) seems to be essentially independent of L .^{255,257}

Other models leading to fractal surfaces and interfaces include tethered membrane models,²⁵⁸⁻²⁶⁴ fracture models^{265,266} and impurity roughening models.²⁶⁷⁻²⁷¹ These interesting recent developments are beyond the scope of this review.

The interdiffusion of miscible materials placed into contact with each other is a process of considerable practical importance in materials science and engineering. Sapoval et al.²⁷² investigated a simple two dimensional lattice model in which A particles (sites) with a constant density of 1 at the edge of a lattice are allowed to diffuse onto the lattice. The diffusion process can be represented by nearest neighbor steps in randomly selected directions (the particles follow random walk trajectories). The average time dependent density profile is given by

$$\rho(x, \ell_D) = \text{erfc}(x/\ell_D) = 1 - (2/\pi^{1/2}) \int_0^x e^{-\mu^2} d\mu \quad (124)$$

where ℓ_D is the diffusion length $2(Dt)^{1/2}$ at time t and D is the diffusion coefficient. Instead of simulating the diffusion process by randomly moving the A sites, the sites at a distance x from the edge of the lattice are randomly occupied by A sites with a probability given by equation (124). A diffusion front for the advancing A sites can be defined in the same way as the hull of a percolation cluster (see above). On length scales smaller than that of the width of the diffusion front the diffusion front was found to have a fractal dimensionality of 1.76 ± 0.02 , a value very similar to that associated with the hull of a percolation cluster. Based on their simulation results and theoretical arguments, Sapoval et al. conjectured that the fractal dimensionality of the diffusion front is related to the percolation correlation length exponent ν (equation (11)) by

$$D = (1+\nu)/\nu = 7/4 . \quad (125)$$

This result has been confirmed by subsequent work.^{195,196,273} The width σ_f of the diffusion front is related to the diffusion length ℓ_D by

$$\sigma_f \sim \ell_D^{\alpha_\sigma} \quad (126)$$

where

$$\alpha_\sigma = \nu/(\nu+1) . \quad (127)$$

These results stimulated Rosso et al.²⁷⁴ to explore the more simple problem of percolation with a linear occupation probability gradient. From the dependence of the mean position of the diffusion front on the concentration gradient a quite accurate value for the square lattice site percolation threshold probability was obtained ($p_c = 0.592802 \pm 10^{-5}$). Subsequently, much more accurate values for p_c ($0.592745 \pm 2 \times 10^{-6}$) have been obtained using a hull generating walk in a concentration gradient.^{20,275} It appears that the uncertainties in p_c estimated by Rosso et al. were too optimistic. In three dimensions the situation is quite different.²⁷⁶ The site percolation threshold probability on the cubic lattice is about $0.311605 \pm 0.000010^{20}$ so that both components can be above their percolation thresholds over a considerable range of concentrations (p_c to $1-p_c$). Consequently, the interface between the two components (A and B) in the diffusion front, becomes a three dimensional structure over the range $p_c \leq p_A \leq (1-p_c)$ where p_A is the density of A sites.

Kolb et al.²⁷⁷ have simulated the effects of attractive and repulsive interactions on diffusion fronts. For weak interactions, the systems behave like the non-interacting system, but for strong interactions phase separation occurs. The two regimes are separated by a critical point. At the critical point the large critical fluctuations retard the diffusion process. Kolb et al. related their model to the kinetic Ising model with Kawasaki^{278,279} (local conservation of the two components, A and B, i.e., spin exchange not spin flips) dynamics and show that the critical point in their diffusion model corresponds to that of the two dimensional Ising model.

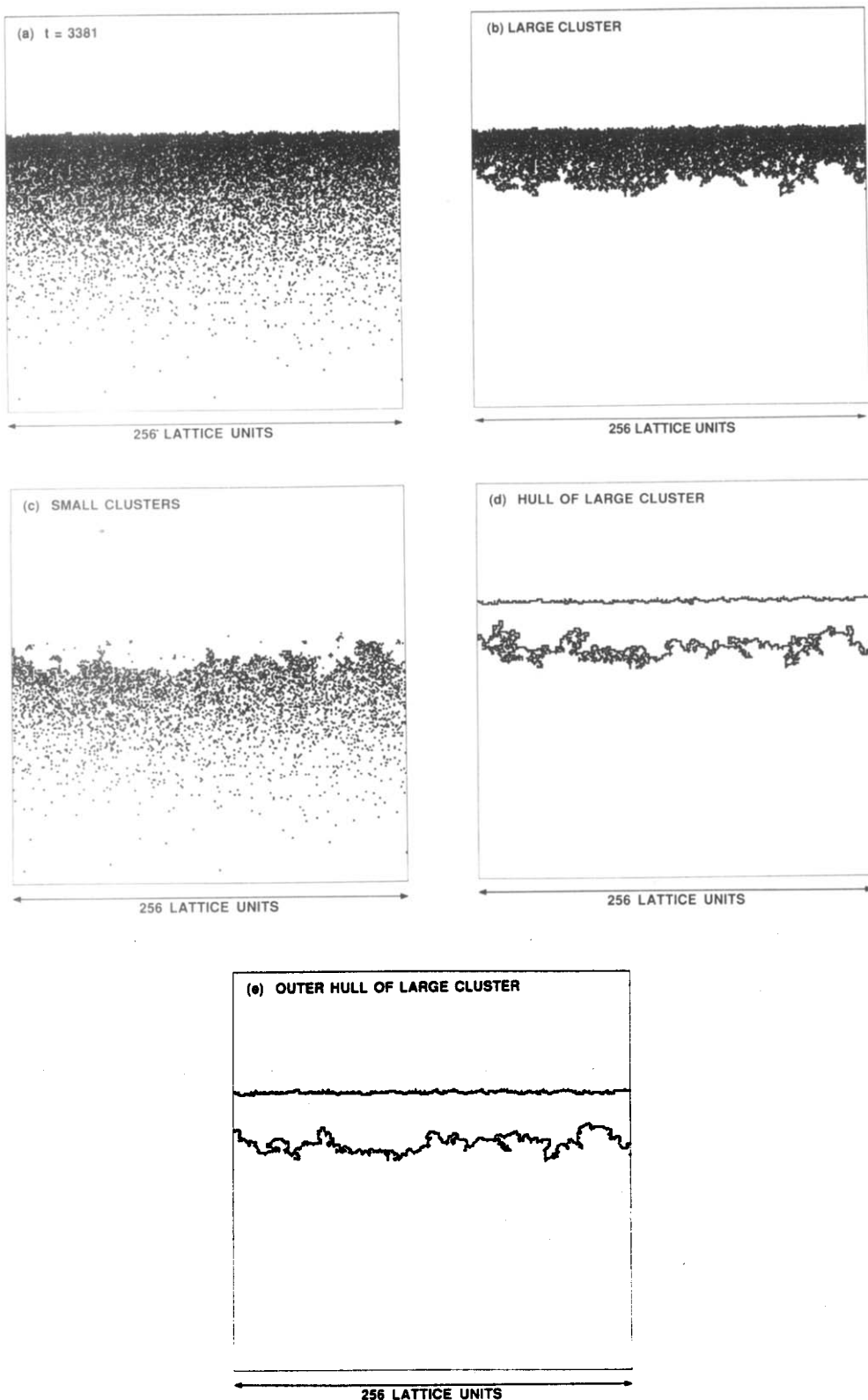


Fig. 41 Results from a simple diffusion-limited solid state reaction model ($A + B \rightarrow 2C$). Figure 41a shows the location of the product (C) sites at a time t of 3881.3. Figures 41b and 41c show the largest C cluster and all of the smaller C clusters respectively, while Figures 41d and 41e show the hull and the outer hull of the largest C cluster.

Figure 41 shows some results obtained from a simple model for a two dimensional diffusion-limited solid state reaction.²⁸⁰ In this model only one (B) of the two reactants (A and B) is allowed to diffuse. This diffusion is represented by random walks. At the start of a simulation the top half of a square lattice is filled with A sites and the bottom half with B sites. As the simulation proceeds B sites that are adjacent to A sites or product (C) sites are selected randomly and an attempt is made to move the selected site in a randomly selected direction. If the selected B site attempts to move onto a site occupied by A, then both sites are converted to C to represent the process



If a B site attempts to move on a C site, the two site labels are exchanged. Figure 41a shows the results of a simulation carried out on a 512x512 site square lattice with periodic boundary conditions at a time (in units of moves per B interface site) of 3881.3. At this stage 22978 sites were converted to product (C). Figure 41a shows all of the "C" sites in a portion of the system at this time. Figure 41b shows all of the sites in the largest cluster of C sites and Figure 41c shows those sites associated with all of the smaller clusters. Finally, Figures 41d and 41e show the hull and the outer hull respectively of the largest cluster of C sites. It is evident that the B-C interface has an irregular fractal structure while the A-C interface is smooth on all but quite short length scales. This behavior can be understood in terms of the models already discussed. The B-C interface is formed by an interdiffusion process so that the hull is self-similar and has a fractal dimensionality of 7/4 while the outer hull has a dimensionality of 4/3 (see above) on length scales up to a correlation length, ξ . The A-C interface is formed by a diffusion-limited annihilation process. Consequently, we expect that the surface thickness or perpendicular correlation length ξ will be quite small and will grow only logarithmically with increasing L or time (see above).

One interesting characteristic of growing two dimensional diffusion fronts is the large fluctuations in their geometry. Large clusters of sites will frequently become attached to and removed from the interface. This may result in large fluctuations in properties such as A/C conductivity and may provide a means of studying the growth of interfaces in pseudo two-dimensional systems.

Fractal Surfaces and Multifractals

One of the most important applications of multifractals is to processes occurring at the surface of fractal structures.^{29,87} For example, Figure 42 shows the results of a simulation²⁸¹ in which the surface of a two dimensional percolation cluster grown on a square lattice was "probed" using random walkers. The simulation resembles very closely that used to grow DLA clusters (see above). When the random walker enters an unoccupied perimeter site the random walk is terminated and a "counter" which records how many times that site has been entered is incremented. After a sufficiently large number of probe particles have been released and adsorbed, the "scores" recorded by each of the counters provide an estimate of the first contact probability for random walks. The probability distribution over the surface generated in this manner is a probability measure known as the "harmonic measure" since the random walkers simulate a field ϕ that obeys the Laplace (harmonic) equation with absorbing boundary conditions on the fractal and a fixed value for ϕ at "infinity". The harmonic measure is a multifractal measure and its multifractal properties can be measured via the correlation functions given in equations (7), (8) and (22) where the density $\rho(r)$ is replaced by $\mu(r)$ or $\mu(r)p$. In a lattice model $\mu(r)$ is the fraction of the random walkers adsorbed by the site at position r . In particular the two point correlation functions $C_p\mu(r)$ given by

$$C_p\mu(r) = \langle (\mu(r_0))^p (\mu(r_0+r))^p \rangle_{|r|} = r \quad (129)$$

can be used to characterize multifractal measure via the corresponding fractal dimensionalities D_p .²⁸¹ It is clear that for $p = 0$ the fractal dimensionality D_p is the dimensionality of the support of the measure which in this case

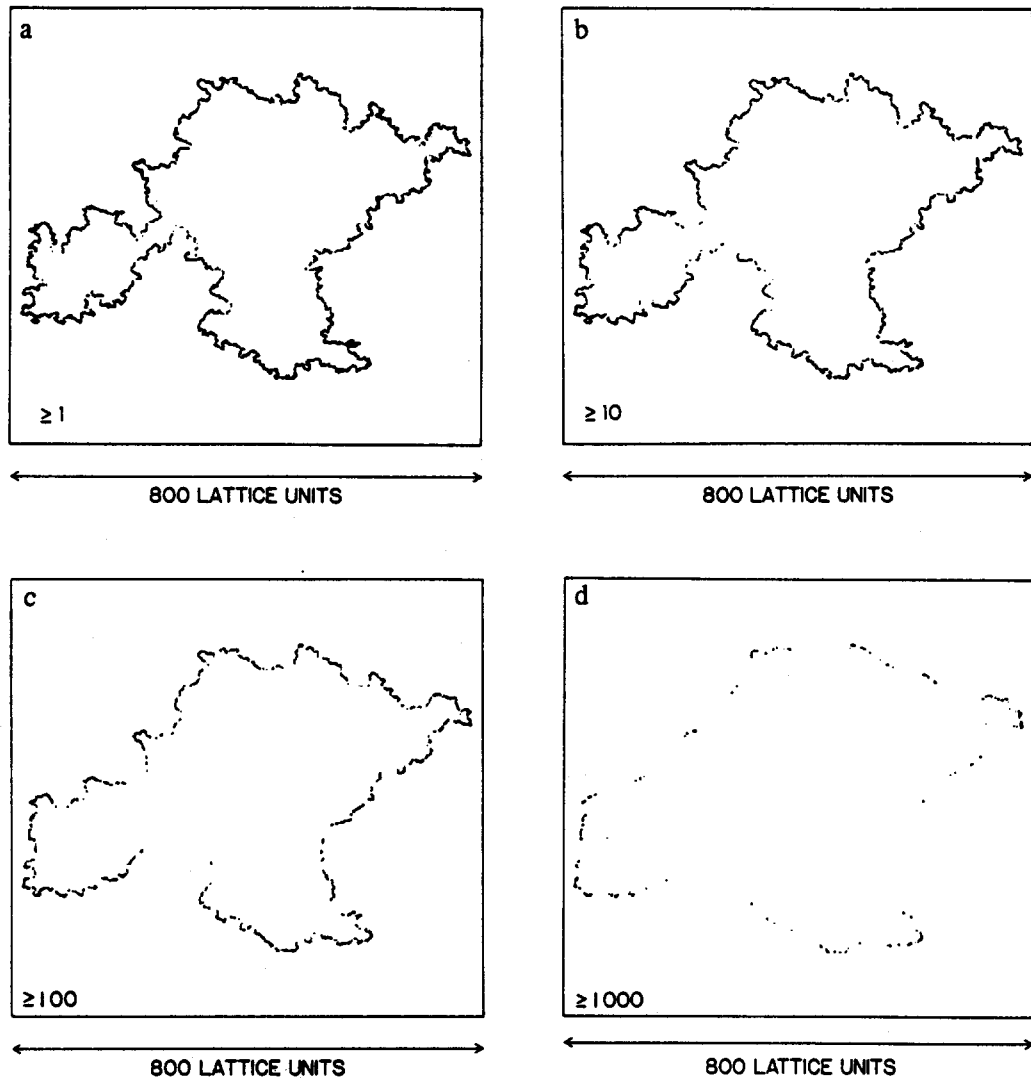


Fig. 42. This figure shows some of the results obtained by probing a percolation cluster with 100,000 random walkers. Fig. 42a shows all sites that were contacted, Fig. 42b shows those sites that were contacted ten or more times, Fig. 42c shows the sites that were contacted 100 or more times, and Fig. 42d shows the sites that were contacted at least 1000 times. The random walks were terminated immediately after contacting the cluster.

is $4/3$ (the outer hull of the two dimensional percolation cluster).

Several other approaches to the characterization of multifractal measures have been developed and tested more thoroughly. One of these is to measure the quantities D_q given in equation (34) where the partition function $Z_q(\epsilon)$ is defined in terms of the measure by equation (69).⁹⁰ The function $\tau(q)$ can be obtained using equation (72). The $f(\alpha)$ curve can then be obtained via a Legendre transformation (equations (77) and (78)). Much of the work on applications of multifractals to real space structures was stimulated by the idea that if we knew more about the distribution of growth probabilities in DLA it might be possible to obtain a better understanding of how this fractal structure is formed.^{113,114,282-289} Figure 43 shows the results of a simulation similar to that illustrated in Figure 42. In this case 5×10^6 off-lattice random walkers were used to probe the surface of a 50,000 particle off-lattice DLA cluster. Even after 5×10^6 probe particles had been released, only 8305 particles in the cluster had been contacted and the maximum number of contacts was 39,175. The broad distribution of growth probabilities that grows algebraically with increasing system size (L/ϵ) is one of the characteristics that distinguishes multifractal distribution from more homogeneous (and more familiar) distributions. Figure 44

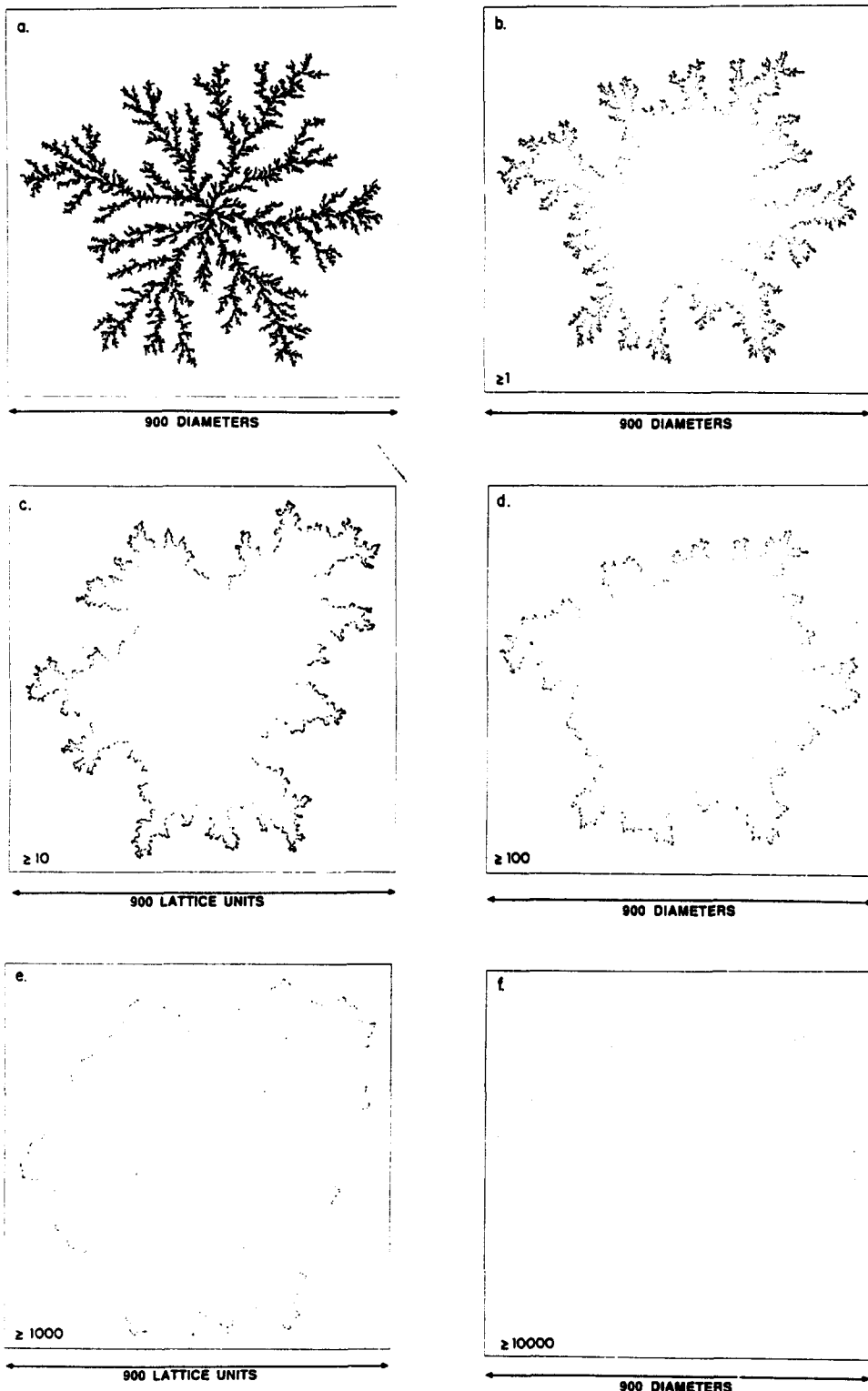


Fig. 43. Estimation of the harmonic measure for off-lattice DLA. Here the results of a simulation in which a 50,000 particle two dimensional DLA cluster (Fig. 43a) was probed by 5×10^6 discs (of the same size as those comprising the cluster) following random walk trajectories. Fig. 43b shows the 8305 particles that were contacted one or more times. Similarly, Figs. 43c, 43d, 43e and 43f show particles that were contacted 10 or more times, ≥ 100 times, ≥ 1000 times and $\geq 10,000$ times respectively.

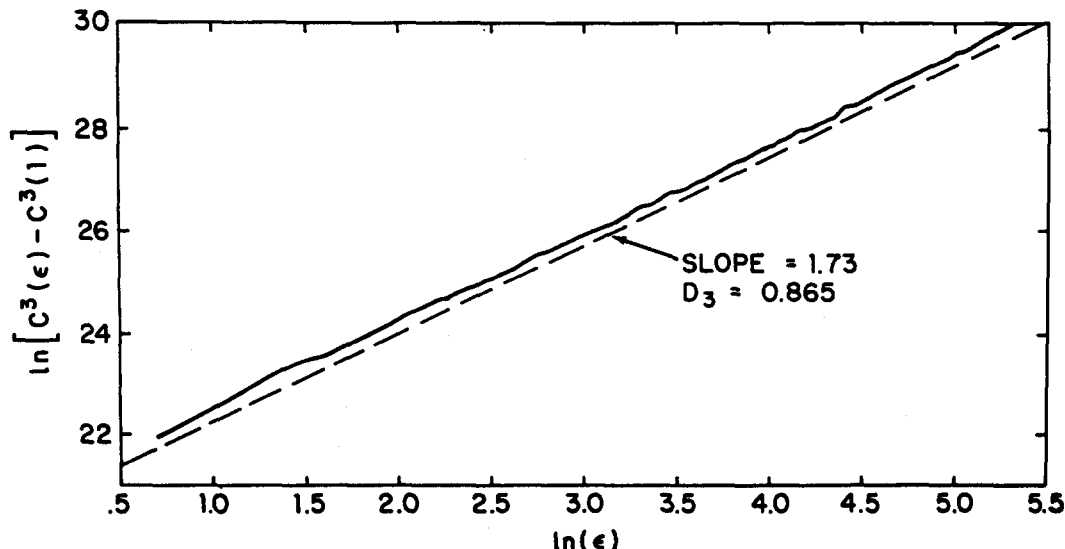


Fig. 44. Determination of D_q from simulations similar to that illustrated in Figure 43. The quantity $C^3(\epsilon)$ (equivalent to $Z_3(\epsilon)$ - equation (69)) was measured by covering the clusters with grids of size ϵ and measuring the number of contacts for all of the particles in each grid element.

shows the measurement of one of the exponents D_q obtained from simulations like that illustrated in Figure 43. In practice the measurement of D_q in this fashion for a large number of q values is not a convenient procedure. More frequently $f(\alpha)$ is determined by measuring Z_q (equation (69)) for a fixed value of ϵ (typically one lattice unit in a simulation) and a range of total system sizes (L). The exponents $\tau(q)$ are then determined from the dependence of $Z_q(\epsilon, L)$ on L via equation (71). The determination of $\tau(q)$ in this manner is fraught with the same uncertainties as the determination of any other exponent or fractal dimensionality. Corrections to scaling may be quite large and convergence of the exponents $\tau(q)$ to their asymptotic values may be slow.

Another approach to the determination of $f(\alpha)$ for surface measures is via a family of surface sizes S_n ²⁸² defined as

$$S_n = \left[\frac{1}{N} \sum_{i=1}^N \mu_i^{n+1} \right]^{1/n} \quad (130)$$

where μ_i is that part of the normalized measure associated with the i th surface site and N is the number of surface sites.

This approach was motivated by the idea that different physical or chemical processes occurring at a surface or interface might depend on different moments of an appropriate measure or probability distribution. For a uniform (or bounded) measure on a fractal object the dependence of the surface sizes S_n on the mass M is given by

$$S_n \sim M^\gamma \quad (131)$$

where the exponent γ is equal to $1/D_\sigma$ and D_σ is fractal dimension of the surface. However, for a fractal measure the dependence of S_n on M is given by

$$S_n \sim M^{\gamma_n} \quad (132)$$

where the exponent γ_n depends on the moment n . The dimensionalities D_q and the exponents γ_n are related by

$$(D_q)|_{q=j+1} = D\gamma_j \quad (133)$$

where D is the fractal dimensionality of the support of the measure (D_0). Consequently, $\tau(q)$ and $f(\alpha)$ can be obtained via the exponents γ_n . Figure 45 shows the dependence of the surface sizes (S_n) on cluster mass, M (number of occupied sites) for two dimensional percolation clusters that have been grown to sizes in the range $100 \leq M \leq 10^5$ and their harmonic measures estimated using random walk probes. Figure 45 shows the dependence of $\ln(S_n)$ on $\ln(M)$ for $n = 1-9$. The linearity of these curves supports equation (132) and the observation that all the slopes are different indicates that the harmonic measure on a percolation cluster is a multifractal measure. The exponents γ_n for negative n are dominated by the parts of the measure that have the smallest values. These correspond to the most deeply buried accessible sites on the surface that are only rarely reached by random walk probes. Consequently, this approach cannot be used to evaluate γ_n for negative values of n and it is not possible to measure all of the $f(\alpha)$ curve. It can be argued that in most cases only the positive moments are important to most physical processes. However, a considerable interest has developed in the distribution of the smallest growth probabilities in DLA despite the fact that this probably has little to do with the way that DLA grows. To investigate the smallest growth probabilities, numerical relaxation,²⁵⁹ Green's function^{113,284} or exact enumeration¹⁶⁹ methods can be used. These approaches, if properly implemented, can give very accurate values for the growth probability distribution but are restricted to relatively small system sizes. It appears that the simple picture presented here may not be adequate for DLA and that some part of the (harmonic) growth probability measure decreases exponentially with increasing cluster size.^{169,172} Fractal measures have also been shown to be an appropriate way of describing phenomena such as the force distribution on fractals embedded in an elastic medium²⁹⁰ or moving through a quiescent fluid.²⁹¹⁻²⁹⁴ Other applications include current distributions²⁹⁵⁻²⁹⁷ and stress distribution in random networks.^{266,298}

There does not appear to be a unique relationship between the exponent $\alpha(p,q)$ describing correlation functions of moments of fractal measures such as those given in equation (129)

$$CP^q \mu(r) = \langle (\mu(r_0)) P(\mu(r_0+r))^q \rangle |r| = r \quad (134a)$$

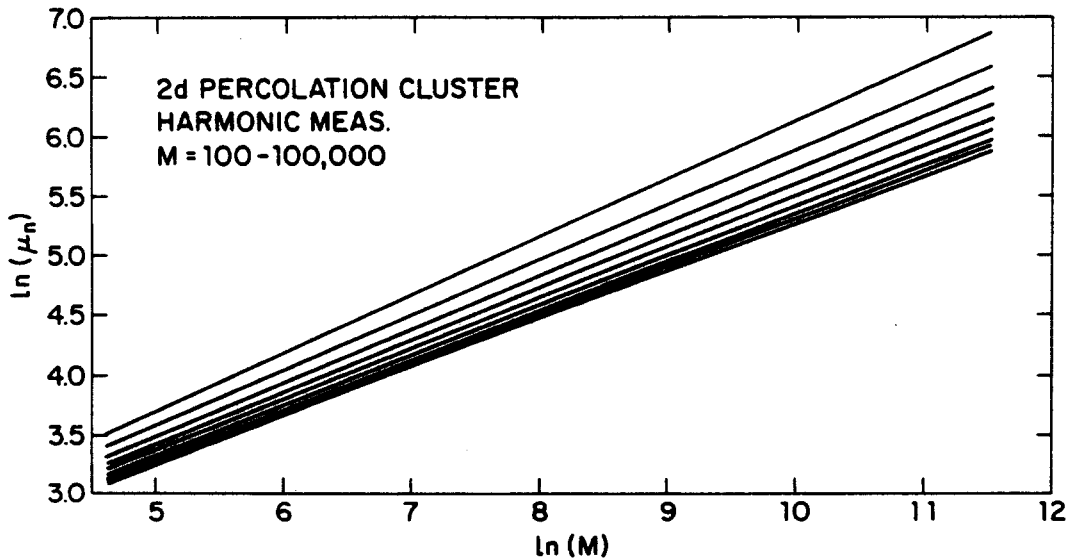


Fig. 45. Dependence of the surface sizes μ_n (equivalent to S_n in equation (130)) on cluster mass M for the harmonic measure on percolation clusters. Here results for $n = 1-9$ are shown.

$$C_p q \mu(r) \sim r^{-\alpha(p,q)} \quad (134b)$$

and the exponents $\tau(q)$ or D_q . Cates and Deutsch²⁹⁹ suggest that

$$\alpha(p,q) = D_0 + \tau(q) + \tau(p) - \tau(p+q) \quad (135)$$

However, Meneveau and Chhabra³⁰⁰ and Lee and Halsey³⁰¹ have shown that equation (135) is not valid for all values of p and q .

APPLICATIONS TO EXPERIMENTS

A wide variety of structures have now been analyzed in terms of fractal geometry. These range from polymer molecules,^{302,303} gels^{302,304,305} and proteins,³⁰⁶ on the 10^{-10} - 10^{-7} meter length scale range to the distribution of mass in the universe³⁰⁷⁻³⁰⁹ on the 10^{17} to 10^{22} (10^{25} ?) meter length scale range. In the majority of these systems evidence for fractal scaling is ambiguous. The problem is that in many systems effective power law behavior in scattering curves, correlation functions, etc., is seen over only about one order of magnitude in length scales. In computer simulations this range of length scales can be extended by improving algorithms or using more computer time (or faster machines). The cost can be considerable but this process is relatively straightforward. In experimental systems it can often be very difficult to extend the range of fractal scaling because the range of conditions over which a single process leading to the formation of a fractal structure is dominant may be quite small. Nevertheless, good evidence for fractal geometry has been found in many systems and it is now clear that fractal geometry provides an appropriate framework for describing and understanding many natural phenomena. It would not be practical to survey these applications. Instead, a few examples that are relevant to the models discussed in the previous section and/or are of particular interest in solid state chemistry are described here.

Percolation Fractals

Percolation has been studied in a wide variety of systems for several decades and many hundreds of experimental papers concerned with percolating systems have been published. In most cases these studies have been concerned with how properties such as elasticity, conductivity and other transport properties depend on composition near to the percolation threshold. There have been few attempts made to measure directly the fractal structure of percolation clusters. The main reason for this is that the percolation geometry depends on connectivity information that is not easily obtained in a three dimensional system.

Percolation is believed to be an appropriate model for polymer gels³¹⁰ near to the gel point. For systems undergoing strong (irreversible) gelation large clusters can be isolated by carrying out a gelation reaction until the gel point is approached, quenching the reaction and isolating the clusters by dilution. However, when the system is diluted the sol that penetrates the large cluster is replaced by solvent and this reduces the screening of the interaction within the incipient gel molecules causing them to swell. This swelling reduces their fractal dimensionality from a value of about 2.5 (that of percolation clusters on a three dimensional lattice or space) to a lower value. Theoretical arguments^{311,312} indicate that the swollen "gel" should have a fractal dimensionality of 2.0 (that of lattice animals³¹³ on a three dimensional lattice). These ideas seem to be confirmed by recent experiments³¹⁴ but there are many subtleties and difficulties associated with these experiments.³¹⁵ An up-to-date and concise review of the fractal properties of polymers and gels can be found in reference.³⁰² It is much easier to observe percolation fractals in two dimensional systems. Good examples of this are provided by the work of Voss³¹⁶ et al. and Kapitulnik and Deutscher.³¹⁷ In the experiment of Voss et al. (Figure 44) gold was deposited on Si₃B₄ windows to a thickness of 6 to 10 nm. The gold does not cover the substrate uniformly but instead forms interpenetrating ramified clusters whose perimeter is proportional to their area on length scales

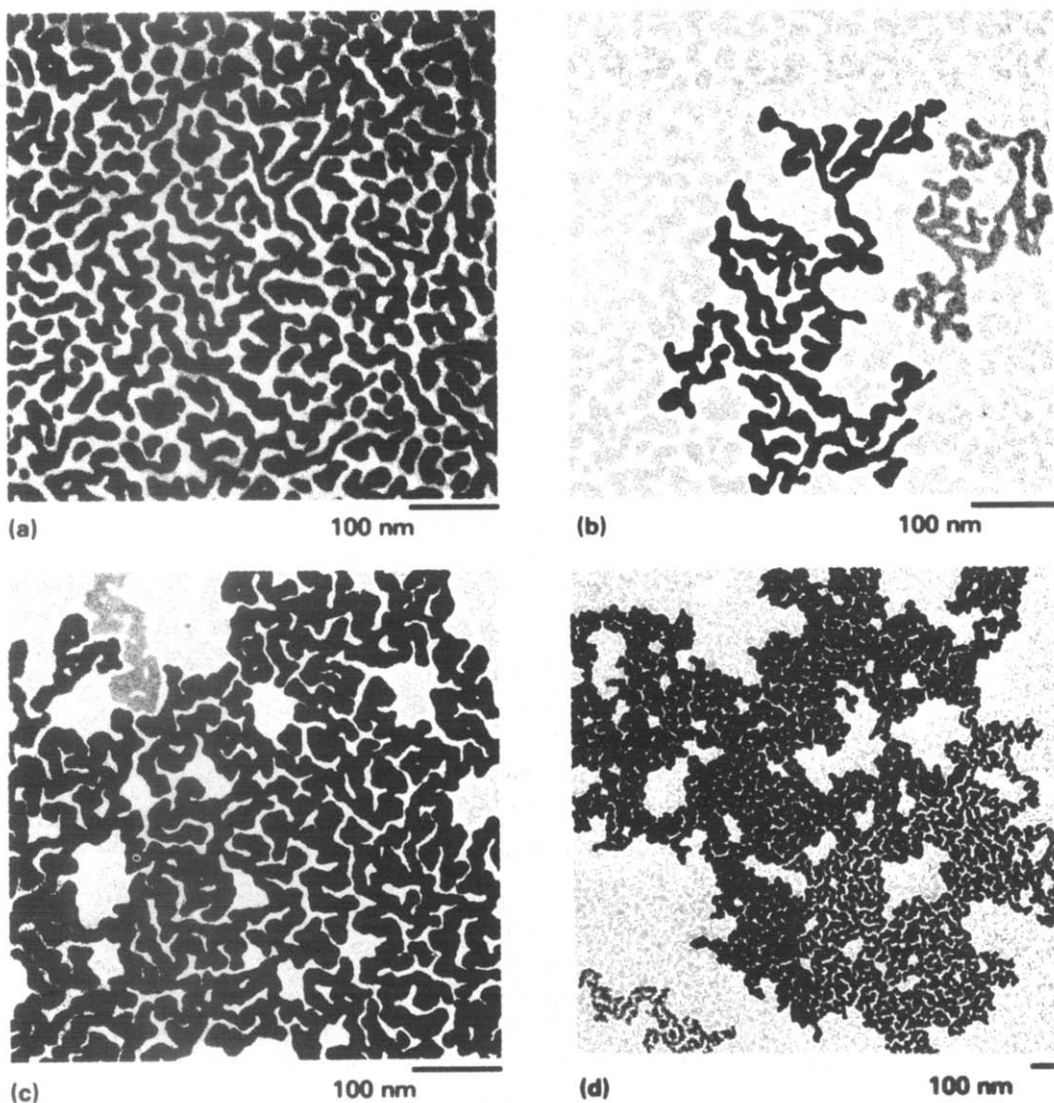


Fig. 46. (a) Halftone representation of a digitized Au cluster transmission electron micrograph, (b) Connectivity analysis of (a) with $p = 0.64$ with the largest clusters shown darkest, (c) Au clusters with $p = 0.75$, (d) Au clusters with $p = 0.71$ at a factor of 3 lower magnification. This figure was taken from ref. 316 (R.F. Voss, R.B. Laibowitz and E.I. Allessandrini, *Phys. Rev. Lett.* **49**, 1441 (1982)).

greater than that of the film thickness. From digitized images (like those shown in Figure 46) the fractal dimensionality and size distribution of clusters was measured for systems near to the percolation threshold which is found at a gold coverage of about 0.74. The values obtained for D and τ (equation (9)) were ≈ 1.89 and ≈ 2.05 respectively. These values are close to the theoretical values of $91/48$ ($1.8958\cdots$) and $187/91$ ($2.049\cdots$ or $(D+d)/D$) expected for two dimensional percolation. A similar morphology has been found by Reich³¹⁸ in phase separated polymer films.

A well established model that leads to the formation of fractal structures is the invasion percolation model.^{5,319-323} In this model randomly selected "threshold" values are associated with all of the sites (or bonds) on a lattice and a cluster is grown, starting from a single occupied site, by always filling the unoccupied perimeter site with the lowest threshold (for the site invasion percolation model) or the perimeter site accessible via the bond with the lowest threshold value for bond invasion percolation. This model has been used extensively to model the slow displacement of a wetting fluid by a non-wetting fluid in a pseudo two dimensional

porous medium^{5,324-326} or the advance of drying fronts in a porous medium confined to a narrow gap between two parallel sheets of glass.^{327,328} If the two fluids are incompressible, it is appropriate to prevent perimeter sites from growing in those regions that have become enclosed by the growing cluster. This model is called invasion percolation with trapping.³²⁹ It has been established^{330,331} that the structure generated by invasion percolation without trapping has the same fractal scaling properties as ordinary percolation clusters at the percolation threshold (i.e., $D = 91/48 \approx 1.89583$ for $d = 2$). For invasion percolation with trapping computer simulations indicate that $D \approx 1.82$ ^{319,33,332,333} and that the exponent τ describing the distribution of "defender" clusters trapped by the "invader" (i.e. the distribution of hole sizes in the invasion percolation cluster with trapping) is given by 332,333

$$\tau = \frac{D+d}{d} \approx \frac{1.82+2}{2} \approx 1.91 \quad (136)$$

(rule 7, see above). Since trapping is a long range phenomenon (like the excluded volume effect in self avoiding random walks) it is not unreasonable for the fractal dimensionality to be lowered by this effect. Theoretical arguments have been presented to support the idea that the fractal dimensionality for invasion percolation should be the same as that for percolation³²⁹ and that the size distribution exponent τ for the trapped defender clusters is given by

$$\tau = \frac{D+d}{D} = 187/91 . \quad (137)$$

However, equation (137) corresponds to the size distribution for fractal ($D = 91/48$) percolation clusters in a Euclidean space not the distribution of compact holes in a fractal.

Figure 47a shows an "invasion percolation" pattern generated by a fluid-fluid displacement experiment.³³² Figure 47b shows, for comparison, a cluster of 2×10^5 sites generated on a square lattice using a bond invasion percolation model with trapping.³³³ On a three dimensional cubic lattice trapping is a quite rare event and only very small regions (cluster of defender sites) can be isolated in this fashion. Consequently, it seems safe to assume that the fractal dimensionality is the same for invasion percolation with and without trapping.

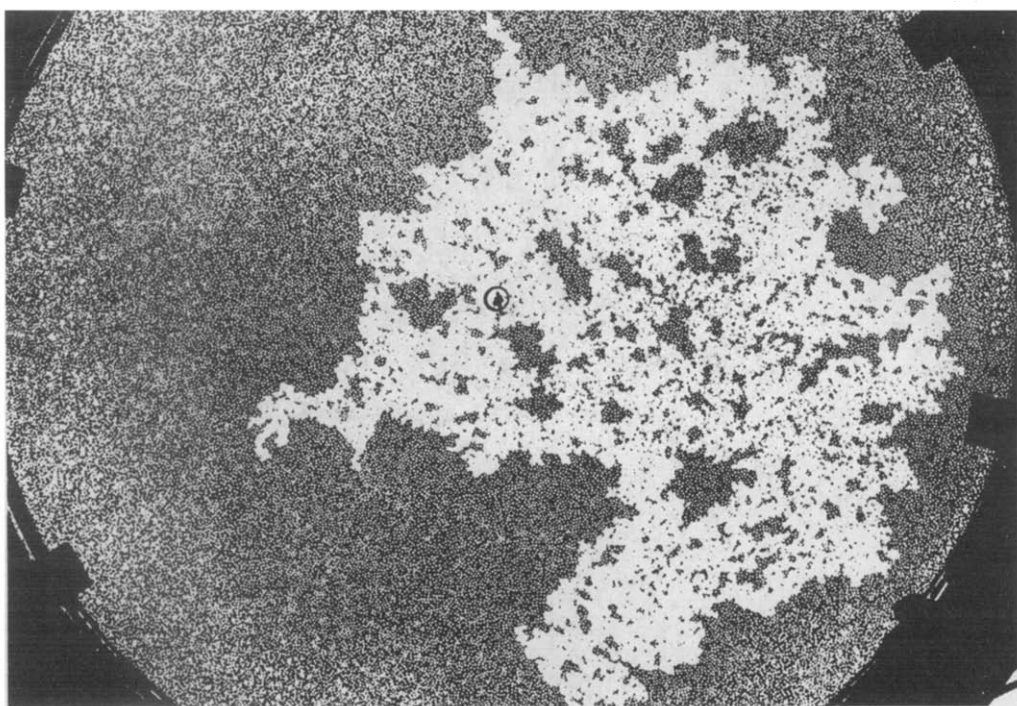
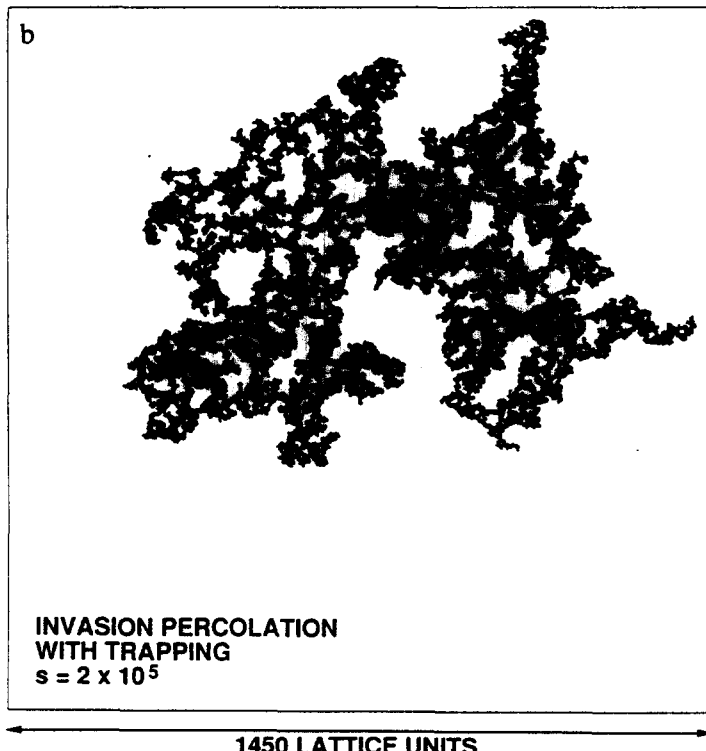
Diffusion Limited Aggregation

One of the first experimental realizations of the diffusion-limited aggregation model was a three dimensional experiment in which copper was electrodeposited onto the exposed end of an otherwise insulated copper wire.³³⁴ Almost all other experiments have been carried out using pseudo two dimensional systems (Hele Shaw cells, filter papers, thin films, etc.). Examples of processes leading to DLA-like patterns include dielectric breakdown, fluid-fluid displacement processes, random dendritic growth, electrodeposition, dissolution of porous materials, and a variety of biological processes such as the growth of bacterial colonies, vascular systems and nerve cells. Most of these applications have been reviewed previously.^{29,335-337}

One of the most dramatic examples comes from the dissolution experiment of Daccord and Lenormand.^{338,339} In these experiments water is slowly injected into plaster of Paris ($\text{CaSO}_4 \cdot 0.5 \text{ H}_2\text{O}$). The flow of water through the porous plaster of Paris is described by Darcy's law

$$U = -k\mu \nabla P \quad (138)$$

where U is the fluid velocity, μ is the fluid viscosity, k is the permeability of the porous medium and P is the fluid pressure inside the porous medium. For an incompressible fluid equation (138) and conservation of the

a**b**

INVASION PERCOLATION
WITH TRAPPING
 $s = 2 \times 10^5$

1450 LATTICE UNITS

Fig. 47. Invasion percolation. Figure 47a shows a pattern generated by the slow displacement of a wetting fluid by a non-wetting fluid in a pseudo two dimensional porous medium. Figure 47a was taken from ref. 332 (J. Feder, T. Jossang, K.J. Maloy and U. Oxaal, *Ann. Israel Phys. Soc.* 8, 531 (1986)). Figure 47b shows a similar pattern generated by a two dimensional bond threshold invasion percolation model with trapping.

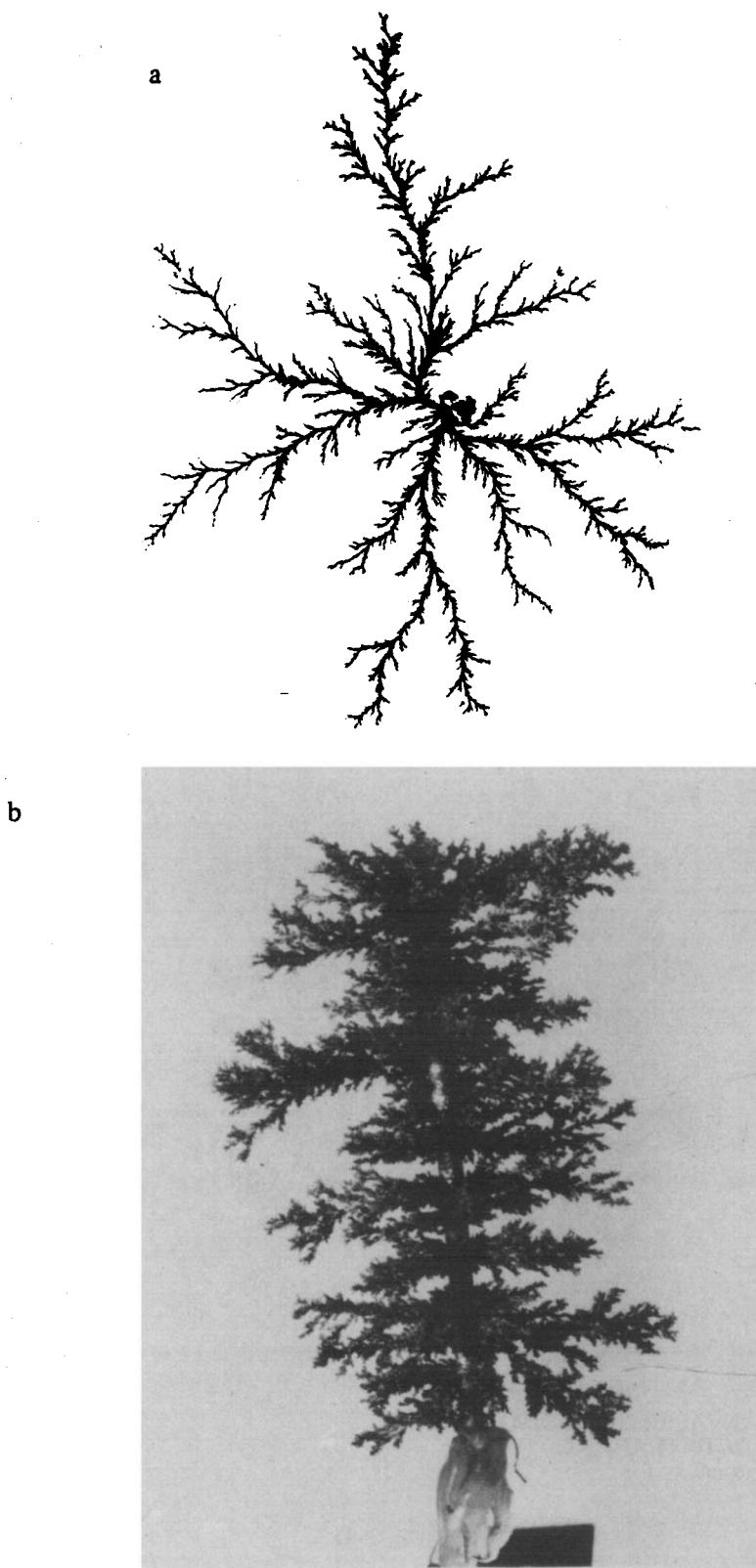


Fig. 48. Dissolution patterns in plaster of Paris. Figure 48a shows a Woods metal casting of a cavity obtained by injecting water into a thin layer of plaster of Paris confined between two parallel sheets of glass. Figure 48b shows the results of a three dimensional experiment in which the water was injected through a hole drilled into a block of plaster of Paris that had been cast into a tube. This figure was provided by G. Daccord and is reproduced with the permission of Dowell Schlumberger.

fluid volume gives the Laplace equation

$$\nabla^2 P = 0 \quad (139)$$

for the water pressure distribution inside the plaster of Paris. The plaster of Paris has a small solubility in water but the equilibrium CaSO_4 concentration in the water is reached quite rapidly. Consequently, the dissolution of the plaster of Paris occurs at the interface between the water saturated plaster of Paris and the region that has been dissolved. The rate of dissolution is proportional to the flux density of water through this interface. The process is random as a consequence of the random structure of the plaster of Paris and the distribution of the rates of growth on the growing interface is controlled by a field (the pressure field inside the porous medium) that obeys the Laplace equation. The pressure drop inside the cavity etched into the plaster of Paris is negligible because there is no friction with a porous medium. Consequently, we have all the ingredients for a DLA process.

Figure 48a shows the result of an experiment in which a narrow (1 mm) gap between two parallel sheets of glass (radius 125 mm) was filled by casting plaster of Paris. Water was then injected at a constant rate through a hole at the center of one of the glass sheets. After a "cavity" had been etched into the plaster of Paris layer the cell was dried and Woods metal was injected into the cavity. Figure 48a shows one of the Woods metal castings. A fractal dimensionality of 1.60 ± 0.10 (in reasonably good agreement with the DLA value of about 1.71) was obtained from the two point correlation functions of digitized images.³³⁸

Figure 48b shows a dissolution pattern obtained using a cylindrical sample 50 mm in diameter and 60 mm long into which water was injected via a 2 mm diameter hole drilled along its axis. The outer surface of the cylinder was exposed ($P = 1 \text{ atm}$). Because of the linearity of the Laplace equation, the magnitude of pressure gradient at the surface of the dissolution pattern (which controls the dissolution rate) is the same as that which would be obtained with a pressure of 0 inside the cavity and a fixed pressure at the surface of the cylinder. Consequently, this process can be simulated using a DLA model with random walkers "coming in" from "outside" despite the fact that the water flows from "inside" to "outside". The pattern shown in Figure 48b resembles quite strongly that obtained using a DLA model of deposition onto a fiber. The fractal properties of structures like that shown in Figure 48b were measured from the kinetics of the dissolution process and a novel approach based on capillary effects.^{340,341} The results obtained were in good agreement with DLA simulations.¹⁴⁴

Rough Surfaces

Rough surfaces and interfaces are important in many commercial and natural processes and the growth of rough surfaces has become a subject of considerable interest from the theoretical and computer simulation point of view (see above). Unfortunately, there are relatively few high quality experimental results that can be used to evaluate the relevance of the computer models and theoretical ideas outlined above. This is an area that deserves much more attention than it has received in recent years. Avnir and his collaborators³⁴²⁻³⁴⁸ have presented evidence to support the idea that the surfaces of most materials are fractal on molecular length scales. This work was based on a large body of previously published data concerning the absorption of molecules of different sizes onto rough surfaces. In this approach the number of molecules per gram of adsorbent (n) is measured as a function of cross-sectional area (σ) or radius (r) of the molecules and an effective fractal dimensionality D , on molecular length scales, is obtained via the relationship

$$N \sim \sigma^{-D/2} \quad (140)$$

or

$$N \sim r^{-D} \quad (141)$$

Alternatively, the size of the adsorbed molecules can be kept fixed and the size of the adsorbing particles varied. In this case a fractal dimensionality is obtained using the relationship

$$N \sim R^{D-3}. \quad (142)$$

This method measures an effective fractal dimensionality on length scales corresponding to the particle radii (R). Without a careful study of the original literature cited by Avnir et al., it is difficult to assess the significance of these results. In many cases data seem to be available over only a relatively short range of length scales and there are substantial uncertainties associated with the details of how molecules adsorb onto irregular heterogeneous surfaces. A concise discussion of some of the caveats associated with these methods is given in reference 346. Taken as a whole, however, this work provides overwhelming evidence for fractal geometry in all manner of surfaces and provides a strong impetus for more detailed studies of individual systems. In one of a number of subsequent more detailed studies of specific systems Rojanski et al.³⁴⁹ used a combination of adsorption, electronic energy transfer and small angle x-ray scattering to study a porous silica gel. All three techniques indicated that the fractal dimensionality of the surface of this material is close to 3.0. This is illustrative of the sort of study that is needed to firmly establish fractal geometry of real surfaces but the result ($D \approx 3$) is disappointing from a "fractal" point of view.

Pfeifer et al.³⁵⁰ have proposed a model for physical adsorption on a fractal surface that leads to an expression of the form

$$N \sim [\ln(P_0/P)]^{(D-3)/3} \quad (143)$$

for the surface coverage. Here P/P_0 is the relative vapor pressure. They have used equation (143) to interpret experiments in which nitrogen is adsorbed at 77°K onto rough silver surfaces that have been obtained by electron beam evaporation onto quartz crystals. From their analysis a fractal dimensionality of 2.30 was obtained. This result was confirmed by scanning-tunneling-microscopy experiments on similar samples. Since the ballistic deposition models described above indicate that surfaces formed by deposition models described above are most probably self-affine the fractal dimensionality of 2.3 should probably be interpreted in terms of a self-affine fractal with a local fractal dimensionality ($D_\epsilon, \epsilon \rightarrow 0$) of about 2.3 and a Hurst exponent of about 0.7. Kardar and Inedeku³⁵¹ have reinterpreted the results of Pfeifer et al. in terms of a self-affine surface with a Hurst exponent of about 0.37 rather than 0.7. This would be in quite good agreement with the value of about 0.35-0.40 obtained from simulations using simple ballistic deposition models (see above).

Avnir and Jaroniec³⁵² have obtained a quite different adsorption isotherm

$$N \sim [\ln(P_0/P)]^{(D-3)} \quad (144)$$

from that of Pfeifer et al.³⁵⁰ (equation 143) based on the work of Dubinin³⁵³. It appears that the absence of surface tension effects in the model of Pfeifer et al. might account for the difference between the two theoretical adsorption isotherms^{352,354}. The adsorption isotherms in equations (143 and 144) are intended to describe multilayer adsorption processes in contrast to the monolayer adsorption model that is used to obtain equations (140-142). A further complication arises from the observation that much of the roughness in the surface of the silver film might be a consequence of roughness in the quartz substrate.³⁵⁵ At present there is good experimental evidence^{350,352,354-357} for adsorption isotherms of the form

$$N \sim [\ln(P_0/P)]^k \quad (145)$$

However, it is not clear how the exponent k in equation (145) is related to the fractal dimensionality. In some cases chemical heterogeneities may play an important role. This is an active area of research that should receive considerable attention in the near future because of its theoretical and practical importance.

Mandelbrot et al.³⁵⁸ have measured the fractal dimensionality of the surface of fractured stainless steel. After the steel sample has been fractured nickel is plated (by an electroless plating technique) onto the fracture surface. The specimen is then mounted in epoxy and polished in a direction parallel to the plane of fracture. The nickel-steel boundary on the polished surface has a complex fractal geometry that can be measured from the perimeter-area relationship for islands of nickel in steel or steel in nickel.

$$\mathcal{L}_p \sim A^{D/2} \quad (146)$$

where \mathcal{L}_p is the perimeter length and A is the island area. A value of about 1.28 was obtained for D from equation (146) corresponding to a value of 2.28 for the fractal dimensionality of the metal surface. Since the fracture surface is probably self-affine, this result can be interpreted in terms of a Hurst exponent of about 0.72 (equation 42).

The specimens were also sectioned in a direction perpendicular to the fracture surface and the fractal nature of the surface (iron-nickel interface) profiles were characterized using Fourier analysis.³⁵⁹ (The interface power spectrum has the form $k^{-(6-2D)}$ or k^{-2H} (from equation (49)). The value obtained for D (about 2.26) or H (about 0.74) was in good agreement with that obtained from the horizontal cross section ("slit Island") method.

Langford et al.³⁶⁰ have recently used the slit island method to measure the fractal characteristics of epoxy. The fractured material was coated with gold and potted in a clear epoxy before polishing to obtain the slit islands. A fractal dimensionality of 1.32 ± 0.03 was obtained using the slit island model (equation 146) corresponding to a value of 2.32 ± 0.03 for the full surface (a Hurst exponent of 0.68 ± 0.03). The time series data for the photon emission intensity were also interpreted in terms of a self-affine fractal curve with a local fractal dimensionality of 1.35 ± 0.03 ($H = 0.65 \pm 0.03$). It seems quite reasonable that the structure of the fracture surface and the photon emission signal should be strongly correlated, but it is not clear why the Hurst exponent should be the same for both the fracture surface and the photon emission signal. Several attempts have been made to relate material properties (such as toughness) to the fractal dimensionality of fracture surfaces.^{358,361,362} Most fracture processes are complex and still quite poorly understood.²⁶⁶ There is, at present, no theoretical understanding of the relationship between D and material fracture processes.

Random Walks, Diffusion, Brownian Motion and Fractals

The paths followed by small particles in a solid or fluid can often be described in terms of fractal geometry. For example, the distance (or root mean square distance) L moved by a particle undergoing Brownian motion in a fluid is related to the length s measured along its own path (or to time t) by

$$L \sim s^v \sim t^v \quad (147)$$

the exponent v is well known to have a value of $1/2$ and the trajectory followed by the particle has a fractal dimensionality D_t given by $D_t = 1/v = 2$. In a low pressure gas the particle (or molecule) will follow a linear trajectory over a substantial distance but in the asymptotic ($t \rightarrow \infty$) limit equation (147) will be obeyed. For a large ensemble of particles we can anticipate that dependence of $\langle L \rangle$ on s (or t) will be given by

$$\langle L \rangle \sim s f(s/s^*) \quad (148)$$

where the function $f(x)$ has the form $f(x) = \text{const.}$ for $x \ll 1$ and $f(x) \sim x^{-1/2}$ for $x \gg 1$. Similarly, if the particle is influenced by an external field or potential gradient in a dense fluid, its motion will be described by equation (147) on short length scales but its trajectory will have an asymptotic fractal dimensionality of 1. In this event we can anticipate that

$$\langle L \rangle \sim s^{1/2} g(s/s^*) \quad (149)$$

where $g(x) = \text{const}$ for $x \ll 1$ and $g(x) \sim x^{1/2}$ for $x \gg 1$. In equation (148) the crossover length s^* can be interpreted as a mean free path or persistent length. In equation 149 the length s^* is the path length over which the particle trajectory appears to be a Brownian trajectory.

A closely related problem that provides an additional motivation for calling $1/\nu$ a fractal dimension is the use of random walks to describe random polymer chains. In this case the polymer mass (M) or number of steps in the walk (N_s) is related to the spatial extent of the walk (the mean end-to-end distance or the radius of gyration, for example) by

$$M \sim L^{1/\nu} \quad (150)$$

or

$$N_s \sim L^{1/\nu} \quad (151)$$

For a random walk the exponent ν has a value of $1/2$ ($D_t = 2$) for all Euclidean spaces and lattices. For the "self-avoiding" random walk that is used to represent the structure of polymer molecules in a "good" solvent, the results given below are obtained from mean field arguments^{363,364}

d	1	2	3	4	5	6
D_t	1	$4/3$	$5/3$	2	2	2

For $d < d_c = 4$ (the critical dimensionalities for the embedding space) $D_t = (d+2)/3$ and for $d > d_c$ $D_t = 2$.

Diffusion plays a central role in almost all areas of science and technology and equation (147) (with $\nu = 1/2$) has been confirmed experimentally in many different ways. In some cases equation (147) has been verified experimentally for up to five orders of magnitude in length scales. For random walks on a fractal lattice (with a fractal dimensionality of D) the dependence of L on s can also be represented by equation (147) and the fractal dimensionality of the walk (D_t) is $1/\nu$. Here L is the distance moved by the random walker in the Euclidean embedding lattice. If $D_t > D$, then the walk compactly explores the lattice (if a lattice site is visited once it will, on average, be visited an infinite number of times by an infinitely long walk). On the other hand, if $D_t < D$, sites are visited only a finite number of times and the total number of sites visited by the walk (F) is proportional to the total length of the walk (N_s) in the asymptotic limit $N_s \rightarrow \infty$. Many of the properties of fractal systems (such as the vibrational density of states) can be described in terms of the fracton or spectral dimensionality³⁶⁵⁻³⁶⁷ (D_s) given by

$$D_s = 2D/D_t \quad (152)$$

If $D_s > 2$, then the walk will be non-compact and if $D_s < 2$, the walk will be compact. For Euclidean lattices $D_t = 2$ so that $D_s = D = d$. For percolation clusters, Alexander and Orbach³⁶⁵ have proposed that $D_s = 4/3$ for all d greater than 2. For $d > d_c = 6$ the result is exact and for $d < 6$ this proposal (known as the Alexander-Orbach conjecture) provides at least a good approximation though it is not generally believed to be exact. The Alexander-Orbach conjecture seems to be approximately true for a wide variety of fractals except for those in which loops are not important.³⁶⁸ In any event random walks on random fractals seem to be almost invariably compact.

The random walk process can be described in terms of a master equation for the probability $P_i(t)$ that the position will be occupied at a time t .

$$d P_i(t)/dt = \sum_j (W_{ji} P_j(t) - W_{ij} P_i(t)) \quad (153)$$

A similar equation describes the propagation of vibrational excitation (within the harmonic approximation)³⁶⁹

$$\frac{d^2(\delta_i)}{dt^2} = \sum_j (K_{ji}\delta_j - K_{ij}\delta_i) \quad (154)$$

where the δ_i are the displacements associated with the vibrational excitation³⁶⁹. The matrices W and K have the same structure. Consequently, an intimate relationship exists between diffusion on a fractal network and the propagation of phonons on the same network.³⁷⁰

For a vibrating Euclidean network the density of states at low frequencies ω is given by

$$N(\omega) \sim \omega^{d-1} \quad (155)$$

Alexander and Orbach³⁷¹ have shown that for a fractal this equation must be replaced by

$$N(\omega) \sim \omega^{D_s-1} \quad (156)$$

where D_s is the fracton or spectral dimensionality introduced in equation (146). The vibrational density of states is important for processes such as thermal conductivity and properties such as the specific heat. The density of state $N(\omega)$ and hence D_s can be measured using Brillouin scattering, neutron scattering, ultrasound attenuation, etc., as well as low temperature specific heat and thermal conductivity measurements. Additional information concerning diffusion and vibrational excitations on fractals can be found in recent reviews^{371,372}. The existence of fractons in tenuous mass fractals has been demonstrated and their nature elucidated by computer simulations.³⁷³⁻³⁷⁵ The existence in real structures has been demonstrated in a beautiful series of experiments by Courtens et al.^{40,376-380} on silica aerogels. This work included small angle neutron scattering, Brillouin scattering and Raman scattering. Low temperature specific heat, thermal conductivity, internal friction and sound velocity measurements were carried out on the same materials by a group at CEN in Grenoble.^{381,382} It appears from these studies that the fractal dimensionality is about 2.4-2.5 in these materials and that D_s has a value of about 1.3-1.4. These studies and work by others on low density aggregates provides a firm experimental foundation for fractons. Fractons have also been observed in the magnetic spin dynamics of randomly diluted antiferromagnetic materials.^{383,384} On the other hand, the existence of fractons in glasses and crosslinked polymers³⁸⁵⁻³⁸⁷ is still a very controversial subject.

Multifractals

Multifractal scaling has been applied with considerable success to the analysis of experimental studies of turbulence^{388,389} and convection.^{390,391} Multifractal $f(\alpha)$ curves have also been measured in driven diode resonator systems³⁹² (here the classification as an experiment or an analog simulation is a matter of taste). In most other cases the large quantity of high quality data needed to obtain reliable $f(\alpha)$ curves seems to have presented a serious barrier. Nittmann et al.³⁹³ have described the distribution of growth probabilities on the surface of two-dimensional viscous fingers. However, the "growth probabilities" were obtained from a numerical solution of the Laplace equation using a digitized image of the viscous fingering pattern as a boundary of zero potential.³⁹⁴ Consequently, this work cannot be cited as experimental evidence for multifractality. A multifractal analysis of the distribution of growth velocities on the surface of two dimensional viscous fingering patterns in a pseudo two-dimensional porous medium has been described by Maloy et al.^{395,396} The results of Maloy et al. strongly support the idea that the growth probability measure can be described in terms of multifractal concepts. Unfortunately, experiments of this type are difficult and this pioneering work did not lead to quantitatively reliable results for the shape of the $f(\alpha)$ curve.

Subfractals

Although "subfractals" such as the Devil's staircase are encountered quite frequently in problems related to non-linear dynamics, they have not (so far) been much utilized in the description of real space phenomena. One interesting example is provided by the work of Thompson, Katz and Raschke³⁹⁷ on the injection of mercury into porous materials (sandstones and sintered glass spheres). They find that the electric resistance decreases as a function of the injection pressure in a series of steps that have a power law distribution over four orders of magnitude. The experimental results are consistent with a percolation model that predicts that the resistance jumps should form a Devil's staircase. Hinrichsen³⁹⁸ has described the distribution of "tree" sizes along the substrate for diffusion-limited deposition on a line in terms of a Devil's staircase.

CHEMISTRY AND PHYSICS IN FRACTALS

The main emphasis of this review is the structure of fractal objects. However, one of the major reasons for being interested in fractal structure is the effects that this structure has on their chemical and physical behavior. Many of the familiar laws of physics and chemistry are quite different for processes occurring in, on and around fractals than they are for more regular Euclidean systems. For example, in recent years considerable interest has developed in simple diffusion-limited reactions³⁹⁹⁻⁴⁰³ represented by



and



on low dimensional Euclidean and fractal lattices. More than ten years ago Ovchinnikov and Zeldovich⁴⁰⁴ showed that for the two species annihilation process (equation (158)) the asymptotic time (t) dependence of the concentrations of A and B were proportional to $t^{-3/4}$ instead of the t^{-1} dependence expected from classical chemical kinetics. Toussaint and Wilczek⁴⁰⁵ carried out simulations for both the one species (equation (157)) and two species process. They showed that the mean field equations of chemical kinetics and the Smoluchowski theory⁴⁰⁶⁻⁴⁰⁷ for diffusion-limited processes do not adequately describe the kinetics of the simple annihilation reactions represented by equations (157) and (158).

For the diffusion-limited one species annihilation process simulated on a hypercubic lattice the density of surviving A covered sites (ρ_A) is given by

$$\rho_A(t) \sim F(t)^{-1} \quad (159)$$

where $F(t)$ is the average number of sites visited by the random walkers after a time t (after t steps). For simple lattices the function $F(t)$ is well known⁴⁰⁸ and equation (159) leads immediately to the result

dimensionality	1	2	3	4
time dependence	$t^{1/2}$	$\log(t)t^{-1}$	t^{-1}	t^{-1}

For $d \geq 3$ the results are in good agreement with the classical chemical kinetics but for the critical dimensionality ($d_c = 2$) important logarithmic corrections are found and for $d = 1$ a $t^{-1/2}$ dependence in the species concentration is predicted. These results have been confirmed by computer simulations⁴⁰⁵ including the logarithmic correction for $d = 2$.⁴⁰⁹

For random walks on a random fractal the fractal substrate is compactly explored throughout a region of

spatial extent L given by

$$L \sim t^{1/D_t} \quad (160)$$

Consequently, the number of sites visited (F) is given by

$$F \sim L^D \sim t^{D/D_t} \sim t^{D_g/2} \quad (161)$$

This means that the density of surviving A species will be given by

$$\rho_A \sim t^{D_g/2} \quad (162)$$

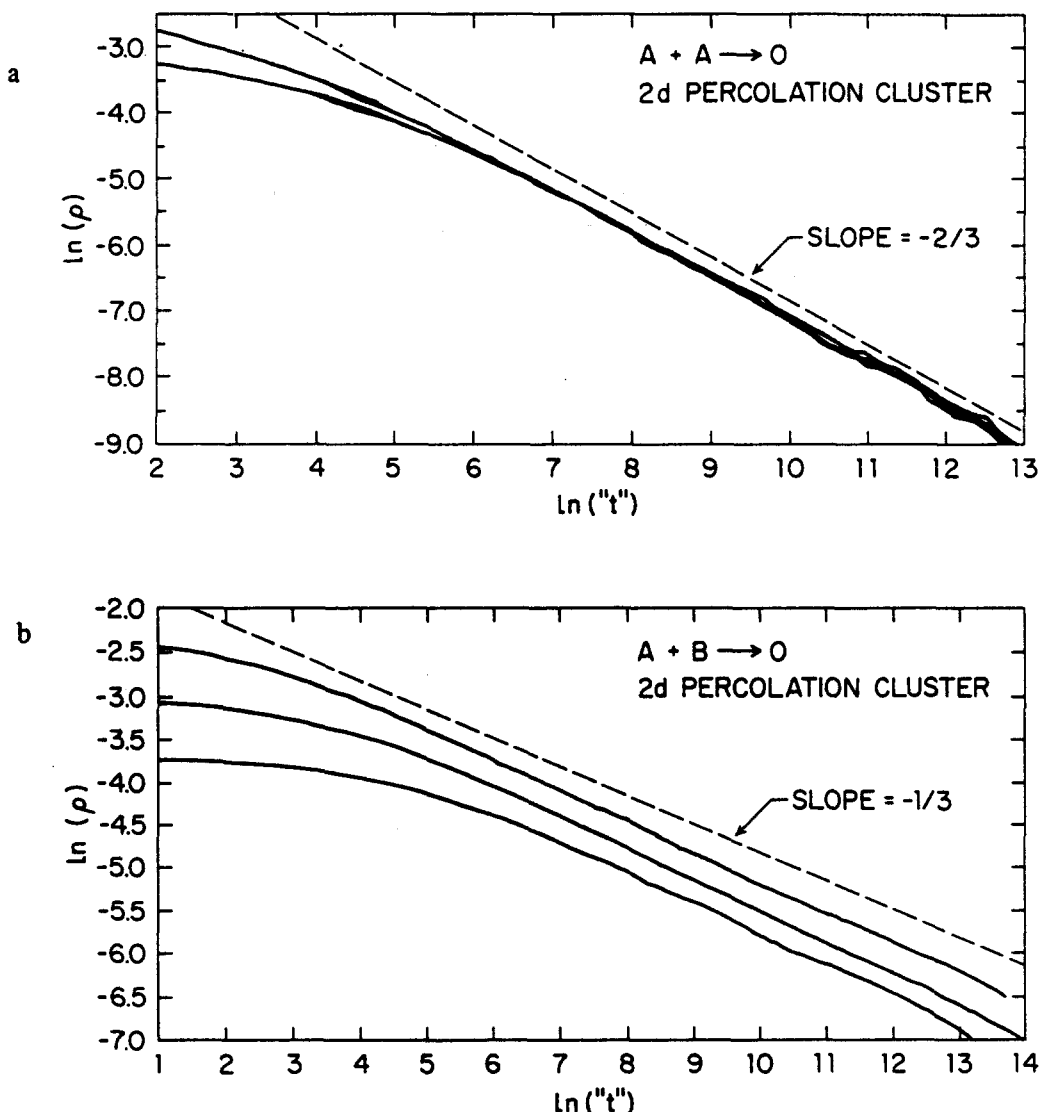


Fig. 49. Time dependence of diffusion-limited annihilation processes on two dimensional square lattice site percolation clusters. Figure 49a shows results for the $A + A \rightarrow O$ process and Figure 49b shows results for the two species $A + B \rightarrow O$ processes. In both cases sites on the percolation cluster were selected randomly (avoiding multiple occupancy) and filled with A "particles" (Figure 49a) or filled alternately with either A or B particles (Figure 49b) at the beginning of each simulation.

Since $D_s \leq 4/3$ for percolation clusters (see above) a $t^{-2/3}$ time dependence is expected. Figures 49a shows the results obtained from simulations carried out on two dimensional percolation clusters.⁴⁰⁹ These simulations were carried out on the "infinite" cluster at the percolation threshold. The expected power law decay with an exponent of about 2/3 is quite well supported by these simulations. Very similar results (also with an exponent of about 2/3) were obtained for the one species annihilation process (equation (157)) on three dimensional percolation clusters.

For the $A + B \rightarrow 0$ two species annihilation process (with equal numbers of A and B) the system evolves into a state that consists of regions which contain only A sites and regions which contain only B sites. This segregation process is a result of fluctuations which are not included in the classical framework of chemical kinetics.

The sizes (correlation length, ξ) of A and B regions is controlled by the diffusion process so that

$$\xi \sim t^{1/D_t} \quad (163)$$

and

$$V\xi \sim t^{D/D_t} \quad (164)$$

where $V\xi$ is the correlation volume.

For uncorrelated random fluctuations the number of sites contained in each of these regions will be given by

$$N\xi \sim (\rho_0 V\xi)^{1/2} \quad (165)$$

where ρ_0 is the initial density so that^{409,410}

$$\rho_A = \rho_B \sim V\xi^{-1/2} \sim t^{D/2D_t} \quad (166)$$

For the special case of Euclidean lattices equation (166) leads to the result

$$\rho_A = \rho_B \sim t^{-d/4} \quad (167)$$

For $d = 1$ and $d = 2$ computer simulations are in good agreement with this theoretical prediction.^{405,409} However, for $d = 3$ the simulations^{409,411} give results which lie between the classical t^{-1} concentration dependence and the $t^{-3/4}$ dependence predicted above. This may be a consequence of the fact that for $d = 3$ the random walks do not compactly explore the cubic lattice and the segregated regions of A and B may themselves have a fractal structure.

For fractal substrates equations (152 and 166) indicated that

$$\rho_A = \rho_B \sim t^{-D_s/4} \quad (168)$$

and if $D_s = 4/3$ then an asymptotic $t^{-1/3}$ particle density is expected. Figure 49b shows results obtained from simulations carried out on two dimensional percolation clusters.⁴⁰⁹ These results are in good agreement with an asymptotic $t^{-1/3}$ decay of the concentration of A and B.

Kopelman et al.⁴¹²⁻⁴¹⁵ have measured the kinetics of triplet-triplet exciton annihilation at low temperatures in naphthalene-hg/naphthalene-dg mixtures. The excitons move (diffuse) on the connected C₁₀H₈ regions and annihilate with the production of light (fluorescence) when two excitons approach each other. The rate of production of singlet excitons (produced by the triplet-triplet annihilation process) can be measured using

the fluorescence intensity (I_F) and the triplet concentration can be measured via its phosphorescence intensity (I_P). Near to the percolation threshold Kopelman et al. found that the ratio $I_F/(I_P)^2$ showed an algebraic time dependence

$$I_F/(I_P)^2 \sim t^{-h} \quad (169)$$

where the exponent h had a value of about 1/3. This corresponds to a $t^{-2/3}$ dependence for the triplet exciton concentration in accord with equation (162) and a value of 4/3 for the spectral dimensionality. This experiment does not correspond to the simulation shown in Figure 49a since the simulation was carried out on a single large percolation cluster while in the experiment the diffusion-limited annihilation process is taking place on the entire distribution of cluster sizes. Since the size distribution exponent (τ) at the percolation threshold has a value of 187/91 (greater than 2) most of the mass of the system will be contained in relatively small clusters at the threshold concentration of naphthalene-dg. As this concentration is exceeded, a larger fraction of the naphthalene will belong to the "infinite" cluster and over some range of concentrations the fraction of naphthalene-dg in the infinite cluster may be large enough and the correlation length ξ large enough for the kinetics to be dominated by a process that is essentially diffusion-limited annihilation on a percolation fractal. This idea is supported by the fact that Kopelman et al. obtained essentially the same value for h over a range of naphthalene-dg concentrations near and above the percolation threshold while a different value ($h \approx 0.45$) was obtained at lower concentrations.

The $t^{D_s/2}$ time dependence for the one species annihilation process and $t^{D_s/4}$ time dependence for the two species annihilation process is quite general and can be used for a wide range of substrates. For example, Martin and Albano⁴¹⁶ and Meakin⁴¹⁷ have obtained simulation results which are consistent with these predictions for one species^{416,417} and two species⁴¹⁸ annihilation on geometrically Euclidean "chemically" heterogeneous substrates with a multifractal distribution of site occupation probabilities.

Strong segregation effects have been found for the two species annihilation reaction (equation (158)) when the reactants (A and B) are fed randomly at a constant rate into a fractal lattice⁴¹⁸ or low dimensional Euclidean lattice⁴¹⁹. Here segregation is driven by the fluctuations in the deposition of A and B into the system and is inhibited by diffusion. For fractal substrates diffusion is inefficient (D_t is large and D_s is small) and segregation is promoted.

The simulation results described in this section were carried out using lattice models. The use of a lattice model may influence the short time behavior but the asymptotic (long time) time dependence is expected to be independent of the details of the lattice structure and should accurately reflect the behavior of continuous systems.

Farin et al.⁴²⁰⁻⁴²² have shown that published data concerning the activity of supported metal catalysis can, in many cases, be summarized by the algebraic expression

$$a \sim R^{D_R} \quad (170)$$

where a is the activity (per particle), R is the metal particle radius and D_R is an exponent that Farin et al. call the "reaction dimensionality". They cite 37 examples, taken from the literature of processes such as hydrogenation, oxidation, isomerization, methanation and ammonia synthesis in which equation (170) describes the dependence of the activity on particle size. The reaction dimensionality can take on a wide range of values ($0 \leq D_R \leq 6$) so that factors other than geometry must make important contributions to D_R .

Relationships similar to equation (170) have also been reported by Farin and Avnir⁴²³ for other processes such as dissolution, thermal decomposition and coal gasification. They suggest that phenomena such as screening, trapping, chemical heterogeneity and morphology changes brought about by the reaction process may contribute to D_R . It is clear that under these circumstances systems must be examined on a case by case basis and that it will be difficult (except for particularly simple systems) to predict the value for D_R . One relatively simple process is the dissolution of a rough particle. It has been observed, empirically, that in a variety of systems the initial rate of dissolution (V) is related to the surface area (s) by^{424,425}

$$V \sim s^m . \quad (171)$$

Silverberg et al.⁴²⁵ suggest that in some cases the exponent m can be understood in terms of a reactive subset on the surface of the particles with a fractal dimensionality \bar{D} . They suggest that the rate of dissolution is proportional to the area of that subset s in contact with the solvent. Since the total surface area (s) is given by equation (142)

$$s \sim R^{D-3} \quad (172)$$

(where D is the fractal dimensionality of the surface) and the area of the reactive surface is given by

$$\bar{s} \sim R^{\bar{D}-3} \quad (173)$$

it follows that the exponent m is given by⁴²⁵

$$m = \frac{\bar{D}-3}{D-3} \quad (174)$$

In more complex systems there might be many subsets each with their own reactivities and fractal dimensionalities. Consequently, the concepts of multifractality might prove to be of value in this area also.

In the limit in which the dissolution process is diffusion-limited and the diffusion length is sufficiently long, the distribution of dissolution rates on the surface of the rough particles can be described by the harmonic measure and the dissolution process can be simulated using random walkers in much the same way that the Laplacian field is simulated using random walkers in DLA simulations.^{425,426}

Many of the physical properties of mass fractals are quite different from those associated with compact structures. For example, the hydrodynamic radius R_h is related to the mass M by

$$R_h \sim M^{1/D} \quad (175)$$

in the asymptotic ($M \rightarrow \infty$) limit.⁴²⁷⁻⁴³⁴ The area of a projection onto a plane is given by

$$\sigma \sim M \quad \text{for } D \leq 2 \quad (176a)$$

$$\sigma \sim M^{2/D} \quad \text{for } D \geq 2 . \quad (176b)$$

This has important implications for properties such as the aerodynamic friction coefficients⁴³⁵ and light scattering.⁴³⁶⁻⁴³⁹

The mechanical properties of fractal structures is also a subject of considerable interest. For a network of particles formed by aggregation or gelation the structure can be expected to be fractal on length scales up to the correlation length given by

$$\xi \sim \rho^{D-d} \quad (177a)$$

or

$$\xi \sim \rho^{D-3} \quad (177b)$$

for a three dimensional embedding space where ρ is the particle density in the network. Brown and Ball⁴⁴⁰ have

shown that for such a system the elastic modulus of the network should depend algebraically on its density

$$G \sim \rho^\mu \quad (178)$$

where the exponent μ is given by

$$\mu = \frac{3 + D_m}{3-D} \quad (179)$$

Here D_m is the minimum path dimensionality that related the minimum distance between two points measured on the fractal, ℓ_{\min} , and the distance, r , between these two points measured in the Euclidean embedding space.

$$\ell_{\min} \sim r^{D_m} \quad (180)$$

Values of 3-5 for the exponent μ are typical for networks formed by processes such as diffusion-limited cluster-cluster aggregation. A variety of experimental studies on low density materials (aerogels, fumed silica, aggregated polymer particles, etc.⁴⁴¹⁻⁴⁴⁶) can be summarized by relationships quite similar to that given in equation (172).

$$G = (\rho - \rho_0)^\mu \quad (181)$$

where ρ_0 has a quite small value (≤ 0.1 that of pore free material) and the exponent μ has a high value (typically 3-6). These properties have important implications in areas such as air and water pollution, the nuclear winter scenario,^{447,448} accretion in the primordial solar nebula^{449,450} and materials processing.^{445,446}

The electrical conductivity of fractal networks is an important property that is amenable to both theoretical and experimental investigation. It is well known that the conductivity of a percolating network above the percolation threshold is given by⁴⁵¹

$$\sigma(L) \sim L^{-t/\nu} f(L/\xi) \quad (182)$$

where $\sigma(L)$ is the average conductivity in a region of size L . In the limit $L/\xi \gg 1$ where the system is uniform on length scales comparable to L the conductivity is independent of L and is given by

$$\sigma \sim \xi^{-t/\nu} \quad (183)$$

or

$$\sigma \sim (p - p_c)^t . \quad (184)$$

If the length L is smaller than the correlation length, ξ , then the conductivity is dependent on L and is given by

$$\sigma \sim L^{-t/\nu} \quad (185)$$

For a fractal structure we expect to find an algebraic relationship between the conductance (g) and the distance (r) between two points on the fractal measured in the embedding space.

$$\langle g \rangle \sim r^\mu \quad (186)$$

The exponent μ in equation (180) can be obtained from the Einstein relationship between conductivity and the diffusion coefficient (D)

$$\sigma \sim D \quad (187)$$

and from this it follows that^{452,453}

$$\mu = D_t - D \quad (188)$$

In a fractal structure the current is carried by a subset of the fractal known as the "backbone" and equation (188) can be applied to this fractal as well

$$\mu = D_{tb} - D_b \quad (189)$$

where D_b and D_{tb} are the fractal dimensionalities of the backbone and of random walks on that backbone. The exponent relating the conductivity (σ) to L (t/v in equation (185)) has a value of $D_t - D + d - 2$ or $D_{tb} - D_b - d - 2$.

In the case of a loopless structure (such as DLA) the exponent μ in equation (186) is equal to the minimum path dimensionality D_m defined in equation (180). For such structure the exponent μ can also be expressed in terms of the spectral dimensionality (D_s). Kaufman et al.⁴⁵⁴⁻⁴⁵⁵ have measured the electric resistance as a function of the distance (r) using two dimensional DLA fractals generated by the diffusion-controlled electrochemical polymerization of pyrrole. A value of 1.04 ± 0.04 was obtained for the exponent μ in equation (186). This result is in good agreement with computer simulations⁴⁵⁶ that indicate that D_m has a value of about 1.0 for $d = 2$. Simulation results indicate that μ (D_m) has a value of about 1.0 for three dimensional DLA also but this has not been tested experimentally. Using values of 1.0 and 1.715 for μ and D in equation (188), gives a value of 2.715 for D_t and 1.26 for D_s . The value for D_s is in good agreement with available simulation results^{457,458} but the statistical uncertainties associated with the simulation results are quite large.

Another topic that has received considerable attention is the "constant phase angle" impedance of ionic solutions in contact with rough electrodes.⁴⁵⁹⁻⁴⁷⁶ Frequently, such electrodes exhibit a characteristic constant phase angle behavior in which the low frequency impedance, $Z(\omega)$, can be described by

$$Z(\omega) \sim (i\omega)^p \quad (190)$$

where the exponent p lies in the range $0 < p < 1$. In general, rough surfaces lead to a smaller value for p . However, no consensus has arisen concerning the relationship between p and the fractal scaling properties of self-affine and self-similar surfaces. In view of the theoretical attention focused on this problem, it seems quite likely that progress will be made during the next 2-3 years.

SUMMARY

Fractal geometry is a rapidly growing but already quite extensive area. As with all such areas much of our knowledge and many techniques will be superceded during the coming years. However, substantial progress has been made and both the basic concepts of fractal geometry and many of its applications will have lasting value. In this review I have described the ideas and approaches that I have found to be of most value in applying fractal geometry to the results of computer experiments. The same methods have been applied successfully by others to a wide variety of experiments on real systems.

The development and eventual popularization of fractals by B. B. Mandelbrot has stimulated a renewed interest in the science of complex and random systems. This background and the introduction of the diffusion-limited aggregation model by Witten and Sander²¹ has led to a broad interest in non-equilibrium growth models. Here I have attempted to illustrate some of the progress that has been made in this area and use it to show how

fractal geometry can be applied to problems in the physical sciences. There has also been a large quantity of concomitant experimental work. The examples of experiments and simulations have been selected to illustrate how fractal geometry can be applied in solid state chemistry. Consequently, I have neglected, for the most part, the quite extensive experimental work on fractal colloidal aggregates.

A description of multifractals has been included. Interest in this aspect of fractal geometry is quite recent (though its origins are much older). There are, as yet, few applications in areas relevant to solid state chemistry. However, there are strong indications that this approach will eventually prove to be of value in understanding phenomena such as diffusion-limited reactions at rough interfaces, mechanical and dielectric breakdown phenomena, catalysis and other phenomena of importance in solid state chemistry.

Despite the substantial progress that has been made in recent years, much work remains to be done. Our basic understanding of even very simple processes leading to the formation of fractal structures is still, in most cases, quite inadequate. In many areas there is still an urgent need for high quality experimental studies that will help to determine the scope of applications of fractal geometry to real systems and assess the quality of understanding what can be achieved in this manner.

A comprehensive survey of fractal geometry and its applications is no longer a practical undertaking. There are now a substantial number of books, reviews and conference proceedings devoted to fractal geometry and its applications. The Mandelbrot classics (particularly *The Fractal Geometry of Nature*, W. H. Freeman and Company, New York (1982)) are still the major sources of information. In addition, there are two excellent intermediate level books that I would strongly recommend to anyone interested in applying fractal geometry to solid state chemistry. These are *Fractals* by J. Feder (Plenum, New York (1989)) and *Fractal Growth Phenomena* by T. Vicsek (World Scientific, Singapore (1989)). Of the many multiauthor books and conference proceedings, *The Fractal Approach to Heterogeneous Chemistry: Surfaces, Colloids, Polymers* (D. Avnir, ed., Wiley, Chichester (1989)) and *Fractals in Physics: Essays in Honor of Benoit B. Mandelbrot* (A. Aharony and J. Feder, eds., North Holland, Amsterdam (1989)) would be of particular interest to readers of *Progress in Solid State Chemistry*.

ACKNOWLEDGMENT

My interest in and understanding of fractal geometry are a consequence of interactions with many colleagues and collaborators. Some of the work described in this review was carried out with R. C. Ball, R. Botet, A. Coniglio, J. P. Eckmann, T. C. Halsey, R. Jullien, J. Krug, I. Procaccia, H. E. Stanley, S. Tolman, L. M. Sander, T. A. Witten and R. Zeitak. I would also like to thank G. Daccord, J. Feder, J. E. Martin, P. W. Schmidt and R. F. Voss for providing figures used in this review.

REFERENCES

- (1) B.B. Mandelbrot, *Les Objets Fractales: Forme, Hasard et Dimension*, Flammarion, Paris, 1975.
- (2) B.B. Mandelbrot, *Fractals: Form, Chance and Dimension*, W. H. Freeman and Company, San Francisco, 1977.
- (3) B.B. Mandelbrot, *The Fractal Geometry of Nature*, W. H. Freeman and Company, New York, 1982.
- (4) B.B. Mandelbrot, *Encyclopedia of Physical Science and Technology*, Vol. 5 (Academic Press, New York), 1987, p. 579.
- (5) J. Feder, *Fractals*, Plenum Press, New York, 1988.
- (6) B.B. Mandelbrot in *Fractals in Physics*, Proceedings of the Sixth International Symposium on Fractals in Physics, L. Pietronero and E. Tosatti, eds., ICTP, North Holland, Amsterdam, 1986, p. 3.
- (7) T. Vicsek, *J. Phys. A* **16**, L647 (1983).
- (8) E.E. Fournier D'Albe, *Two New Worlds, I. The Infra World, II. The Supra World*, Longmans Green, London, 1907.

- (9) S.R. Broadbent and J. M. Hammersley, *Proc. Camb. Phil. Soc.* **53**, 629 (1957).
- (10) J.M. Hammersley, *Proc. Camb. Phil. Soc.* **53**, 642 (1957).
- (11) J.W. Essam in *Phase Transitions and Critical Phenomena*, C.S. Domb and M.S. Green, eds., Academic, London, 1972, Vol. 2, p. 192.
- (12) S. Kirkpatrick, *Rev. Mod. Phys.* **45**, 574 (1973).
- (13) D. Stauffer, *Phys. Rep.* **54**, 1 (1979).
- (14) D. Stauffer, *Introduction to Percolation Theory*, Taylor and Francis, London, 1985.
- (15) P.L. Leath, *Phys. Rev. B* **14**, 5046 (1976).
- (16) Z. Alexandrowicz, *Phys. Lett.* **80A**, 284 (1980).
- (17) M.P.M. den Nijs, *J. Phys. A* **12**, 1857 (1979).
- (18) R.B. Pearson, *Phys. Rev. B* **22**, 2579 (1980).
- (19) B. Nienhuis, E.K. Riedel and M. Schick, *J. Phys A* **13**, L189 (1980).
- (20) R.M. Ziff and G. Stell, unpublished.
- (21) T.A. Witten and L.M. Sander, *Phys. Rev. Lett.* **47**, 1400 (1981).
- (22) K. Kremer and J.W. Lyklema, *Phys. Rev. Lett.* **54**, 267 (1985).
- (23) Z.V. Djordjevic, I. Majid, H.E. Stanley and R.J. dos Santos, *J. Phys. A* **16**, L519 (1983).
- (24) J.W. Lyklema and K. Kremer, *Phys. Rev. B* **31**, 3182 (1985).
- (25) Y. Kantor and T.A. Witten, *J. Phys. (Paris)*, **45**, L675 (1984).
- (26) T.A. Witten and L.M. Sander, *Phys. Rev. B* **27**, 5686 (1983).
- (27) W.T. Elam, S.A. Wolf, J. Sprague, D.U. Gubser, D. Van Vechten, G.L. Bairz, Jr. and P. Meakin, *Phys. Rev. Lett.* **54**, 701 (1985).
- (28) R. Jullien and R. Botet, *Aggregation and Fractal Aggregates*, World Scientific, Singapore, 1987.
- (29) P. Meakin, in *Phase Transitions and Critical Phenomena*, C. Domb and J.L. Lebowitz, eds., Vol. 12, Academic, New York, 1988, p. 335.
- (30) P. Meakin, *Phys. Rev. Lett.* **51**, 1119 (1983).
- (31) M. Kolb, R. Botet and R. Jullien, *Phys. Rev. Lett.* **51**, 1123 (1983).
- (32) J.E. Martin and A.J. Hurd, *J. Appl. Crystallogr.* **20**, 61 (1987).
- (33) J. Teixeira in *On Growth and Form: Fractal and Non-Fractal Patterns in Physics*, H. E. Stanley and N. Ostrowsky, eds., NATO ASI series E100, Martinus Nijhoff, p. 145.
- (34) P.W. Schmidt in *The Fractal Approach to Heterogeneous Chemistry: Surfaces, Colloids, Polymers*, D. Avnir, ed., Wiley, Chichester, 1989, p. 67.
- (35) R. Klein, D.A. Weitz, M.Y. Lin, H.M. Lindsay, R.C. Ball and P. Meakin, preprint.
- (36) D.A. Weitz and M. Oliveria, *Phys. Rev. Lett.* **52**, 1433 (1984).
- (37) J. Kjems and T. Freloft in *Scaling Phenomena in Disordered Systems*, R. Pynn and A.T. Skjeltorp, eds., NATO ASI Series B133, Plenum Press, New York, 1985, p. 133.
- (38) D.W. Schaefer, J.E. Martin, P. Wiltzius and D.S. Cannell, *Phys. Rev. Lett.* **52**, 2371 (1984).
- (39) S.K. Sinha, T. Freloft and J. Kjems in *Kinetics of Aggregation and Gelation*, F. Family and D.P. Landau, eds., North Holland, Amsterdam, 1984, p. 87.
- (40) R. Vacher, T. Woignier, J. Pelous and E. Courtens, *Phys. Rev. B* **37**, 6500 (1988).
- (41) G. Allain and M. Cloitre, *Phys. Rev. B* **33**, 3566 (1986).
- (42) M.Y. Lin, H.M. Lindsay, D.A. Weitz, R.C. Ball, R. Klein and P. Meakin, *Nature* **339**, 360 (1989).
- (43) P. Dimon, S.K. Sinha, D.A. Weitz, C.R. Safinya, G.S. Smith, W.A. Varady and H.M. Lindsay, *Phys. Rev. Lett.* **57**, 595 (1986).
- (44) J.D.F. Ramsay, *Chem. Soc. Rev.* **15**, 335 (1986).
- (45) J.E. Martin and B.J. Ackerson, *Phys. Rev. A* **31**, 1180 (1985).
- (46) P.W. Schmidt, *J. Appl. Crystallogr.* **15**, 567 (1982).
- (47) J.E. Martin, *J. Appl. Crystallogr.* **19**, 25 (1986).
- (48) A. Guinier and G. Fournet, *Small Angle Scattering of X-Rays*, Wiley, New York, 1955.
- (49) C. Aubert and D.S. Cannell, *Phys. Rev. Lett.* **56**, 738 (1986).

- (50) M. Kolb and R. Jullien, *J. Physique Lett.* **45**, L977 (1984).
- (51) R. Jullien and M. Kolb, *J. Phys. A* **17**, L639 (1984).
- (52) W.D. Brown and R.C. Ball, *J. Phys. A* **18**, L517 (1985).
- (53) P. Meakin and F. Family, *Phys. Rev. A* **36**, 5498 (1987).
- (54) P. Meakin and F. Family, *Phys. Rev. A* **38**, 2110 (1988).
- (55) H.D. Bale, M.D. Carlson, M. Kalliat and P.W. Schmidt in *The Chemistry of Low-Rank Coal*, H.H. Schobert, ed., ACS Symposium Series No. 264, American Chemical Society, Washington, D. C., 1984, p. 79
- (56) H.D. Bale and P. Schmidt, *Phys. Rev. Lett.* **53**, 596 (1984).
- (57) H.G.E. Hentschel and I. Procaccia, *Physica* **8D**, 435 (1983).
- (58) P. Meakin and Z.R. Wasserman, *Chem. Phys.* **91**, 391 (1984).
- (59) F. Argoul, A. Arneodo, G. Grasseau and H.L. Swinney, *Phys. Rev. Lett.* **61**, 2558 (1989).
- (60) G. Li, L.M. Sander and P. Meakin, *Phys. Rev. Lett.* **63**, 1322 (1989).
- (61) T. Tel and T. Vicsek, *J. Phys. A* **20**, L835 (1987).
- (62) T. Tel, A. Fulop and T. Vicsek, *Physica A* **159**, 155 (1989).
- (63) T. Tel, *Z. Naturforsch.* **43a**, 1154 (1988).
- (64) J.P. Hansen, J.M. McCauley, J. Muller and A.T. Skjeltorp in *Random Fluctuations and Pattern Growth: Experiments and Models*, H.E. Stanley and N. Ostrowski, eds., Kluwer Dordrecht, 1988, p. 310.
- (65) J. Feder, private communication.
- (66) B.B. Mandelbrot, *Physica Scripta*, **32**, 257 (1985).
- (67) H.E. Hurst, *Trans Am. Soc. Civil Eng.* **116**, 770 (1951).
- (68) H.E. Hurst, R.P. Black and Y.M. Simaika, *Long-Term Storage: An Experimental Study*, Constable, London, 1965.
- (69) R.F. Voss in *Scaling Phenomena in Disordered Systems* NATO ASI Series B133, R. Pynn and A.T. Skjeltorp, eds., Plenum Press, New York, 1986.
- (70) P.-Z. Wong, *Phys. Rev. B* **32**, 7417 (1985).
- (71) S. Alexander, preprint.
- (72) B.B. Mandelbrot and J.R. Wallis, *Water Resour. Res.* **4**, 909 (1968).
- (73) B.B. Mandelbrot and J.R. Wallis, *Water Resour. Res.* **5**, 321 (1969).
- (74) B.B. Mandelbrot and J.R. Wallis, *Water Resour. Res.* **5**, 228 (1969).
- (75) B.B. Mandelbrot and J.R. Wallis, *Water Resour. Res.* **5**, 242 (1969).
- (76) B.B. Mandelbrot and J.R. Wallis, *Water Resour. Res.* **5**, 260 (1969).
- (77) B.B. Mandelbrot and J.R. Wallis, *Water Resour. Res.* **5**, 967 (1969).
- (78) J. Froyland, J. Feder and T. Jossang, to be published.
- (79) B. Dubuc, J.F. Quiniou, C. Roques-Carmes, C. Tricot and S.W. Zucker, *Phys. Rev. A* **39**, 1500 (1989).
- (80) M.V. Berry and Z.V. Lewis, *Proc. Roy. Soc. (London) A* **370**, 459 (1980).
- (81) C. Tricot, *Gaz Sci. Math. Quebec*, **10**, 3 (1986).
- (82) B.B. Mandelbrot and J.W. Van Ness, *SIAM Rev.* **10**, 422 (1968).
- (83) J.D. Farmer, *Phys. Rev. Lett.* **55**, 351 (1985).
- (84) R. Ekholt and D.K. Umberger, *Phys. Rev. Lett.* **57**, 2333 (1986).
- (85) C. Grebogi, S.W. McDonald, E. Ott and J.A. Yorke, *Physics Lett. A* **110**, 1 (1985).
- (86) P.P. Pfeifer and M. Obert in *The Fractal Approach to Heterogeneous Chemistry: Surfaces, Colloids, Polymers*. D. Avnir, ed., Wiley, Chichester, 1989, p. 11.
- (87) H.E. Stanley and P. Meakin, *Nature* **335**, 6189 (1988).
- (88) B.B. Mandelbrot, *J. Fluid Mech.* **62**, 331 (1974).
- (89) B.B. Mandelbrot in *Fractals' Physical Origin and Properties*, L. Pietronero, ed., Plenum, New York, 1989, p. 3.

- (90) T.C. Halsey, M.H. Jensen, L.P. Kadanoff, I. Procaccia and B. Shraiman, *Phys. Rev. A* **33**, 1141 (1986).
- (91) P. Meakin, *Phys. Rev. A* **34**, 710 (1986).
- (92) P. Meakin, *Phys. Rev. A* **35**, 2234 (1987).
- (93) B.B. Mandelbrot in *Random Fluctuations and Pattern Growth*, NATO ASI Series E157, H.E. Stanley and N. Ostrowsky, eds., Kluwer Dordrecht, 1988, p. 279.
- (94) A. Chhabra and R.V. Jensen, *Phys. Rev. Lett.* **62**, 1327 (1989).
- (95) A. Atmanspacer, H. Scheingraber and G. Wiedenmann, preprint.
- (96) R.E. Amritkar and N. Gupte, *Phys. Rev. Lett.* **60**, 245 (1988).
- (97) A.B. Chhabra, R.V. Jensen and K.R. Sreenivasan, *Phys. Rev. A* **40**, 4593 (1989).
- (98) M.E. Cates and J.M. Deutch, *J. Stat. Phys.* **35**, 4907 (1987).
- (99) S.J. Lee and T.C. Halsey, preprint (1990).
- (100) B.B. Mandelbrot in *Statphys. 17*, C. Tsallis, ed., North Holland, Amsterdam, 1990.
- (101) P. Bak, C. Tang and K. Wiesenfeld, *Phys. Rev. Lett.* **59**, 381 (1987).
- (102) P. Bak, C. Tang and K. Wiesenfeld, *Phys. Rev. A* **38**, 364 (1988).
- (103) C. Tang and P. Bak, *J. Stat. Phys.* **60**, 2347 (1988).
- (104) C. Tang and P. Bak, *J. Stat. Phys.* **51**, 797 (1988).
- (105) T. Hwa and M. Kardar, *Phys. Rev. Lett.* **62**, 1813 (1989).
- (106) D. Dhar and R. Ramaswamy, *Phys. Rev. Lett.* **63**, 1659 (1989).
- (107) Y.-C. Zhang, *Phys. Rev. Lett.* **63**, 470 (1989).
- (108) L.P. Kadanoff, S.R. Nagel, L. Wu and S.-M. Zhou, *Phys. Rev. A* **39**, 6524 (1989).
- (109) P. Bak and K. Chen, *Physica D* **38**, 5 (1989).
- (110) J.-P. Eckmann, P. Meakin, I. Procaccia, and R. Zeitak, *Phys. Rev.* **39**, 3185 (1989).
- (111) J.-P. Eckmann, P. Meakin, I. Procaccia and R. Zeitak, *Phys. Rev. Lett.* **65**, 52 (1990).
- (112) P. Meakin, F. Leyvraz and H.E. Stanley, *Phys. Rev. A* **31**, 1195 (1985).
- (113) L.A. Turkevich and H. Scher, *Phys. Rev. Lett.* **55**, 1026 (1985).
- (114) T.C. Halsey, P. Meakin and I. Procaccia, *Phys. Lett.* **56**, 854 (1986).
- (115) R.C. Ball, *Physica* **104A**, 62 (1986).
- (116) R.C. Ball, M.J. Blunt and O. Rath Spivack, *Proc. Roy. Soc. (London)* **423**, 1 (1989).
- (117) M. Muthukumar, *Phys. Rev. Lett.* **50**, 839 (1983).
- (118) R.C. Ball and T.A. Witten, *Phys. Rev. A* **29**, 2966 (1984).
- (119) A. Gould, F. Family and H.E. Stanley, *Phys. Rev. Lett.* **50**, 686 (1983).
- (120) L. Pietronero, A. Erzan and C. Evertsz, *Phys. Rev. Lett.* **61**, 861 (1988).
- (121) M. Eden, *Proceedings of the Fourth Berkeley Symposium on Math, Statistics and Probability*, F. Neyman, ed., University of California Press, Berkeley, CA, 1961.
- (122) R. Jullien and R. Botet, *Phys. Rev. Lett.* **54**, 2055 (1985).
- (123) R. Jullien and R. Botet, *J. Phys. A* **18**, 2279 (1985).
- (124) P. Freche, D. Stauffer and H.E. Stanley, *J. Phys. A* **15**, L1163 (1985).
- (125) R. Hirsch and D.E. Wolf, *J. Phys. A* **19**, L251 (1986).
- (126) J.G. Zabolitzky and D. Stauffer, *Phys. Rev. A* **34**, 1523 (1986).
- (127) P. Meakin, R. Jullien and R. Botet, *Europhys. Lett.* **1**, 609 (1986).
- (128) D. Richardson, *Proc. Cambridge Philos. Soc.* **74**, 515 (1973).
- (129) P. Meakin, *Phys. Rev. A* **38**, 418 (1988).
- (130) C. Tang, *Phys. Rev. A* **31**, 1977 (1985).
- (131) J. Kertsz and T. Vicsek, *J. Phys. A* **19**, 2257 (1986).
- (132) S.R. Forrest and T.A. Witten, *J. Phys. A* **12**, L109 (1979).
- (133) R. Jullien, *Ann. Telecommun.* **41**, 343 (1986).
- (134) L. M. Sander, *Nature* **322**, 789 (1986).
- (135) P. Meakin, *Advances in Colloid and Interface Sci.*, **28**, 249 (1988).

- (136) P. Meakin, *Ann. Rev. Phys. Chem.* **39**, 237 (1988).
- (137) T. Vicsek, *Fractal Growth Phenomena*, World Scientific, Singapore, 1988.
- (138) T.A. Witten and M.E. Cates, *Science*, **232**, 1607 (1986).
- (139) R. Jullien and R. Botet, *Aggregation and Fractal Aggregates*, World Scientific, Singapore, 1987.
- (140) P. Meakin, *J. Phys. A* **18**, L661 (1985).
- (141) R.C. Ball and R.M. Brady, *J. Phys. A* **18**, L809 (1985).
- (142) S. Tolman and P. Meakin, *Phys. Rev. A* **40**, 428 (1989).
- (143) P. Meakin, *Phys Rev. A* **27**, 2616 (1983).
- (144) P. Meakin, *Phys. Rev. B* **30**, 4207 (1984).
- (145) R. Jullien, M. Kolb and R. Botet, *J. Phys. (Paris)* **45**, 395 (1984).
- (146) P. Meakin and F. Family, *Phys. Rev. A* **34**, 2558 (1986).
- (147) K. J. Maloy, private communication.
- (148) M. Matsushita, Y. Hayakawa and Y. Sawada, *Phys. Rev. A* **32**, 3814 (1985).
- (149) G. Helgesen in *Time Dependent Effects in Disordered Materials*, R. Pynn and T. Riste, eds., NATO ASI Series B167, Plenum Press, New York, 1987, p. 89.
- (150) H. van Damme in *The Fractal Approach to Heterogeneous Chemistry: Surfaces, Colloids, Polymers*", D. Avnir, ed., Wiley, Chichester, 1989, p. 199.
- (151) Z. Racz and T. Vicsek, *Phys. Rev. Lett.* **51**, 2382 (1983).
- (152) P. Meakin and T. Vicsek, *Phys. Rev. A* **32**, 1026 (1985).
- (153) T.C. Halsey and P. Meakin, *Phys. Rev. A* **32**, 2547 (1985).
- (154) M. Kolb, *J. Phys. (Paris) Lett.* **46**, L632 (1985).
- (155) P. Meakin, *Phys. Rev. A* **27**, 604 (1983).
- (156) P. Meakin, *Phys. Rev. A* **27**, 2495 (1983).
- (157) M. Tokayama and K. Kawasaki, *Phys. Lett.* **100A**, 337 (1984).
- (158) M. Matsushita, K. Honda, H. Toyoki, Y. Hayakawa and H. Kondo, *J. Phys. Soc. Japan*, **55**, 2618 (1986).
- (159) M. Matsushita, Y. Hayakawa, S. Sato and K. Honda, *Phys. Rev. Lett.* **59**, 86 (1987).
- (160) K. Honda, H. Toyoki and M. Matsushita, *J. Phys. Soc. Japan*, **55**, 2479 (1986).
- (161) F. Leyvraz, *J. Phys. A* **18**, L941 (1985).
- (162) L. Turkevich and H. Sher, *Phys. Rev. A* **33**, 786 (1986).
- (163) P.M. Morse and H. Feshbach, *Methods of Theoretical Physics*, McGraw Hill, New York, 1963.
- (164) P. Meakin, *Phys. Rev. A* **33**, 3371 (1986).
- (165) R.C. Ball, R.M. Brady, G. Rossi and B.R. Thompson, *Phys. Rev. Lett.* **55**, 1406 (1985).
- (166) P. Meakin, H.E. Stanley, A. Coniglio and T.A. Witten, *Phys. Rev. A* **32**, 2364 (1985).
- (167) P. Meakin, A. Coniglio, H.E. Stanley and T.A. Witten, *Phys. Rev A* **34**, 3325 (1986).
- (168) C. Amitrano, A. Coniglio and F. di Liberto, *Phys. Rev. Lett.* **57**, 1016 (1986).
- (169) J. Lee and H.E. Stanley, *Phys. Rev. Lett.* **61**, 2945 (1988).
- (170) J. Lee, P. Alstrom and H.E. Stanley, *Phys. Rev. A* **39**, 6545 (1989).
- (171) R. Blumenfeld and A. Aharony, *Phys. Rev. Lett.* **62**, 2977 (1989).
- (172) A.B. Harris and M. Cohen, *Phys. Rev. A* **41**, 971 (1990).
- (173) T. Nagatini, *J. Phys. A* **20**, L381 (1987).
- (174) T. Nagatini, *Phys. Rev. A* **35**, 2765 (1987).
- (175) I. Procaccia and R. Zeitak, *Phys. Rev. Lett.* **60**, 2511 (1988).
- (176) P. Alstrom, P. Trufino and H. E. Stanley in *Random Fluctuations and Pattern Growth: Experiments and Models*, H. E. Stanley and N. Ostrowsky, eds., NATO ASI Series E157, Kluwer, Dordrecht, 1988, p. 340.
- (177) H. Gould, F. Family and H. E. Stanley, *Phys. Rev. Lett.* **50**, 686 (1983).
- (178) L. Niemeyer, L. Pietronero and H.J. Wiesmann, *Phys. Rev. Lett.* **52**, 1033 (1984).
- (179) P. Meakin, *J. Theor. Biol.* **118**, 101 (1986).

- (180) M. Matsushita, K. Honda, H. Toyoki, Y. Hayakawa and N. Kondo, *J. Phys. Soc. Japan* **55**, 2618 (1986).
- (181) Y. Hayakawa, H. Kondo and M. Matsushita, *J. Phys. Soc. Japan*, **55**, 2479 (1986).
- (182) S. Tolman and P. Meakin, *Physica A* **158**, 801 (1989).
- (183) C.J.G. Evertsz, *Laplacian Fractals*, Thesis, Rijksuniversiteit, The Cheese Press, Edam, The Netherlands, 1989.
- (184) H.J. Wiesmann and L. Pietronero in *Fractals in Physics*, Proc. Sixth Int. Symp. on Fractals in Physics ICTP, L. Pietronero and E. Tosatti, eds., North Holland, Amsterdam, 1986, p. 151.
- (185) J. Nittmann and H.E. Stanley, *Nature* **321**, 663 (1986).
- (186) P. Meakin, *Proc. Roy. Soc. (London) A* **423**, 133 (1986).
- (187) M.J. Vold, *J. Colloid Sci.*, **18**, 684 (1963).
- (188) D.N. Sutherland, *J. Colloid Interface Sci.* **22**, 300 (1966).
- (189) P. Meakin, *J. Colloid Interface Sci.*, **105**, 240 (1985).
- (190) D. Bensimon, B. Shraiman and S. Liang, *Phys. Lett.* **102A**, 238 (1984).
- (191) M.J. Vold, *J. Colloid Sci.* **14**, 168 (1959).
- (192) M.J. Vold, *J. Phys. Chem.* **63**, 1608 (1959).
- (193) R. Jullien and P. Meakin, *Europhys. Lett.* **4**, 1385 (1987).
- (194) R.F. Voss, *J. Phys. A* **17**, L373 (1984).
- (195) H. Saleur and B. Duplantier, *Phys. Rev. Lett.* **58**, 2325 (1987).
- (196) A. Coniglio, N. Jan, I. Majid and H.E. Stanley, *Phys. Rev. B* **35**, 3617 (1987).
- (197) R.M. Ziff, *Phys. Rev. Lett.* **56**, 545 (1986).
- (198) B. Sapoval, M. Rosso and J.F. Gouyet, *J. Phys. (Paris)* **46**, 2149 (1985).
- (199) T. Grossman and A. Aharony, *J. Phys. A* **19**, L745 (1986).
- (200) S. Havlin, R. Nossal, B. Trus and G.H. Weiss, *J. Phys. A* **17**, L957 (1984).
- (201) S. Kirkpatrick, *AIP Conf. Proc.* **40**, 99 (1978).
- (202) H.E. Stanley, *J. Phys. A* **10**, L211 (1977).
- (203) P. Meakin and J. Krug, *Europhys. Lett.* **11**, 7 (1990).
- (204) F. Family and T. Vicsek, *J. Phys. A* **18**, L75 (1985).
- (205) D.J. Henderson, M.H. Brodsky and P. Chaudhari, *J. Appl. Phys. Lett.* **25**, 641 (1974).
- (206) S. Kim, D.J. Henderson and P. Chaudhari, *Thin Solid Films*, **47**, 155 (1977).
- (207) A.G. Dirks and H.J. Leamy, *Thin Solid Films*, **47**, 219 (1977).
- (208) H.J. Leamy and A.G. Dirks, *J. Appl. Phys.* **49**, 33430 (1978).
- (209) H.J. Leamy, G.H. Gilmer and A.G. Dirks in *Current Topics in Materials Science*, E. Kaldis, ed., North Holland, Amsterdam, 1980.
- (210) P. Meakin, *Critical Reviews in Solid State and Materials Science*, **13**, 143 (1984).
- (211) P. Personne and C. Duroure, *J. Phys. (Paris)* **48**, C1-413 (1987).
- (212) J.G. Amar and F. Family, *Phys. Rev. Lett.* **64**, 543 (1990).
- (213) M. Kardar, G. Parisi and Y.-C. Zhang, *Phys. Rev. Lett.* **56**, 889 (1986).
- (214) P. Meakin, P. Ramanlal, L.M. Sander and R.C. Ball, *Phys. Rev. A* **34**, 5091 (1986).
- (215) J.M. Kim and M. Kosterlitz, *Phys. Rev. Lett.* **62**, 2289 (1989).
- (216) J. Krug, *Phys. Rev. A* **36**, 5465 (1987).
- (217) J. Krug and H. Spohn, preprint.
- (218) J. Halpin-Healy, *Phys. Rev. Lett.* **62**, 442 (1989).
- (219) D.E. Wolf and J. Kertesz, *J. Phys. A* **20**, L257 (1987).
- (220) J. Kertesz and D.E. Wolf, *J. Phys. A* **32**, 747 (1988).
- (221) J. Krug, *J. Phys. A* **22**, L769 (1989).
- (222) P. Meakin and R. Jullien, *Europhys. Lett.* **4**, 1385 (1987).
- (223) P. Meakin, *Phys. Rev. A* **38**, 994 (1988).
- (224) J. Krug and P. Meakin, *Phys. Rev. A* **40**, 2064 (1989).

- (225) J.M. Burgers, *The Nonlinear Diffusion Equation*, Reidel, Boston, 1974.
- (226) R. Jullien and P. Meakin, *J. Phys. (Paris)* **48**, 1651 (1987).
- (227) F. Family, *J. Phys. A* **19**, L441 (1986).
- (228) S.F. Edwards and D.R. Wilkinson, *Proc. Roy. Soc (London) A* **381**, 17 (1982).
- (229) P. Meakin and R. Jullien, unpublished.
- (230) G.Y. Onoda and J. Toner, *Phys. Rev. Lett.* **57**, 1340
- (231) J.P. Pellegrini and R. Jullien, *Phys. Rev. Lett.* **64**, 1745 (1990).
- (232) J.P. Pellegrini and R. Jullien, preprint.
- (233) H. Yan, D. Kessler and L.M. Sander, *Phys. Rev. Lett.*, **64**, 926 (1990).
- (234) J.G. Amar and F. Family, *Phys. Rev. A* **41**, 3399 (1990)
- (235) J. Krug and H. Spohn, *Phys. Rev. Lett.* **64**, 2332 (1990).
- (236) J.M. Kim, T. Ala-Nissila and J.M. Kosterlitz, *Phys. Rev. Lett.* **64**, 2333 (1990).
- (237) D.A. Huse, J.G. Amar and F. Family, *Phys. Rev. A* **41**, 7075 (1990).
- (238) J. Krug and P. Meakin, preprint.
- (239) H. van Beijeren, R. Kotter and H. Spohn, *Phys. Rev. Lett.* **54**, 2026 (1985).
- (240) G.I. Sivashinski, *Acta Astronautica*, **6**, 569 (1979).
- (241) S. Zalesky, *Physica D*, to be published.
- (242) M. Kardar, *Phys. Rev. Lett.* **55**, 2923 (1985).
- (243) J.D. Weeks, G.N. Gilmer and H.J. Leamy, *Phys. Rev. Lett.* **31**, 549 (1973).
- (244) Y. Saito and H. Muller-Krumbhaar in *Applications of the Monte Carlo Method in Statistical Physics*, K. Binder, ed., Springer-Verlag, Berlin, 1984, p. 223.
- (245) D. Jasnow, *Rep. Prog. Phys.* **47**, 1059 (1984).
- (246) G.H. Gilmer, *J. Crystal Growth* **35**, 15 (1976).
- (247) Z. Jiang and C. Ebner, *Phys. Rev. B* **38**, 6766 (1988).
- (248) D. Bedeaux, J.D. Weeks and B.J.A. Zielinska, *Physica*, **130A**, 88 (1985).
- (249) F.P. Buff, R.A. Lovett and F.H. Stillinger, *Phys. Rev. Lett.* **51**, 621 (1983).
- (250) D. Bedeaux and J.D. Weeks, *J. Chem. Phys.* **82**, 972 (1985).
- (251) N.A. Metropolis, A.W. Rosenbluth, M.N. Rosenbluth, A.H. Teller and E. Teller, *J. Chem. Phys.* **21**, 1087 (1953).
- (252) *Applications of the Monte Carlo Method in Statistical Physics*, K. Binder, ed., Springer Berlin, 1984.
- (253) G.S. Bales, R. Bruinsma, E.A. Eklund, R.P.U. Karunasiri, J. Rudnick and A. Zangwill, *Science* **249**, 264 (1990).
- (254) P. Meakin, unpublished.
- (255) P. Meakin and J.M. Deutch, *J. Chem. Phys.* **85**, 2320 (1986).
- (256) L. Patterson, *Phys. Rev. Lett.* **53**, 1621 (1984).
- (257) J. Krug and P. Meakin, preprint.
- (258) Y. Kantor and D.R. Nelson, *Phys. Rev. Lett.* **58**, 2774 (1987).
- (259) Y. Kantor and D.R. Nelson, *Phys. Rev. A* **36**, 4020 (1987).
- (260) Y. Kantor, M. Kardar and D.R. Nelson, *Phys. Rev. Lett.* **57**, 791 (1986).
- (261) Y. Kantor, M. Kardar and D.R. Nelson, *Phys. Rev. A* **35**, 3056 (1987).
- (262) M. Plischke and Z. Racz, *Phys. Rev. A* **38**, 4943 (1988).
- (263) D. Nelson in *Random Fluctuations and Pattern Growth: Experiments and Models*, NATO ASI Series E157. H.E. Stanley and N. Ostrowsky, eds., Kluwer Dordrecht, 1988, p. 193.
- (264) M. Plischke and D. Boal, *Phys. Rev. A* **38**, 4943 (1988).
- (265) Y. Termonia and P. Meakin, *Nature* **320**, 429 (1986).
- (266) *Statistical Models for the Fracture of Disordered Media*, H. Herrmann, ed.
- (267) M. Kardar in *Disorder and Fracture*, J.C. Charlot, ed., NATO ASI Series, Plenum, 1990, to be published.
- (268) J. Villain, *Phys. Rev. Lett.* **52**, 1543 (1984)

- (269) M. Kardar and Y.C. Zhang, *Europhys. Lett.* **8**, 233 (1989).
- (270) G. Grinsein and J. Fernandez, *Phys. Res. B* **29**, 6389 (1984).
- (271) R. Bruinsma and G. Aeppli, *Phys. Rev. Lett.* **52**, 1547 (1984).
- (272) B. Sapoval, M. Rosso, and J.F. Gouyet, *J. Phys. (Paris) Lett.* **46**, L149 (1985).
- (273) A. Bunde and J.F. Gouyet, *J. Phys. A* **18**, L285 (1985).
- (274) M. Rosso, J. F. Gouyet, and B. Sapoval, *Phys. Rev. B* **32**, 6053 (1985).
- (275) R. M. Ziff and B. Sapoval, preprint.
- (276) M. Rosso, J.F. Gouyet and B. Sapoval, *Phys. Rev. Lett.* **57**, 3195 (1986).
- (277) M. Kolb, J. F. Gouyet and B. Sapoval, *Europhys. Lett.*, **3**, 33 (1987).
- (278) K. Kawasaki in *Phase Transitions and Critical Phenomena*, Vol. 2, C. Domb and M.S. Green, eds., Academic Press, New York, 1972, p. 442.
- (279) K. Kawasaki in *Phase Transitions and Critical Phenomena*, Vol. 5a, C. Domb and M.S. Green, eds., Academic Press, New York, 1976, p. 165.
- (280) P. Meakin, unpublished.
- (281) P. Meakin, *Phys. Rev. A* **33**, 1365 (1986).
- (282) P. Meakin, H.E. Stanley, A. Coniglio and T.A. Witten, *Phys. Rev. A* **32**, 2364 (1985).
- (283) P. Meakin, A. Coniglio, H.E. Stanley and T.A. Witten, *Phys. Rev. A* **34**, 3325 (1986).
- (284) C. Amitrano, A. Coniglio and F. di Liberto, *Phys. Rev. Lett.* **57**, 1016 (1986).
- (285) T. Nagatini, *Phys. Rev. A* **36**, 5812 (1987).
- (286) R.C. Ball, R.M. Brady, C. Rossi and B.R. Thompson, *Phys. Rev. Lett.* **55**, 1406 (1985).
- (287) R.C. Ball and M. Blunt, preprint.
- (288) Y. Hayakawa, S. Sato and M. Matsushita, *Phys. Rev.* **36**, 1963 (1987).
- (289) M. Blunt and R. C. Ball, preprint
- (290) P. Meakin, *Phys. Rev. A* **36**, 325 (1987).
- (291) M.E. Cates and T.A. Witten, *Phys. Rev. Lett.* **56**, 2497 (1986).
- (292) P. Meakin and J.M. Deutch, *J. Chem. Phys.* **86**, 4648 (1987).
- (293) P. Meakin, *J. Chem. Phys.* **88**, 2042 (1988).
- (294) M. Blunt, *Phys. Rev. A* **39**, 5801 (1989).
- (295) L. de Arcangelis, S. Redner and A. Coniglio, *Phys. Rev. B* **31**, 4725 (1983).
- (296) R. Rammal, C. Tannous, P. Breton and A.M.S. Tremblay, *Phys. Rev. Lett.* **54**, 1718 (1985).
- (297) R. Blumenfeld, Y. Meir, A. Aharony and A. Brooks Harris, *Phys. Rev. B* **35**, 3524 (1987).
- (298) A. Hansen, S. Roux and H.J. Herrmann, *J. Phys. (France)* **50**, 733 (1989).
- (299) M. Cates and J. Deutsch, *Phys. Rev. A* **35**, 4907 (1987).
- (300) C. Meneveau and A. Chhabra, preprint (1989).
- (301) S.J. Lee and T.C. Halsey, preprint (1990).
- (302) M. Doud and J.E. Martin in *The Fractal Approach to Heterogeneous Chemistry: Surfaces, Colloids, Polymers* D. Avnir, ed., p. 109.
- (303) P. Meakin, *Encyclopedia of Polymer Science and Engineering*.
- (304) C.J. Brinker and G.W. Shiner *Sol-Gel Processing*, Academic, 1989.
- (305) D. Stauffer, A. Coniglio and M. Adam in *Advances in Polymer Science*, Vol. 44, K. Dusek, ed., Springer-Verlag, Berlin, 1982.
- (306) H.J. Stapleton, J.P. Allen, C.P. Flynn, D.G. Stinson, and S.R. Kurtz, *Phys. Rev. Lett.* **45**, 1456 (1980).
- (307) P.J.E. Peebles, *Physica D* **38**, 273 (1989).
- (308) L. Pietronero, *Physica* **144**, 257 (1987).
- (309) P.H. Coleman in *Fractals' Physical Origin and Properties*, L. Pietronero, ed., Plenum, New York, 1990, p. 349.
- (310) P.G. de Gennes, *Scaling Concepts in Polymer Physics*, Cornell, Ithaca, 1979.
- (311) P.G. de Gennes, *C.R. Acad. Sci.* **291**, 17 (1980).

- (312) M. Daccord, F. Family and G. Jannink, *J. Phys. (Paris) Lett.* **45**, 199 (1984).
- (313) J. Isaacson and T.C. Lubensky, *J. Phys. (Paris) Lett.* **41**, L469 (1980)
- (314) E. Bouchard, M. Delsanti, M. Adam, M. Daoud and D. Durand, *J. Phys. (Paris) Lett.* **47**, 1273 (1986).
- (315) J.E. Martin, J. Wilcoxan and D. Adolf, preprint.
- (316) R.F. Voss, A.B. Laibowitz and E.I. Allessandrini, *Phys. Rev. Lett.* **49**, 1441 (1982).
- (317) A. Kapitulnik and G. Deutscher, *Phys. Rev. Lett.* **49**, 1444 (1982).
- (318) S. Reich, preprint.
- (319) D. Wilkinson and J.F. Willemsen, *J. Phys. A* **16**, 3365 (1983).
- (320) D. Wilkinson and M. Barony, *J. Phys. A* **17**, L129 (1984).
- (321) R. Lenormand and S. Bories, *C.R. Acad. Sci. (Paris) B* **291**, 279 (1980).
- (322) R. Chandler, J. Koplik, K. Lerman and J.F. Willemsen, *J. Fluid Mech.* **119**, 249 (1982).
- (323) L. Furberg, J. Feder, A. Aharony, and T. Jøssang, *Phys. Rev. Lett.* **61**, 2117 (1988).
- (324) R. Lenormand and C. Zarcone, *Phys. Rev. Lett.* **54**, 2226 (1985).
- (325) K. J. Maløy, F. Boger, J. Feder and T. Jøssang, in *Time Dependent Effects in Disordered Materials*, R. Pynn and T. Riste, eds., NATO ASI Series B167, Plenum, New York, 1987.
- (326) R. Lenormand and C. Zarcone, Soc. Petrol. Eng. paper 13264 (1984).
- (327) T.M. Shaw, *Phys. Rev. Lett.* **59**, 1671 (1987).
- (328) A.T. Skjeltorp, private communication.
- (329) M.M. Dias and D. Wilkinson, *J. Phys. A* **19**, 3131 (1986).
- (330) J.T. Chayes, L. Chayes and C.M. Newman, *Ann. Probab.* **15**, 1272 (1987).
- (331) J.T. Chayes, L. Chayes and C.M. Newman, *Commun. Math. Phys.* **101**, 383 (1985).
- (332) J. Feder, T. Jøssang, K.J. Maloy and U. Oxaal in *Fragmentation Form and Flow in Fractured Media*, R. Englman and Z. Jaeger, eds., *Ann Israel Phys Soc* **8**, 531 (1986).
- (333) P. Meakin, unpublished.
- (334) R.M. Brady and R.C. Ball, *Nature*, **309**, 225 (1984).
- (335) R.C. Ball in *On Growth and Form: Fractal and Non-Fractal Patterns in Physics*, H.E. Stanley and N. Ostrowsky, eds., NATO A11 Series E100, Martinus Nijhoff, Dordrecht, 1986, p. 69.
- (336) M. Matsushita in *The Fractal Approach to Heterogeneous Chemistry: Surfaces, Colloids, Polymers* D. Avnir, eds., Wiley, Chichester, 1989, p. 161.
- (337) H. Van Damme in *The Fractal Approach to Heterogeneous Chemistry: Surfaces, Colloids, Polymers*, D. Avnir, ed., Wiley, Chichester, 1989, p. 199.
- (338) G. Daccord and R. Lenormand, *Nature* **325**, 41 (1987).
- (339) G. Daccord, *Phys. Rev. Lett.* **58**, 479 (1987).
- (340) R. Lenormand, A. Soucemarianadin, E. Touboul and G. Daccord, *Phys. Rev. Lett.* **36** (1987).
- (341) G. Daccord in *The Fractal Approach to Heterogeneous Chemistry: Surfaces, Colloids, Polymers*, D. Avnir, ed., Wiley, Chichester, 1989.
- (342) D. Avnir, *Nature* **308**, 261 (1984).
- (343) D. Avnir and P. Pfeifer, *Nouv. J. Chim.* **7**, 71 (1983).
- (344) D. Avnir, D. Farin and P. Pfeifer, *J. Chem. Phys.* **79**, 3566 (1983).
- (345) D. Farin, D. Avnir, and P. Pfeifer, *Part. Sci. Technology* **2**, 27 (1984).
- (346) D. Farin and D. Avnir in *The Fractal Approach to Heterogeneous Chemistry: Surfaces, Colloids, Polymers*, D. Avnir, ed., Wiley, Chichester, 1989, p. 271.
- (347) D. Avnir, D. Farin and P. Pfeifer, *J. Colloid Interfae Sci.* **103**, 112 (1985).
- (348) P. Pfeifer, D. Avnir and D. Farin, *J. Stat. Phys.* **36**, 699 (1984).
- (349) D. Rojanski, D. Huppert, H.D. Bale, X. Dacai, P.W. Schmid, D. Farin, A. Seri-Levy, and D. Avnir, *Phys. Rev. Lett.* **56**, 2505 (1986).
- (350) P. Pfeifer, Y.J. Wu, M.W. Cole and J. Krim, *Phys. Rev. Lett.* **62**, 1997 (1989).
- (351) M. Kardar and J.O. Indekeu, preprint.

- (352) D. Avnir and M. Jaroniec, *Langmuir*, **5**, 1431 (1989).
- (353) M.M. Dubinin in *Characterization of Porous Solids*, K.K. Unger, J. Rouquerol, K.S.W. Sing and H. Kral, eds., Elsevier, Amsterdam , 1988, p. 127.
- (354) P. Pfeifer, J. Kennterer and M.W. Cole, *Proceedings of Conference of Fundamentals of Adsorption*, Sonthofen, 1989.
- (355) J. Krim and V. Panella, *Proceedings of IUPAC Symposium on Characterization of Porous Solids* (COPS II) Alicante, Spain (1990).
- (356) C.L. Wang, J. Krim and M.F. Toney, *J. Vac. Sci. Tech A* **7**, 2481 (1989).
- (357) J. Krim and E.T. Watts, *Proceedings of the 3rd International Conference on Fundamentals of Adsorption*, Sonthofen, W. Germany (1989).
- (358) B.B. Mandelbrot, D.E. Passoja and A.J. Paullay, *Nature* **308**, 731 (1978).
- (359) D.E. Passoja and D.J. Aniborski, *Microstruct. Sci.* **6**, 143 (1978).
- (360) S.C. Langford, M. Zhenyi and J.T. Dickinson, *J. Mater. Res.* **4**, 1272 (1989).
- (361) T.J. Mackin, D.E. Passoja and J.J. Mechlosky in *Fractal Aspects of Materials: Disordered Systems*, A.J. Hurd, D.A. Weitz and B.B. Mandelbrot, eds., Materials Research Society , 1989.
- (362) C.S. Pande, *Acta Metal.* **35**, 1633 (1987).
- (363) P.J. Flory, *Principles of Polymer Chemistry*, Cornell University Press, Ithaca, New York, 1971.
- (364) P.J. Flory, *J. Chem. Phys.* **17**, 303 (1949).
- (365) S. Alexander and R. Orbach, *J. Physique Lett.* **43**, 625 (1982).
- (366) D. Ben Avraham and D. Havlin, *J. Phys. A* **15**, L691 (1982).
- (367) R. Rammal and G. Tolouse, *J. Physique Lett.* **44**, L13 (1983).
- (368) F. Family and A. Coniglio, *J. Phys. A* **17**, L285 (1984).
- (369) C. Kittel, *Introduction to Solid State Physics* (Sixth Edition), John Wiley and Sons, Inc., New York 1986.
- (370) S. Alexander, J. Bernasconi, W.R. Schneider and R. Orbach, *Rev. Mod. Phys.* **53**, 175 (1981).
- (371) R. Orbach, *Scaling Phenomena in Disordered Systems*, NATO ASI Series B133, P. Pynn and A.T. Skjeltorp, eds., Plenum, New York, 1986.
- (372) A. Aharony, O. Entin-Wohlman and R. Orbach in *Time Dependent Effects in Disordered Materials*, NATO ASI, Geilo, Norway.
- (373) G.S. Grest and I. Webman, *J. Phys. (Paris)* **45**, L1155 (1984).
- (374) K. Yahubo and T. Nakagama, *Phys. Rev. B* **36**, 8933 (1987).
- (375) R. Orbach, *Physica B* **38**, 266 (1989).
- (376) E. Courtens, R. Vacher and E. Stoll, *Physica D* **38**, 41 (1989).
- (377) R. Vacher, T. Woignier, J. Pelous and E. Courtens, *Phys. Rev. B* **37**, 6500 (1988).
- (378) R. Vacher, E. Courtens, G. Goeldens, J. Pelous and T. Woignier, *Phys. Rev. B* **39**, 7384 (1989).
- (379) Y. Tsujimi, E. Courtens, J. Pelous and R. Vacher, *Phys. Rev. Lett.* **60**, 2757 (1988).
- (380) E. Courtens and R. Vacher, *Proc. Roy. Soc. (London) A* **423**, 55 (1989).
- (381) R. Calemzuk, A.M. de Goer, B. Salce, R. Maynard and A. Zarembowich, *Europhys. Lett.* **3**, 1205 (1987).
- (382) A.M. de Goer, R. Calemzuk, B. Salce, J. Bon, E. Bonjour and R. Maynard, *Phys. Rev. B*, to be published.
- (383) Y.J. Uemura and R.J. Birgeneau, *Phys. Rev. Lett.* **57**, 1947 (1986).
- (384) Y.J. Uemura and R.J. Birgeneau, *Phys. Rev. Lett.* **36**, 7024 (1987).
- (385) P.F. Tua, S.J. Patterson and R. Orbach, *Phys. Lett. A* **98**, 357 (1983).
- (386) S. Alexander, C. Laermans, R. Orbach and H.M. Rosenberg, *Phys. Rev. B* **28**, 4615 (1983).
- (387) R. Orbach, *Science*, **231**, 814 (1986).
- (388) R.R. Prasad, C. Meneveau and K.R. Sreenivasan, *Phys. Rev. Lett.* **61**, 74 (1988).
- (389) C. Meneveau and K.R. Sreenivasan, *Nucl. Phys. B. Proc. Suppl.* **2**, 49 (1987).
- (390) M.H. Jensen, L.P. Kadanoff, A. Libchaber, I. Procaccia and J. Stavans, *Phys. Rev. Lett.* **55**, 2798

- (1985).
- (391) M.H. Jensen in *Random Fluctuations and Pattern Growth: Experiments and Models*, NATO ASI Series E157, H.E. Stanley and N. Ostrowsky, eds., Kluwer Dordrecht, 1988, p. 292.
- (392) Z. Su, R.W. Rollins and E.R. Hunt, *Phys. Rev. A* **36**, 3515 (1987).
- (393) J. Nittmann, H.E. Stanley, E. Touboul and G. Daccord, *Phys. Rev. Lett.* **58**, 619 (1987).
- (394) H.E. Stanley in *Time Dependent Effects in Disordered Materials*, NATO ASI Series B167, R. Pynn and T. Riste, eds., Plenum, New York, 1987, p. 145.
- (395) K.J. Maloy, F. Boger, J. Feder and T. Jossang in *Time Dependent Effects in Disordered Materials* NATO ASI Series B167. R. Pynn and T. Riste, eds., Plenum, New York, 1987, p. 111.
- (396) J. Feder, K.J. Maloy and T. Jossang in *Hydrodynamics of Dispersed Media*, J.P. Hulin, A.M. Cazabat, E. Guyon and F. Carmona, eds., Elsevier (North Holland) Amsterdam, 1990.
- (397) A.H. Thompson, A.J. Katz and R.A. Raschke, *Phys. Rev. Lett.* **58**, 29 (1987).
- (398) E.L. Hinrichsen, *Structure and Geometry of Two Dimensional Random Systems*, Thesis, University of Oslo (1989).
- (399) R.M. Noyes, *Prog. Reac. Kinet.* **1**, 128 (1961).
- (400) D.F. Calef and J.M. Deutch, *Ann. Rev. Phys. Chem.* **34**, 493 (1983).
- (401) A. Blumen, J. Klafter and G. Zumofen in *Optical Spectroscopy of Glasses*, I. Zschokke, ed., Reidel, 1986, p. 199.
- (402) P. Meakin in *Reactions in Compartmentalized Fluids*, W. Knoche, ed.
- (403) A. Blumen and G.H. Kohler, *Proc. Roy. Soc. A* **423**, 189 (1989).
- (404) A.A. Ovchinnikov and Y.B. Zeldovich, *Chem. Phys.* **28**, 215 (1976).
- (405) D. Toussaint and F. Wilczek, *J. Chem. Phys.* **78**, 2642 (1983).
- (406) M. von Smoluchowski, *Z. Phys.* **17**, 585 (1916).
- (407) M. von Smoluchowski, *Z. Phys. Chem.* **92**, 129 (1917).
- (408) G.H. Weiss and R.J. Rubin, *Adv. Chem. Phys.* **52**, 363 (1983).
- (409) P. Meakin and H.E. Stanley, *J. Phys. A* **17**, L173 (1984).
- (410) K. Kang and S. Redner, *Phys. Rev. Lett.* **52**, 955 (1984).
- (411) D.C. Torney and T.T. Warnock, *International J. Supercomputer Appl.* **1**, 33 (1987).
- (412) R. Kopelman, *Science*, **241**, 1620 (1988).
- (413) R. Kopelman, *J. Stat. Phys.* **42**, 185 (1986).
- (414) P. Klymko and R. Kopelman, *J. Phys. Chem.* **86**, 3686 (1982).
- (415) P. Klymko and R. Kopelman, *J. Phys. Chem.* **87**, 4565 (1983).
- (416) H.O. Martin and E.V. Albano, *Phys. Rev. A* **39**, 6003 (1989).
- (417) P. Meakin, *Physica A* **155**, 21 (1989).
- (418) L.W. Anaker and R. Kopelman, *Phys. Rev. Lett.*, **58**, 289 (1987).
- (419) K. Lindenberg, B.J. West and R. Kopelman, *Phys. Rev. Lett.*, **60**, 1777 (1988).
- (420) D. Farin and D. Avnir, *J. Amer. Chem. Soc.* (1988).
- (421) D. Farin and D. Avnir, Proc. IUPAC Symposium on *Characterization of Porous Solids*, K.K. Unger, D. Behrens and H. Kral, eds., Elsevier, Amsterdam (1987).
- (422) D. Farin and D. Avnir, *Proc. 9th Int. Congress Catalysis*, Calgary, Canada (1988).
- (423) D. Farin and D. Avnir, preprint.
- (424) G.R. Holdren and P.M. Speyer, *Geochim. Cosmochim Acta*, **49**, 675 (1985).
- (425) M. Silverberg, D. Farin, A. Ben-Shaul and D. Avnir, *Ann. Israel Phys. Soc.* **8**, 451 (1986).
- (426) P. Meakin, *Ann. Israel Phys. Soc.* **8**, 490 (1986).
- (427) Z.-Y. Chen, J.M. Deutch and P. Meakin, *J. Chem. Phys.* **80**, 2982 (1985).
- (428) P. Meakin, Z.-Y. Chen and J.M. Deutch, *J. Chem. Phys.* **82**, 3786 (1985).
- (429) W. Hess, H.L. Frisch and R. Klein, *Z. Phys. B* **64**, 65 (1986).
- (430) W. Van Saarloos, *Physica A* **147**, 280 (1987).
- (431) P. Wiltzius, *Phys. Rev. Lett.* **58**, 710 (1987).

- (432) Z.-Y. Chen, P. Meakin and J.M. Deutch, *Phys. Rev. Lett.* **59**, 2121 (1987).
- (433) P.N. Pusey, J.G. Rarity, R. Klein and D.A. Weitz, *Phys. Rev. Lett.* **59**, 2122 (1987).
- (434) P. Wiltzius and W. Van Saarloos, *Phys. Rev. Lett.* **59**, 2123 (1987).
- (435) P. Meakin, B. Donn and G.W. Mulholland, *Langmuir*, **5**, 510 (1989).
- (436) M.V. Berry and I.C. Percival, *Optima Acta*, **33**, 577 (1986).
- (437) Z. Chen, P. Sheng, D.A. Weitz, M.H. Lindsay, M.Y. Lin and P. Meakin, *Phys. Rev. B* **37**, 5232 (1988).
- (438) Z.-Y. Chen, P. Weakliem, W.M. Gelbart and P. Meakin, *Phys. Rev. Lett.* **58**, 1996 (1987).
- (439) E.L. Wright, preprint.
- (440) W.D. Brown and R.C. Ball, unpublished.
- (441) D. Deptuk, J.P. Harrison and P. Zawadzki, *Phys. Rev. Lett.* **54**, 913 (1985).
- (442) J. Forsman, J.P. Harrison and A. Rutenberg, *Can. J. Phys.* **65**, 767 (1987).
- (443) M. Gronauer, A. Kaduc and J. Fricke in *Aerogels*, J. Fricke, ed., Springer Berlin, 1986, p. 167.
- (444) T. Woignier, J. Phalippou, R. Sempere and J. Pelous, *J. Phys. (Paris)* **49**, 289 (1988).
- (445) R. Buscall, P.D.A. Mills, J.W. Goodwin and D.W. Lawson, *J. Chem. Soc. Faraday Trans.* **84**, (1988).
- (446) R. Buscall, I.J. McGowan, P.D.A. Mills, R.F. Stewart, D. Sutton, L.R. White and G.E. Yates, *J. Non-Newtonian Fluid Mech.* **24**, 183 (1987).
- (447) M.V. Berry, *Physica D* **38**, 29 (1989).
- (448) J. Nelson, *Nature*, **339**, 611 (1989).
- (449) P. Meakin and B. Donn, *The Astrophysical Journal* **328**, L39 (1988).
- (450) S.J. Weidenschilling, B. Donn and P. Meakin in *The Formation and Evolution of Planetary Systems*, H.A. Weaver and L. Donly, eds., Space Telescope Science Institute Symposium Series, Cambridge University Press, Cambridge, 1989.
- (451) A. Aharony in *Scaling Phenomena in Disordered Systems*, R. Pynn and A.T. Skjeltorp, eds., Plenum, New York, 1985, p. 289.
- (452) H.E. Stanley and A. Coniglio, *Phys. Rev. B* **29**, 522 (1984).
- (453) T.A. Witten and Y. Kantor, *Phys. Rev. B* **30**, 4093 (1984).
- (454) J.H. Kaufman, A.I. Nazzal, O.R. Melroy and A. Kapitulnik, *Phys. Rev. B* **35**, 1881 (1987).
- (455) J.H. Kaufman, C.K. Baker, A.I. Nazzal, M. Flickner, O.R. Melroy and A. Kapitulnik, *Phys. Rev. Lett.* **56**, 1932 (1986).
- (456) P. Meakin, I. Majid, S. Havlin and H.E. Stanley, *J. Phys. A* **17**, L975 (1984).
- (457) P. Meakin and H.E. Stanley, *Phys. Rev. Lett.* **51**, 1457 (1983).
- (458) M. Sahimi, M. McKarnin, T. Nordahl and M. Tirrell, *Phys. Rev. A* **32**, 590 (1985).
- (459) A. Le Mehaute and G. Crepy, *Solid State Ionics* **9**, 17 (1983).
- (460) S.H. Liu, *Phys. Rev. Lett.* **55**, 529 (1985).
- (461) T. Kaplan and L.J. Gray, *Phys. Rev. B* **32**, 7360 (1983).
- (462) B. Sapoval, *Solid State Ionics*, **23**, 253 (1987).
- (463) T.C. Halsey, *Phys. Rev. A* **35**, 3512 (1987).
- (464) R. de Levie, *Electrochimica Acta* **35**, 1045 (1990).
- (465) L. Nyikos and T. Pajkossy, *Electrochimica Acta*, **30**, 1533 (1985).
- (466) J.P. Clerc, A.M.S. Tremblay, G. Allsinet and C.D. Mitescu, *J. Phys. (Paris)*
- (467) M. Keddam and H. Takenouti, *C.R. Acad. Sci. Ser. 2*, **302**, 281 (1986).
- (468) M. Blunt, *J. Phys. A* **22**, 1179 (1989).
- (469) B. Sapoval, J.N. Chazaviel and J. Peyriere, *Phys. Rev. A* **38**, 5867 (1988).
- (470) T.C. Halsey, *Phys. Rev. A* **36**, 5877 (1987).
- (471) T.C. Halsey and M. Leibig, preprint.
- (472) J.B. Bates, Y.T. Chu and W. Stribling, *Phys. Rev. Lett.* **60**, 627 (1988).
- (473) B. Sapoval in *Fractals and Disordered Systems*, A. Bunde and S. Havlin, eds., Springer-Verlag,

- Heidelberg, 1991, to be published.
- (474) R.D. Armstrong and R.A. Burnham, *J. Electroanal. Chem.* **72**, 237 (1976)
- (475) M. Keddam and H. Takenouti, *Electrochim. Acta* **33**, 445 (1988).
- (476) A. LeMehaute in *The Fractal Approach to Heterogeneous Chemistry: Surfaces, Colloids, Polymers*, D. Avnir, ed., Wiley, Chichester, 1989, p. 311.